THE UNIVERSITY OF CHICAGO

DENDRITIC CELL-INTRINSIC PTPN22 NEGATIVELY REGULATES ANTI-TUMOR IMMUNITY AND ANTI-PD-L1 EFFICACY

A DISSERTATION SUBMITTED TO
THE FACULTY OF THE DIVISION OF THE BIOLOGICAL SCIENCES
AND THE PRITZKER SCHOOL OF MEDICINE
IN CANDIDACY FOR THE DEGREE OF
DOCTOR OF PHILOSOPHY

COMMITTEE ON CANCER BIOLOGY

BY
SANTIAGO ACERO BEDOYA

CHICAGO, ILLINOIS
JUNE 2024

"No medicine cures what happiness cannot."

— Gabriel García Márquez, *Of Love and Other Demons*

TABLE OF CONTENTS

LIST OF FIGURES

LIST OF TABLES

ACKNOWLEDGMENTS

This dissertation serves as a testament to an immeasurable amount of support, encouragement, and love that I have been fortunate enough to receive from a great deal of people throughout my life.

Firstly, to my mentor and advisor, Tom Gajewski, you have endowed in me one of the greatest gifts: curiosity. More specifically, your guidance and perspectives have taught me how to nurture and rigorously test the boundaries of my curiosity and package and present it in a way that can excite and induce further curiosity in others. Your ability to discover and communicate impactful science is second to none, and I will forever be proud to have completed my doctoral work under your tutelage.

To the Gajewski lab, past, present, and future, thank you for creating such a fun and collaborative environment. I owe a great deal to many of you for the growth I have experienced throughout my time in the lab. It is not lost on me how much I have been able to achieve in only three years, and it would not be possible were it not for the supportive environment you all have helped build and foster. Specifically, I want to thank Anna Martinez, Ada Cabanov, and Emily Higgs. To my mentee Anna, mentoring you and watching you grow scientifically has been one of the great privileges of my life. To my co-senior graduate student and friend, Ada, your unshakable persistence and positivity are nothing short of amazing and inspirational. Lastly, to Emily, thank you not only for training me but also for believing in this project and bringing it to life.

Secondly, to my friends, your support and sense of community have meant everything to me. From karaoke to in-depth scientific discussions and exploring the vast possibility of career paths out there, you have helped me more than you know. I came to Chicago alone and will be leaving with lifelong friendships. Specifically, Patrick, Ben, Emma, Colin, Alex, and Sophia from school, Andrew, Liv, Drew, Shuvam, Will, Ted and the entire Nucleate Chicago team. I cannot wait to see what all of you achieve. Thank you also to Shanay,

Greta, Craig, Nick, Keke, and Jessie for bringing tOSU to Chicago. Go Bucks.

The Committee on Cancer Biology, thank you for the opportunity of a lifetime. I will forever be grateful for this opportunity and hope that my achievements will serve as evidence. Specifically, thank you to Kay Macleod and Mat Perez for allowing me to realize that this was the best place for me. A special thank you to my committee Drs. Barbara Kee (chair), Daria Esterhazy, and Phoenix Miao for all of your support and feedback on this body of work. I also want to thank all of the administrators and staff for their critical work; this place wouldn't run without you. Thank you also to my funding sources that have allowed me to pursue my work to the full extent of my interests: IMSD, NSF GRFP, and the NCI F99/K00.

I also want to thank and acknowledge all of my mentors who helped foster my passion for science and creating a better society through innovation: Stephanie Wilson, Medeva Ghee, Michelle Dawson, John Hawse, Asuncion Mejias, and Thomas de Vlaam.

Lastly, I want to thank my family. I wouldn't be here without you. All my success is our success. To my mom and my dad, the sacrifices you have made to allow me to pursue higher education in the United States are beyond what words can describe. I will always strive to be a son you can be proud of. Los amo con toda mi alma.

To my best friend and loving wife, Rosy, who knew our PhDs would turn into a love story? I am better every day because of you. There are no words to describe what you mean to me. This PhD is as much yours as it is mine. You are the Sally to my Harry, and I cannot wait to continue our story in New York (driving in the right direction this time).

ABSTRACT

Checkpoint blockade immunotherapies have revolutionized cancer treatment, yet only a subset of patients benefit. Individuals with a loss-of-function single nucleotide polymorphism in the gene encoding PTPN22 have increased risk for autoimmune diseases and lower incidence of cancer. Moreover, the presence of these alleles in cancer patients is associated with increased survival and favorable responses to checkpoint blockade immunotherapy. Studies in PTPN22 knockout (KO) mice have established it as a negative regulator of T cell responses in cancer models. However, the role of PTPN22 in distinct immune cell compartments, such as dendritic cells (DCs), remains undefined. We developed a novel DC PTPN22 conditional KO (cKO) mouse model that enables specific deletion in $CD11c^+$ cells, targeting DCs in mice. Deletion of PTPN22 in DCs did not alter the immune profiles of naive young (6 weeks) or aged (20 months) mice but resulted in augmented tumor control upon challenge with B16.SIY injected intradermally. $CD8^+$ T cells, but not $CD4^+$ T cells or Tregs, were increased in the tumors of $CD11c^+$ PTPN22 cKO mice. Depleting $CD8^+$ T cells eliminated the tumor growth control, suggesting a reliance on the DC-$CD8^+$ T cell axis. Accordingly, day 7 tumor-bearing mice revealed an increase in IFN-γ-producing SIY-specific T cells, indicating improved $CD8^+$ T cell priming. Analysis of tumor antigen-specific T cells in the tdLN showed a significant increase of $CD8^+$ SIY^+ T cells displaying elevated activation and memory markers. Likewise, there was an overall increase only in the $CD103^+$ DC subset displaying increased activation markers in the tdLN. Together, the number of tumor-infiltrating $CD8^+$ T cells and $CD103^+$ DCs at endpoint correlated with decreased tumor volumes. Furthermore, intratumoral DCs showed significantly higher $Ki67^+$versus activated $Caspase\text{-}3^+$ cells, which led to a greater number of DCs with internalized tumor-derived material in situ. Additional characterization in vitro revealed equal amounts of antigen uptake, but superior antigen processing and subsequent presentation on MHC I only in splenic $CD103^+$ DCs of PTPN22 cKO animals. These observations were also supported by bulk RNAseq of intra-

tumoral DCs showing enrichment of activation gene signatures in PTPN22 cKO DCs and negative regulatory signatures in WT DCs. Improved tumor control and favorable $CD8^+$ T cell and $CD103^+$ DC profiles were also observed in PTPN22 cKO mice challenged with subcutaneous injection of the colon cancer cell line MC38.SIY. Lastly, PTPN22 cKO mice displayed increased survival upon anti-PD-L1 treatment in the B16.SIY model but no appreciable changes in the more immunogenic MC38.SIY model. However, PTPN22 cKO mice challenged with MC38 parental tumors showed decreased tumor growth and increased survival when treated with anti-PD-L1 therapy. In conclusion, deletion of PTPN22 in DCs is sufficient to drive an augmented tumor antigen-specific T cell response, resulting in enhanced tumor control. Mechanistically, this is linked to a shift towards proliferative over apoptotic $CD103^+$ DCs, leading to enhanced antigen presentation to $CD8^+$ T cells in vivo. This work argues that PTPN22 is likely regulating DC proliferative signals and management of acquired antigens, highlighting the potential to modulate anti-tumor immunity through the manipulation of DC signaling.

CHAPTER 1

INTRODUCTION

1.1 Cancer immunology: a new field is born

Everyone has heard of cancer, and odds are, the ravenous disease has touched most individuals in some way or another. However, not everyone appreciates that the term "cancer" represents over 200 different diseases [1]. Thus, it is not surprising that entire careers are dedicated to studying just a single aspect of any given type of cancer. The prominence and complexity of cancer can also be appreciated by its long history, seemingly inherent to life itself. For example, scientists and doctors recently identified the first case of bone cancer (osteosarcoma) in a dinosaur that lived roughly 76 million years ago [2].

In humans, however, the oldest written records we have describing cancer are part of the Edwin Smith Papyrus, an Egyptian document dating back to around 2,000 BC describing different ailments and maladies, including tumors [3]. Observations from the ancient Greeks have proven to be foundational in our understanding of cancer today. For instance, the Greek physician Hippocrates described a variety of cancers, referring to them as "karkinos," giving rise to the modern term *carcinoma* [4, 5]. These observations and others allow us to see how history has long recognized what we now know as cancer.

While descriptions and observations of cancer have been present throughout history, its origins and complexities are active topics of debate and investigation to this day. Today, we appreciate the interaction between the immune system (the body's defense system against pathogens) and cancer, but this crucial interaction was far from obvious, and its history underscores its nuance. It was not until the second century A.D. that the Greek physician Galen began referring to tumors as "oncos" because of their swollen nature, which may be a direct consequence of immune-mediated inflammation [6, 7, 8]. Thus, this is perhaps the first description of the connection between the immune system and cancer.

Despite the early astonishing observations made by the ancient Greeks, it was not until the 19th century that the Polish physician Rudolf Virchow first described the presence of "leucocytes," or white blood cells, inside tumors. Virchow further postulated that the "lymphoreticular infiltrate" suggested the origin of cancer at sites of chronic inflammation [9, 10, 8]. Expanding on this idea, he later coined the term leukemia, describing the pathology of excess white blood cells [11]. These observations helped strengthen the ties between immune cells and tumors but were missing proof of concept studies to truly understand the role of the immune system in the context of cancer. Up to that point, it was clear that immune cells had an involvement, but it was not clear if it was causative or correlative, and certainly not preventative.

It was not until 1891, when William B. Coley made the observation that some patients with incurable cancers underwent spontaneous tumor rejection following concomitant bacterial infections, that the immune system was speculated to play a potential therapeutic role [12, 13]. A bone surgeon at that New York Cancer Hospital (now Memorial Sloan Kettering), Coley studied available literature along with the charts of as many patients as he could find and ultimately deduced that the infections were triggering a response that drove the rejection of established tumors. Coley meticulously tested and different cocktails of bacteria and treated over 1,000 patients with what became known as Coley's Toxins, which became commercially available. [14].

Despite his success, the lack of understanding behind the mechanism of action and the concurrent advancements in radiation therapy resulted in Coley's work falling out of favor, and in 1963, the FDA officially labeled it as an investigations drug, making it illegal to prescribe outside of clinical trial settings. All of this culminated in the importance of Coley's work going largely unrecognized for almost half a century. Following his death, his daughter Helen Coley Nauts worked tirelessly and diligently to ensure her father's legacy was appreciated and not forgotten. Mrs Nauts then went on to found the Cancer Research Institute

in New York in 1953 [15]. Thanks to his daughter, Coley's work is now appreciated, and he is regarded as the "Father of Immunotherapy."

Coley could not explain the mechanism behind his treatments, which we now understand to have been the activation of the innate immune system by the bacteria resulting in adaptive immunity against the tumors, but the postulations of his contemporaries and successors provided explanations. Paul Ehrlich was one of these luminaries. He proposed the "side-chain theory," suggesting that in the presence of toxins, cells would produce extra "nutriceptors" that would shed and accumulate in the bloodstream acting as antitoxins [16, 17, 14]. While incorrect, this led to the discovery and understanding of antibodies and receptors, not to mention it earned him the Nobel Prize in Medicine in 1908. Moreover, Ehrlich was the first to put forth the idea in 1909 that cancers arose spontaneously but were kept in check by the immune system [18]. This idea would change the way scientists thought of cancer and the immune system.

It was not until 50 years later that Macfarlane Burnet and Lewis Thomas refined Ehrlich's ideas backed by experimental data and officially coined the term "immune surveillance," shaping the way we think about anti-tumor immunity today [19, 20]. Macfarlane and Thomas were strong proponents that T-lymphocytes were the dominant immune cells in driving immune surveillance, a highly controversial take at the time. In fact, Macfarlane was awarded the Nobel Prize in 1960 for his work on acquired immunological tolerance, widely attributed to this work in virology. Ironically, Macfarlane died of cancer in 1985. Burnet and Thomas's immune surveillance theory brought widespread popularity to the field of cancer immunology, but it was not long-lived.

The development of athymic nude mice, thought to be completely immunocompromised due to a lack of thymus, allowed Osias Stutman to put the immune surveillance theory to the test in 1974 [21]. In his landmark study, Stutman showed that immunocompromised mice showed no increased incidence or onset of chemically induced tumors when treated with 3-

methylcholanthrene (MCA). Stutman concluded that lymphocytes were thus not necessary for the control of tumors in mice. However, this model system contained unappreciated caveats that resulted in important implications.

At the time, it was not known that nude mice had a leaky system that resulted in the presence of leftover T cells, especially with age. Moreover, what Stutman could not have accounted for was the presence of the innate immune system in nude mice, such as Natural Killer (NK) cells, that could drive tumor rejection [22]. Lastly, Stutman utilized the MCA model that was later shown to be dependent on the activity of aryl hydrocarbon hydroxylase (AHH) [23]. Nude mice have higher levels of AHH activity, making MCA extremely carcinogenic in this model and likely overwhelming whatever immune system these mice retained. Despite careful experimentation from Stutman, the complexities of the model system he was not privy to render his conclusion incorrect, or at the very least incomplete. Nevertheless, they halted the excitement and credibility in the field of cancer immunology.

It was not until the early 2000s that Robert Schreiber's group demonstrated the necessity of T cells and associated pathways for endogenous tumor rejection. These studies were facilitated by the development of $RAG2^{-/-}$ mice that lack an enzyme necessary for somatic recombination, resulting in the absence of mature T and B lymphocytes [24]. $RAG2^{-/-}$ mice allowed Robert Schrieber's group to repeat Osias Stutman's experiments in a model truly lacking T and B cells. This landmark study showed that immunocompromised mice had a greater incidence of tumor development and went on to show that this was dependent on $CD8^{+}$ and $CD4^{+}$ T cells through depletion studies, as well as the importance of the IFN-γ pathway through mice lacking the IFN-γ receptor ($IFNGR1^{-/-}$ mice) [25]. The development of these tools, such as the $RAG2^{-/-}$ mouse model, and the observations made by Schreiber's group helped revive excitement in the field of cancer immunology. But the true potential of cancer immunotherapies would not be appreciated until the development and approval of checkpoint blockade therapies capable of achieving long-term responses.

1.2 Immunotherapies are efficacious anti-cancer treatments

Today, it is impossible to talk about cancer research without taking into account the immune system. Accordingly, research activities, funding opportunities, and biotech and large pharmaceutical companies based around cancer immunotherapies are abundant. However, this wasn't always the case. As previously mentioned, Coley's Toxins are considered to be the first immunotherapies, granting William B. Coley the title of "Father of Immunotherapy." Coley's findings were foundational in establishing a link between the immune system and cancer, but they were also important in driving the realization that manipulation of the immune system could be therapeutic against tumors.

One of the most widely researched modalities for cancer immunotherapies is based on cytokines. In their purest form, cytokines are small secreted proteins that elicit downstream signaling on cells. Their signaling can affect cells nearby (paracrine) or far away (endocrine). Similarly, cytokines can also act on the same cells that secret them (autocrine) [26]. The word originates from the Greek works *cyto*, meaning cavity or cell, and *kine*, meaning movement [27]. While the first identified cytokine was interferon-a in 1957, it was merely seen as a protein that interfered with viral replication [28]. Shortly after, interferon-γ was identified in 1965 as the first lymphocyte-derived mediator [29]. However, it was not until 1972 that Stanely Cohen coined the term "cytokine," based on previous observations that non-lymphoid cells could produce migration inhibitory factor (MIF) as well as other previously described lymphokines [30]. Cohen argued that instead of being a function of the immune system, it was rather more likely a general aspect of host defense. This paradigm helped shape the way for the cytokines that were being discovered and characterized.

Interleukin-2 (IL-2) was first characterized by a group at Yale Medical School in 1972, coincidentally the same year the term "cytokine" was coined. IL-2 was first referred to as a "lymphocyte activating factor" derived from the serum of lymphocytes exposed to bacterial toxins [31]. Further work led to the purification and naming of IL-2 in 1982 [32]. The

purification of IL-2 was of extreme importance as it allowed for T cells to be cultured in vitro for extended periods of time and also allowed for the treatment of patients with the purified cytokine alone or in combination with purified lymphocytes expanded ex-vivo. This work, in particular, was championed by Steven Rosenburg at the National Cancer Institute (NCI) [33, 34]. Optimization of the dosage and treatment regimen eventually led to the FDA approval of high-dose IL-2 in patients with late-stage metastatic melanoma and renal cancer [26]. This would be one of the first FDA approvals granted to immunotherapies and would generate widespread interest in the therapeutic use of cytokines in cancer.

Other cytokines of key importance were also being characterized in the meantime. Specifically, interferon-a, IL-15, and GM-CSF. Interferon-a was first observed to function as an inhibitor of viral replication, but subsequent studies also showed its ability to upregulate MHC I (facilitating antigen presentation, discussed later) and driving dendritic cell maturation and T and B cell activation. This work led to its FDA approval for treating hematological cancers as well as late-stage melanomas [35]. IL-15 functions similarly to IL-2, except it also holds the ability to potentiate memory $CD8^+$ T cell phenotype [36]. On the other hand, GM-CSF proved to be important for the maturation and regulation of granulocytes and macrophages as well as a key regulator of multi-lineage hematopoietic progenitors [37]. While both IL-15 and GM-CSF have shown anti-cancer potential in preclinical models and have been widely investigated in clinical trials, neither has garnered FDA approval, and both remain active areas of research today.

While cytokines represent secreted modulators of immune homeostasis, activators and inhibitors of immune activation through cell-to-cell contact have been discovered, elucidated, and clinically developed over the past four decades. The best examples of these positive and negative regulators affect the function of T cells. As cells with cytotoxic and otherwise inflammatory potential, it is crucial for T cell responses to be tightly regulated. For example, in the presence of a pathogen or a cancer cell, T cells should be activated in order to gain

cytotoxic capabilities and eliminate the threat. However, once the immunological challenge has been cleared, it is imperative for T cell responses to be suppressed in order to avoid damage to healthy tissues. Moreover, uncontrolled or erroneous T cell activation can lead to pathologies aptly classified as autoimmune diseases. Thus, both the positive and negative regulation of T cells is essential for proper immune homeostasis.

In the early 1980s, T cell stimulatory receptors and their ligands were identified. The co-stimulatory ligand was first described as B lymphoblast antigen (BB-1) expressed on activated and malignant B cells, while the co-stimulatory receptor CD28 was first identified as a membrane glycoprotein capable of regulating human T cell proliferation [38, 39]. The role of BB-1, later renamed B7-1 and now known as CD80, remained unclear until further light was shed on its binding partner [40] Meanwhile, CD28 was characterized as a signaling receptor crucial for T cell activation, including cytokine production, as well as being able to bind to the B7/BB-1 molecule [41, 42, 43, 44]. Around this time in the late 1980s came one of the greatest discoveries in the field of immunology: the identification of CTLA-4 [45]. CTLA-4 was first identified from activated T cells and was further shown to be upregulated in models of induced cytotoxicity in T cells. Researchers quickly realized that B7/BB-1 and the related co-stimulatory molecule B7-2 (now known as CD86) bound to CTLA-4 as well as to CD28 [46, 47, 48]. These observations, along with shared homology and chromosomal location between CD28 and CTLA-4, led to different hypotheses regarding their roles [49]. It was not clear at the time, but the characterization of these molecules would eventually go on to change the world.

Despite confusion regarding the roles of CD28 and CTLA-4, clever work utilizing monoclonal antibodies (mAbs) in mouse cancer models would lead to the answer. In 1994, work led by the labs of Jeff Bluestone and Craig Thompson at the University of Chicago showed that CTLA-4 could, in fact, function as a negative regulator of T cell activation [50]. The next year, Jim Allison confirmed that CTLA-4 inhibited T cell activation and cytokine pro-

duction by using mAbs against CTLA-4 (anti-CTLA-4) [51]. Moreover, the development of CTLA-4 knock-out (KO) mice by Arlene Sharpe and Jeff Bluestone, as well as independent characterization by Tak Mak and Craig Thompson, cemented the role of CTLA-4 as a negative regulator of T cell activation [52, 50, 53]. Importantly, these studies also demonstrated that the absence of CTLA-4 in mice resulted in severe lymphoproliferative diseases evidenced by lymphocyte infiltration into organs, leading to fatal tissue destruction. Finally, in 1996, Jim Allison's group published their seminal work on improved anti-tumor immunity through CTLA-4 blockade [54]. This work showed tumor rejections, including in pre-established tumors and secondary challenges. Clinical investigations ultimately were undertaken in humans with the eventual FDA approval of anti-CTLA-4 in 2011 [55, 56, 57, 58]. However, CTLA-4 was not alone, as another key negative regulator was discovered and characterized quickly after.

Tasuko Honjo's group at Kyoto University was focused on identifying molecules associated with apoptosis (cell death). In doing so, they discovered the programmed cell death (PD-1) molecule as being expressed in the thymus and is upregulated upon cell death induction [59] Shortly after, Honjo's group generated a PD-1 KO mouse that elicited spontaneous autoimmune-like pathology, similar to those seen in the CTLA-4 KO mouse [60, 52]. At the same time, Lieping Chen's group at the Mayo Clinic identified a new member of the B7 family termed B7-H1 that seemed to drive a type of T cell activation [61]. It was then shown that this new protein B7-H1 was the ligand of PD-1 and led to negative regulation of T cell activation, leading to its renaming as PD-L1 [62]. Interestingly, researchers also found evidence that PD-L1 was expressed on tumor cells and contributed to immune recognition evasion [63]. Together, these observations led to the hypothesis that similar to anti-CTLA-4, the blockade of the PD-1/PD-L1 interaction could be therapeutic in cancer. This hypothesis proved correct as blockade of either PD-L1 or PD-1 improved anti-tumor immunity in murine cancer models [64, 65]. Clinical evaluation of anti-PD-1 and anti-PD-L1 quickly followed,

leading to their FDA approval in 2014 and 2015 [66, 67, 68, 69]. Due to the remarkable prolonged survival associated with these checkpoint blockade therapies, Jim Allison and Tasuko Honjo were awarded the Nobel Prize in Physiology or Medicine in 2018.

1.3 Cancer and immunity: a complex cycle

The first two sections of this chapter outlined the history of cancer and the development of immunology-based therapies for its treatment, but how do these tumors arise in the first place, and how is the immune system able to prevent and eliminate them? Cells frequently divide and respond to a variety of signals in their environment. Errors in replication and sustained damage from stressors can result in the elimination of these faulty cells to prevent giving rise to cancerous cells. These processes are mediated both intra- and inter-cellularly. For example, accumulation of DNA damage triggers a type of cell death known as apoptosis and errors in DNA that lead to mutations result in mutated peptides that flag cells as defective, targeting them for elimination by the immune system. Cancer is thus a multi-step process that involves the failure to eliminate mutated cells, allowing them to grow uncontrollably. As previously mentioned, the immune system is tasked with surveilling and eliminating these threats, and it is thought to do so efficiently, which is why there is an increased incidence of cancer when the immune system is suppressed [70, 25]. There are multiple mechanisms that allow the immune system to recognize cancerous cells, the mechanisms of which differ between the innate and adaptive immune system.

The innate immune system is comprised of cells that frequently sample their environment for threats. For example, natural killer (NK) cells and macrophages sample cells indiscriminately for "safe or destroy" signals. NK cells achieve this by recognizing class I MHC molecules that present self-antigens to other immune cells [71]. The absence of these MHC I complexes is indicative of mutations or a potentially dangerous cell, driving NK cells to eliminate those cells. Similarly, macrophages are phagocytic cells capable of eating other

cells. However, healthy cells prevent being eaten by macrophages by expressing "don't eat me" signals, marking them as safe [72]. The innate immune system is thus the first line of defense and functions in a non-specific manner. This allows the immune system to respond quickly to threats like pathogens and potentially cancerous cells.

Despite the effectiveness of the innate immune system, pathogens and cancerous cells have the potential to break through by evading recognition or simply overwhelming the innate immune system. This is where adaptive immunity enters in order to elicit a coordinated and specific attack against cellular perpetrators. In fact, innate immune responses induce adaptive immunity through cells specialized cells. These specialized cells primarily function as antigen-presenting cells (APCs). APCs are always sampling their environments, taking up proteins and cellular debris, and presenting on their surface to T cells that are capable of then seeking out cells expressing these antigens and mediating their destruction [73, 74]. These antigen-specific T cells also have the ability to generate special populations of memory T cells that will persist long-term and become quickly activated if they ever encounter a cell expressing that antigen again. Thus, the immune system can function both in a quick and non-specific manner as well as in a coordinated and adaptive manner that generates memory against a given potentially dangerous entity.

In the context of cancer, successful induction of adaptive immunity is crucial for the recognition and elimination of tumor cells. The ability of T cells to eliminate tumor cells is dependent on their ability to identify them in the first place. As mentioned, APCs are continually taking up material from their environment, either shed or secreted by cells or simply as a result of cellular material being released following cell death. While different cells can function as APCs, dendritic cells (DCs) are specialized in these functions and can elicit strong activation of T cells. Specifically, BATF3-lineage DCs signal to cytotoxic $CD8^+$ T cells by presenting antigens on MHC I, while IRF4- and IRF8-lineage DCs signal primarily to helper $CD4^+$ T cells. The DCs are commonly referred to as classical DC1s (cDC1s) and

DC2s (cDC2s). However, the complexity and diversity of DCs is an active area of research [75, 76, 77]. DCs thus play a critical role in the recognition of tumors and the subsequent education and activation of the adaptive immune system against them.

The sequence by which DCs acquire tumor-derived antigens and present them to T cells for the targeted elimination of tumors has been designated as the anti-tumor immunity cycle, highlighted in **Figure 1.1**. DCs must first be able to take up antigens in the tumor, where inflammatory signaling drives the maturation of DCs that travel to tumor-draining lymph nodes (tdLNs). Similarly, DCs can sense cell-free DNA from dying tumor cells, which also drives their activation. In all, a couple of key aspects in this step include 1) the presence of DCs in the tumor and their ability to penetrate the tumor, 2) the availability of antigens that can be presented in MHC molecules, and 3) the additional signals in the environment that at homeostasis drive tolerance and in inflammatory environments drive DC activation and migration into the tdLNs. Once matured/activated, tumor antigen-loaded DCs enter the tdLNs, and they can activate and drive the expansion of antigen-specific $CD8^+$ T cells. This creates a pool of activated, antigen-specific $CD8^+$ T cells that can then travel through the blood vessels, following chemokine gradients, to tumors to penetrate the tumor microenvironment (TME) and have the potential to execute their cytotoxic function. Importantly, there is growing evidence that DCs are critical within the TME for the maintenance and continued activation of $CD8^+$ T cells.

This cycle represents the main process through which the adaptive immune system is able to recognize and eliminate tumors that may arise after bypassing the innate immune system. The understanding of how tumors are able to persist despite these barriers depends on our understanding of the molecular mechanisms of each one of these steps. As a multi-step process, this means that immune evasion by tumors can arise at different points and through a variety of different mechanisms. Thus, therapies that aim to target the immune system for cancer therapies must be designed thoughtfully to maximize efficacy and reduce

toxicity. Moreover, the understanding of this process will also allow the development of future therapies capable of acting at multiple steps resulting in greater therapeutic benefit. Some of these approaches are highlighted in **Figure 1.2**. Of note, despite the presence of different immune cells at various points, DCs are present and crucial at all of the steps of the anti-tumor immunity cycle.

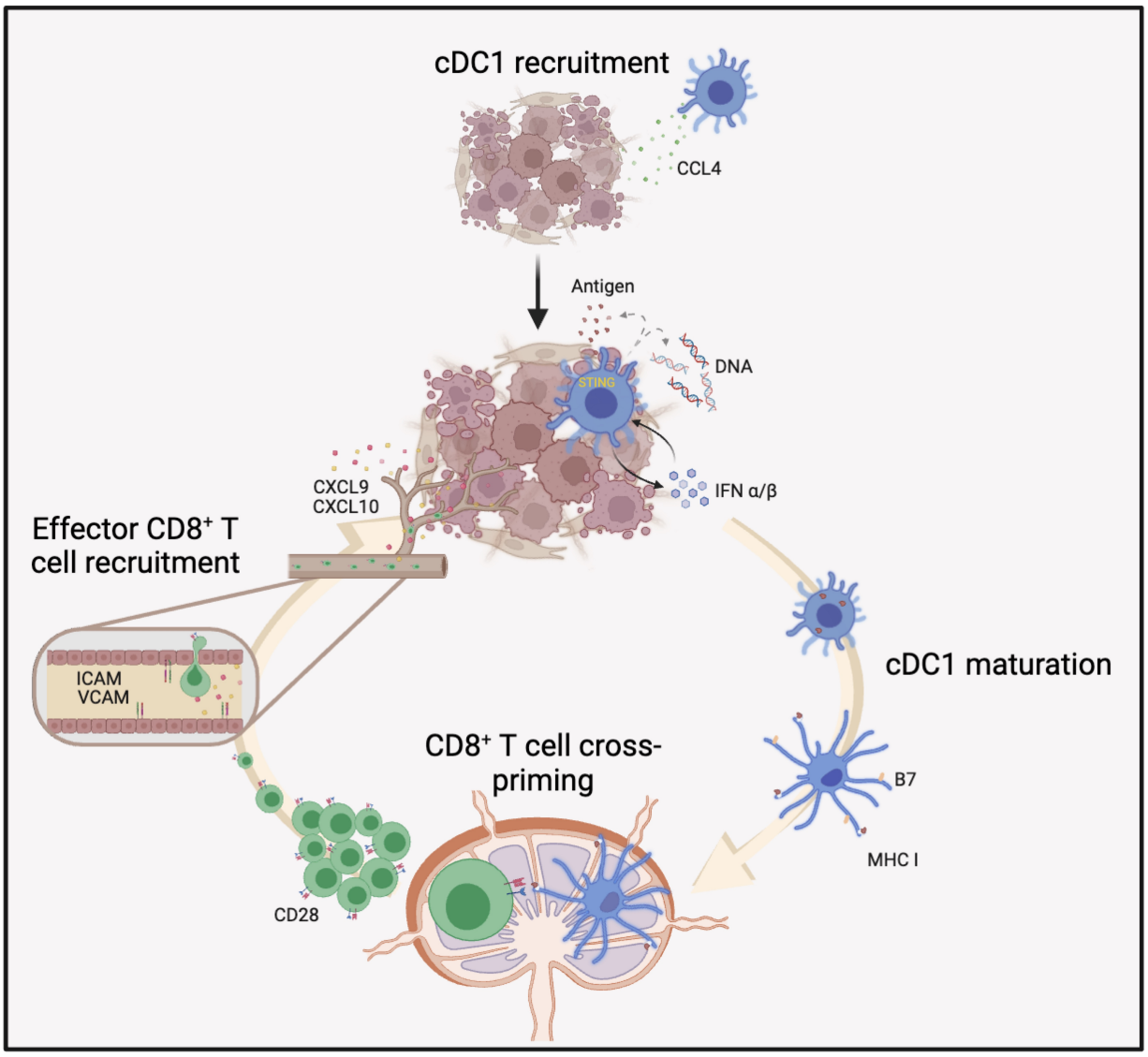

Figure 1.1: Endogenous anti-tumor immunity cycle. Schematic depicting the endogenous anti-tumor immunity cycle. Briefly, DCs (blue) are first shown entering tumors. DC recruitment to tumors is incompletely understood, but data suggest a role of NK cell-mediated recruitment. Once in the tumor, DCs can sense tumor-derived material in a variety of ways, including activation of the STING pathway by cell-free DNA and the overall acquisition of tumor-derived antigens in an inflammatory setting. Antigen-loaded DCs then mature and travel through the lymphatic system to the tumor-draining lymph nodes (tdLNs). The tdLN is the main site of cross-priming, where DCs activate and drive the expansion of antigen-specific $CD8^+$ T cells. Activated $CD8^+$ T cells then travel through the blood vessels down chemokine gradients in search of tumor cells expressing their antigen. These T cells, along with support from DCs, are then able to clear tumor cells at the site of the tumor.

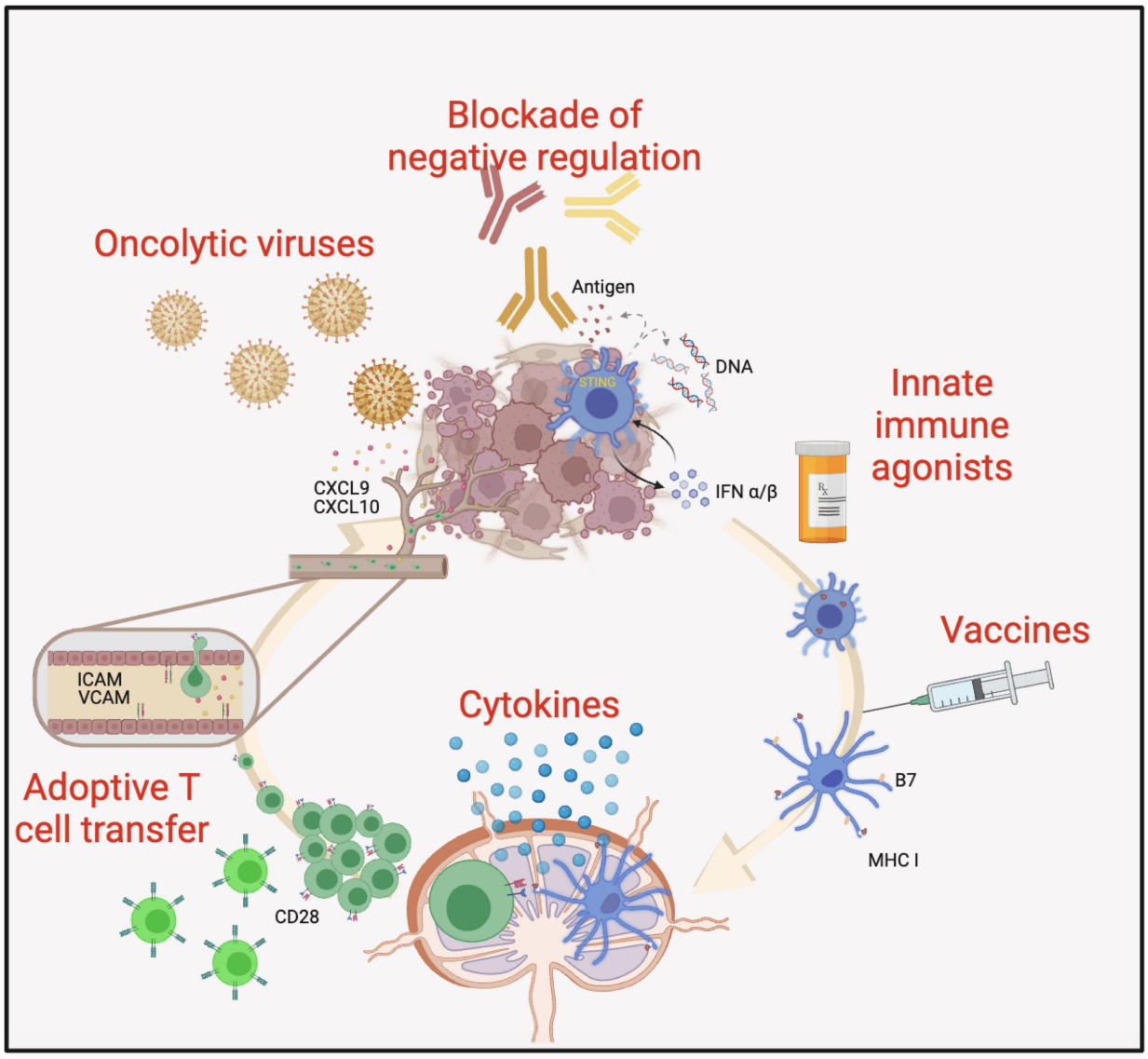

Figure 1.2: Routes of intervention by immunotherapies on the anti-tumor immunity cycle. Different modalities of cancer immunotherapies are shown along the anti-tumor immunity cycle, representing their likely primary sites of action. These highlight the ability to intervene and induce anti-tumor immunity through a variety of therapeutic modalities that act at different steps of this cycle.

1.4 Tumor immune evasion and determinants of immunotherapy response

The anti-tumor immunity cycle described above is representative of the necessary steps to mount an endogenous immune response against tumors. As previously mentioned, failure at any of these nodes can result in the disruption of the entire cycle and a lack of tumor control. However, no two tumors are created equal, and as such immune infiltration is variable amongst tumor types and even within patients bearing the same type of tumor. For example, early studies examining the immune infiltrate of tumors revealed that the presence of lymphocytes was a strong predictor of survival in patients with colorectal cancer [78]. Work from our lab in metastatic melanoma described the segregation of patient tumors by the presence or absence of T cells [79]. These differences have become even more evident through the use of immune checkpoint blockade (ICB) therapy; while some patients may experience complete responses, others either initially respond and become refractory or are refractory from the start.

Differences in ICB efficacy suggested baseline differences in the tumors of patients. Accordingly, examination of tumors from patients treated with ICB revealed that responders to therapy had higher levels of a gene enrichment score associated with the presence and activation of T cells [80]. Together, these observations have led to the broad classification of tumors as either "hot" or "cold." However, this terminology may be a misrepresentation as myeloid cells are one of the major cell types found across all tumors [81, 82]. Therefore, these tumors are more appropriately described as being either T cell-inflamed or non-T cell-inflamed. A schematic highlighting major differences between these two tumor types and their distinct mechanisms for immune evasion is shown in **Figure 1.3**. Understanding the tumor immune microenvironment is thus crucial to determining what patients will benefit most from ICB therapy and identifying potential mechanisms to therapeutically overcome immune exclusion in non-T cell-inflamed tumors.

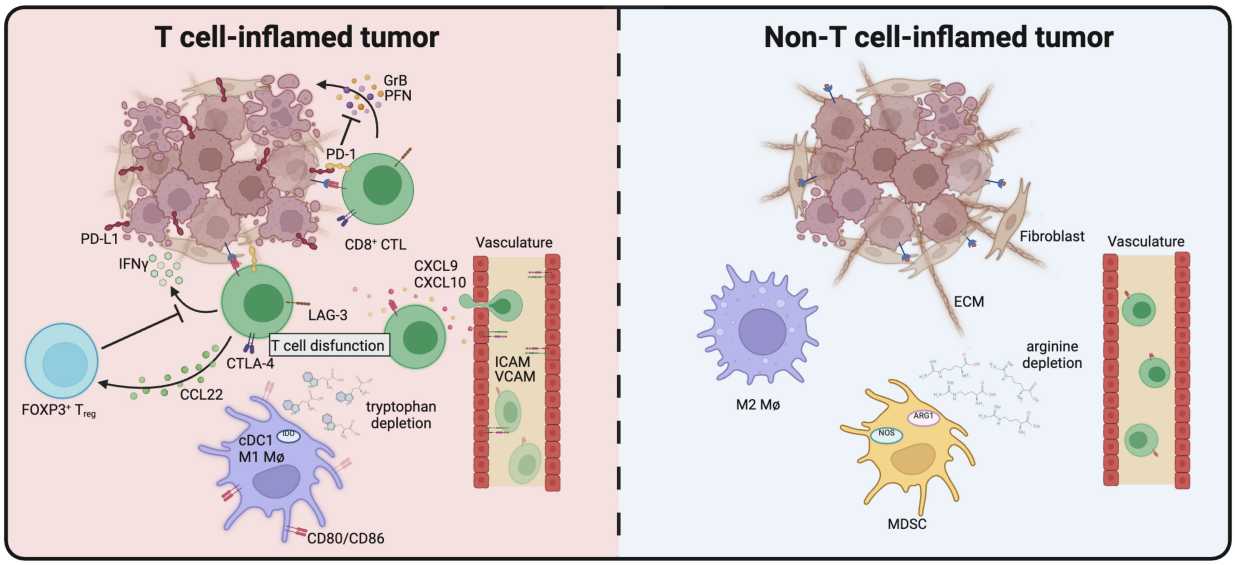

Figure 1.3: T cell and non-T cell-inflamed tumors. The schematic shows scenarios representative of T cell-inflamed tumors and non-T cell-inflamed tumors, colloquially referred to as "hot" and "cold" tumors, respectively. T cell-inflamed tumors are characterized by the presence of $CD8^+$ T cells and an overall type I IFN gene signature. These tumors represent an endogenous anti-tumor response, as described by the anti-tumor immunity cycle. In this case, immune evasion is possible through the engagement of checkpoint molecules. Non-T cell-inflamed tumors are conversely characterized by the overall lack of $CD8^+$ T cells and are rather enriched for suppressive myeloid cells. These tumors achieve immune evasion by the overall exclusion of T cells from tumors.

Understanding mechanisms that dictate T cell infiltration into tumors is imperative to extract maximum benefit from ICB therapies. However, other host-intrinsic pathways also dictate not just T cell responses but also broad immunity (**Figure 1.4**). As tumors arise by the selection of preferential mutations that allow for tumor growth and persistence, it is no surprise that the expression of certain oncogenes can also have an impact on the tumor immune infiltrate. Our group has characterized one such example where the expression of β-catenin in tumors results in the exclusion of DCs and T cells [83]. The gut microbiome is another component that can have drastic implications on immunity and response to ICB therapy. Work from our lab established a role for the gut microbiome as a mediator of ICB response in preclinical models and showed differences in the gut microbiome of patients that either responded or were refractory to ICB therapy [84, 85]. Further work has shown that

interventions targeting the gut microbiome are effective in improving ICB efficacy in some patients [86, 87, 88]. Lastly, there is growing evidence to suggest that host germline genetic differences could play a role in anti-tumor immunity [89, 90, 91, 92]. The present work aims to characterize further potential differences driven by host germline genetic differences in the context of anti-tumor immunity.

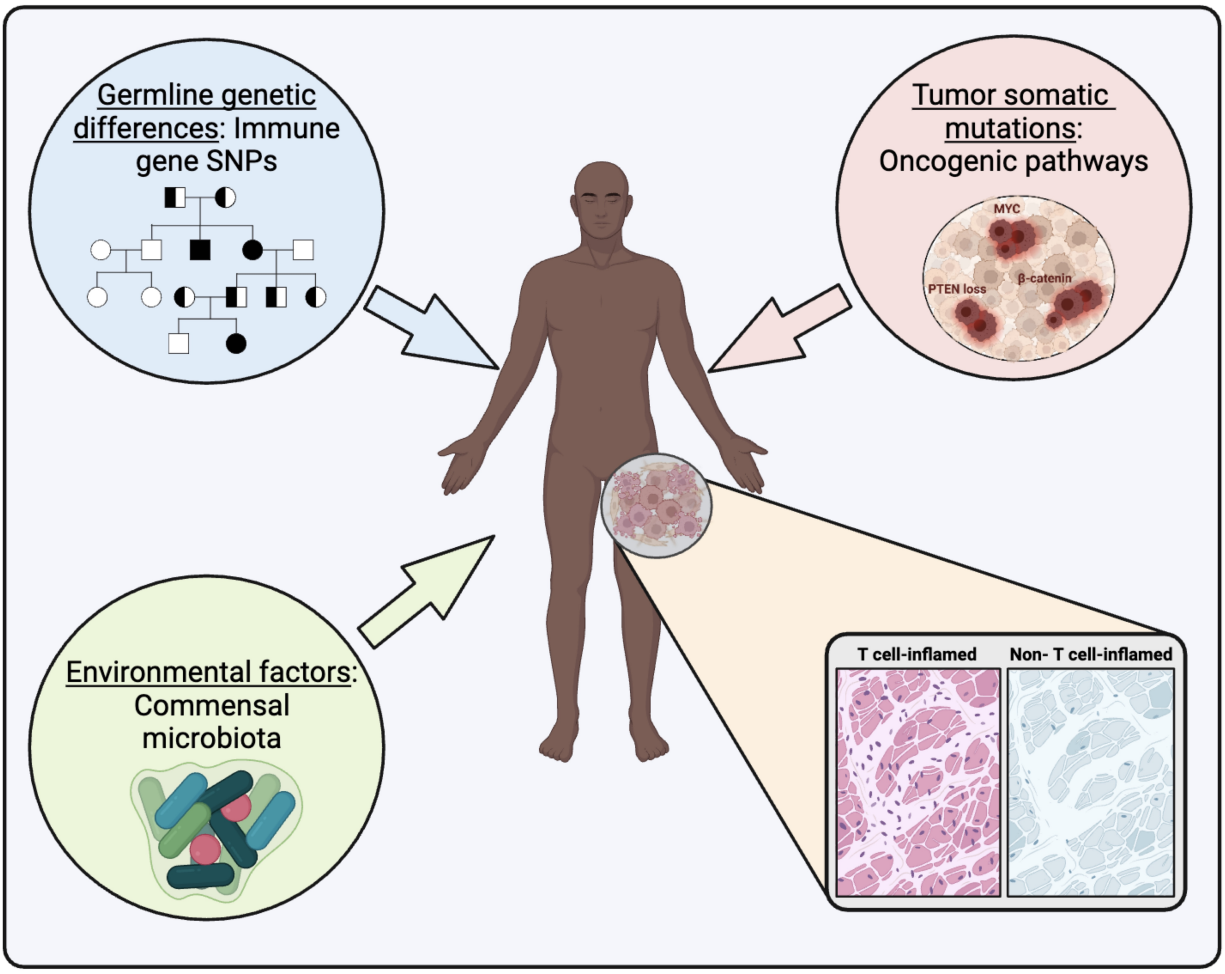

Figure 1.4: Immunotherapy efficacy can be affected by a variety of factors. Schematic showing four main mechanisms that dictate responses to cancer immunotherapy. On the upper left, germline single nucleotide polymorphisms are depicted, especially those affecting the expression of immune regulatory genes. The top right section highlights tumor somatic mutations, such as those leading to oncogenes. The bottom left panel focuses on environmental factors like the gut microbiome. Lastly, the bottom right section emphasizes the impact of T cell infiltration on immunotherapy efficacy.

1.5 Cancer immunotherapy and autoimmunity

The rise of cancer immunology has culminated in the understanding that one of the major reasons tumors arise is the lack of immune-mediated tumor clearance in immunocompetent patients. In other words, the immune system has been turned "off" in a case where it should be "on." Autoimmunity lies on the opposite end of this spectrum, where the immune system is promiscuously activated in the absence of an external immunological challenge. Thus, in autoimmunity, immune cells break self-tolerance and damage healthy tissue, while in cancer, a lack of immunity against cancerous cells allows tumors to persist [93]. This inverse relationship has drawn an increasing amount of attention in recent years, suggesting that the mechanisms of pathology in one disease could serve as therapeutic interventions in the other.

Another example of this is the observation that cancer immunotherapies can result in cytotoxicity termed immune-related associated effects (irAEs), given their resemblance to autoimmunity [94, 95]. One of the best examples of this phenomenon is the development of vitiligo in melanoma patients treated with immune checkpoint inhibitors (ICB) [96, 97]. Vitiligo is a type of autoimmune disease where T cells target and destroy melanocytes, characterized by light patches of skin as a result of a lack of melanin pigmentation. The rate of melanoma-associated vitiligo in patients treated with checkpoint blockade is estimated to be 15-25%, while the incidence in the general population is between 0.05-1.5% [98]. Importantly, across tumor types, irAEs onset is associated with increased survival in patients treated with ICB [99, 96, 97]. In this way, understanding the development and consequences of autoimmune-like sequelae in patients treated with ICB represents is imperative.

Interestingly, recent research has discovered that autoreactive T cells exist in the periphery and are kept dormant through PD-1/PD-L1 interactions [100]. These observations are in stark contrast to the dogma that autoreactive T cells are eliminated during thymic development but supported by a recent report that autoreactive T cells are, in fact, prema-

turely evicted from the thymus and develop into self-tolerant mature T cells in the periphery [101, 102]. These observations are further supported by the observations that loss of function polymorphisms in PD-1/PD-L1 and CTLA-4 are associated with increased incidence of a variety of autoimmune diseases [103, 104]. Similarly, SNPs identified from autoimmune GWAS screens have also been shown to be predictive of the development of irAEs and overall response to ICB therapy [105, 106, 107]. This presents a unique opportunity to mine autoimmune GWAS studies to identify loss of function mutations in immune regulatory genes as novel targets for cancer immunotherapy.

1.6 A SNP in PTPN22 increases risk for autoimmunity

The gene tyrosine-protein phosphatase nonreceptor type 22 (PTPN22), located on chromosome 1p 13.3–13.1, encodes the human protein the cytoplasmic lymphocyte-specific phosphatase (Lyp) made up of 21 exons. The mouse ortholog, located on chromosome 3, is termed PEST domain-enriched tyrosine phosphatase (PEP) and is comprised of 23 exons. The catalytic domains share nearly complete identity (90%) while the protein as a whole has 70% identity per NCBI BLAST [108, 109]. PEP and Lyp are referred to as PTPN22 collectively in the field and will be referred to as such in this dissertation. PTPN22 was first cloned in the early 1990s and identified for its exclusive expression on hematopoietic cells, its function as a tyrosine phosphatase, and its interaction with the TCR regulator Csk [110, 111]. These early identifications suggested its role as an immune regulatory molecule, especially in T cells.

In 2004 gene, gene-wide association (GWAS) studies first identified an SNP in PTPN22 associated with rheumatoid arthritis, type 1 diabetes, and systemic lupus erythematosus (SLE) [112, 113, 114]. Further analyses from other autoimmune-associated GWAS established the SNP rs2476601 as the single most important contributor to autoimmune diseases outside of the HLA locus [115]. This mutation creates a C1858T allele, resulting in an

R620W substitution. Interestingly, mice bearing the homolog R619W mutation and lymphocytes from autoimmune-burned individuals carrying the R620W mutation displayed 50% higher catalytic activity compared to wildtype but is ultimately degraded almost immediately, resulting in a loss-of-function phenotype [116, 117]. The generation of a global PTPN22 mouse revealed an age-associated expansion of immune cells and hyperresponsiveness of T cells ex vivo, confirming its role as a key regulator of immune homeostasis [118]. Interestingly, studies in PTPN22 KO mice have shown both increased incidence of autoimmunity in some cases and protection in others, reflective of similar context-dependent studies in patients [119, 120, 121, 122, 123]. These studies establish PTPN22 as a strong regulatory of immunity, making it attractive to study in immune-related diseases.

1.7 PTPN22 plays multiple roles in lymphocytes and myeloid cells

Mechanistically, PTPN22 has thus far been described to have several functional roles in different immune cell types. Primarily, PTPN22 has been shown to regulate de-phosphorylation of T- and B-cell receptor (TCR and BCR, respectively) signaling proteins and stabilization of TRAF3 in Toll-like receptor (TLR) signaling in myeloid cells. Through these mechanisms, PTPN22 might serve to inhibit TCR/BCR signaling yet may activate TLR signaling [115]. Studies in T cells have revealed that PTPN22 loss leads to 1) increased effector and memory $CD8^+$ T cell responses, 2) increased sensitivity to low-affinity antigens, and 3) dysregulated regulatory T cells (Tregs) activity [118, 124, 125, 126]. The regulation of T cell activity and identity by PTPN22 is further highlighted by the fact that PTPN22 mRNA expression increases with the expression of CD44 in T cells [127]. These studies also showed that PTPN22 KO $CD8^+$ T cells could out-compete WT T cells in $RAG^{-/-}$ hosts and were more resistant to wildtype Treg suppression. However, PTPN22 KO Tregs were also found to be more suppressive than wildtype Tregs and could control PTPN22 KO $CD8^+$ T cells accordingly.

PTPN22 has also been shown to play a role in regulating myeloid cell activity. Chiefly,

it has been shown to promote TLR signaling by driving TRAF3 autoubiquination and stabilization in antiviral responses [121]. However, those studies showed reduced activation of bone marrow-derived dendritic cells (BMDCs) in response to LPS stimulation, contradictory to other results [117]. Others have also shown that in BMDCs, PTPN22 is dispensable for antigen processing and subsequent T cell activation but rather has been implicated as a negative regulator in the presentation of immune complex-derived antigens [128, 129]. However, those experiments again utilized BMDCs and did not distinguish between DC subsets, potentially confounding results.

Further, it has also been proposed that PTPN22 functions as a negative regulator of cDC2 homeostasis and cDC2-driven CD4+ T cell-driven responses [130]. In this case, PTPN22 was found to directly and exclusively impact cDC2 proliferation, though the authors did not thoroughly characterize changes in DC-associated activation markers. Interestingly, earlier work looking at the effect of the autoimmune-associated variant found that BMDCs in this model were also more potent activators of $CD4^+$ T cells in the presence of antigens [117]. These data suggest an important yet incompletely characterized role of PTPN22 in DCs. Lastly, there is also limited evidence that PTPN22 suppresses M1 macrophage polarization and drives the expression of an M2-associated profile, further highlighting the importance of PTPN22 in the myeloid lineage [131]. However, this is the only report of PTPN22-mediated regulation of macrophage polarization, and further work is needed to confirm these findings.

An important caveat of the above-described experiments is that they were carried out using the global PTPN22 KO or global R619W knock-in (KI) mice. In such systems, altered activation of one cellular subset (e.g. T cells) could indirectly result in altered activation of another subset (e.g. DCs). This is an important consideration as $CD4^+$ T cells "license" DCs by stimulating and activating their co-stimulatory receptors. Improved or aberrant licensing in global PTPN22 deficient mice could result in changes in DC states and functionality that are ultimately not cell-intrinsic. Given the strong T cell phenotypes observed in these mice,

it is thus impossible to dissect cell intrinsic vs extrinsic mechanisms mediated by modulation of PTPN22. For this reason, a conditional KO mouse model is desirable to identify cell lineage-intrinsic roles of PTPN22 directly.

1.8 PTPN22 is a functionally relevant target for anti-tumor immunity

The expansion of effector $CD8^+$ in PTPN22 KO mice was first described in 2004, but it was not until 2017 that loss of PTPN22 in immune cells was first described as beneficial in the context of anti-tumor immunity [118, 132]. These initial experiments crossed PTPN22 KO mice with OT-I mice (where $CD8^+$ have transgenic TCRs specific for the OVA peptide). The intraperitoneal administration of PTPN22 KO OT-I T cells in mice bearing OVA-expressing ID8 tumors (established by intraperitoneal injection) showed that these T cells were superior in controlling tumors as compared to WT OT-I T cells. Specifically, these studies showed that PTPN22 KO OT-I T cells could overcome TGFβ suppression through increased expression of IL-2. Memory PTPN22 KO OT-I cells ($CD44^+$ $CD62L^+$) were also shown to control lymphoma tumors expressing OVA upon re-challenge [125]. However, more recent work has shown that general PTPN22 KO in T cell-based therapies does not confer any added protection. Specifically, PTPN22 KO CAR-T cells showed no difference to WT controls in mouse and humanized models. The lack of a substantial effect in PTPN22 KO for T cell-based therapies has been attributed to their increased rate of exhaustion and overall lack of persistence [133, 134]. These data suggest that PTPN22 might be regulating anti-tumor immunity through other cellular compartments.

Others have added to this body of work by testing endogenous tumor control in PTPN22 KO and R619W KI mice. PTPN22 KO mice generated on a BALB/cJ background did not show any differences in the control of colon cancer cell lines MC38 and CT26. However, PTPN22 KO mice responded better to anti-PD-L1 therapy in both models [135]. Moreover,

PTPN22 KO mice were able to reject Hepa1-6 tumor growth without treatment, allowing them to test for the dependency of different immune cells for their control. Depletion studies showed that the rejection of Hepa1-6 tumors in PTPN22 KO mice was dependent on $CD8^+$ and $CD4^+$ T cells and partially through IFNAR signaling. Interestingly, these experiments were accompanied by favorable changes in the T cell compartment, but no differences were observed in DCs or macrophages. Lastly, an analysis of patients treated with anti-PD-L1 revealed that patients homozygous for the pro-autoimmune risk variant R620W had increased survival in comparison to WT carriers.

Improved endogenous tumor control was confirmed in the original PTPN22 KO mice on a C57BL/6 background. Specifically, those experiments showed that PTPN22 KO mice on this background could more efficiently control MC38 tumors and were similarly more responsive to anti-PD-L1 treatment [136]. Unlike mice on the BALB/cJ background, when challenged with tumors, these PTPN22 KO mice showed differences in the myeloid compartment. Specifically, tumor control in this model was associated with the presence of M1-like tumor-associated macrophages in addition to $CD8^+$ T cells. They also described the development of a targeted PTPN22 inhibitor that, under frequent dosing, phenocopied PTPN22 KO animals. Interestingly, using immune cell type deconvolution through CIBERSORT, they showed that decreased expression of PTPN22 was correlated with an activated DC gene signature across multiple tumor types in TCGA data. While this model did not observe specific changes in DCs, recent studies utilizing the R619W KI mouse model did observe an increase in $CD103^+$ DCs in tumor-bearing mice [137]. This work confirms improved endogenous tumor control in PTPN22 KO and R619W KI animals and provides evidence for the involvement of DCs.

Together, these data highlight two main points: 1) global loss of PTPN22 function endows increased tumor control, and 2) immune-mediated tumor control in PTPN22 deficient mice cannot be solely explained by activity in T cells. The establishment of improved anti-tumor

immunity by loss of PTPN22 function is evidenced by data from a variety of independently and commonly used PTPN22 KO and PTPN22 R619W KI mice. Furthermore, careful work focused on the use of PTPN22 KO T cells confirms its role as a potent regulator of TCR signaling but also underscores the contribution of other immune compartments regulated by PTPN22 that are yet to be discovered. Further, data from non-tumor-bearing mice in this context also suggest changes in the myeloid compartment, with an emphasis on DCs. While the details of these effects are confounded by the global loss of PTPN22 in other immune cells involved in cross-activation and signaling, the notion of PTPN22 as a regulator of DC function is also supported by deconvolution of TCGA data showing a negative correlation between PTPN22 expression and DC activation status. The work outlined here thus aims to decipher the cell-intrinsic role of PTPN22 in myeloid cells with an emphasis on DCs through the use of a novel conditional PTPN22 knockout mouse model.

CHAPTER 2

MATERIALS AND METHODS

2.1 Mouse models

All of the animal experiments were performed with mice on the C57BL/6 genetic background. PTPN22$^{fl/fl}$ mice were exclusively for our laboratory by Cyagen. Briefly, loxP sites, along with self-deletion anchor sites, were inserted into the PTPN22 gene locus of mouse embryonic stem cells (ES), flanking exons 2 - 8. ES clones N-1H7 and N-2B5 were injected into C57BL/6 albino embryos, which were then re-implanted into immunocompromised CD-1 pseudo-pregnant females. Desired animals were identified by their coat color, and their germline transmission was confirmed by breeding with C57BL/6 females and subsequent genotyping of the offspring. The company delivered three male heterozygous targeted mice from clone N-1H7 and three male and one female heterozygous targeted mice from clone N-2B5. These mice were subsequently bred with C57BL/6 over several generations to ensure the proper genetic background for future breeding with other mouse models.

For conditional knockouts, PTPN22$^{fl/fl}$ mice were bred with CD11c-Cre mice to target dendritic cells and LysM-Cre mice to target macrophages. However, given the unintended targeting of neutrophils in the LysM-Cre model, a more specific model was sought out. The macrophage-specific CD64-Cre mouse model was a kind gift from Dr. Ming Li from the Memorial Sloan Kettering Cancer Center. CD11c-Cre and LysM-Cre mice were obtained from the Jackson Laboratory (Strain #: 008068 and 004781, respectively).

Mice breeding pairs always included a Cre^{+} (heterozygous) and a Cre^{-} (wild type) mouse, both on the PTPN22$^{fl/fl}$ background, to ensure mixed litters for experiments. Litter mates were utilized in experiments to reduce the impact of genetic drift and gut microbiome differences, as has been previously shown in the laboratory [84]. Mice aged 6 - 12 weeks were used in all of the experiments, ensuring age-matching between experimental groups. Both

male and female mice were used and indicated as necessary.

Target	Primer 1	Primer 2	Primer 3	Primer 4	WT Product	Mutant Product
PTPN22	TATGTGCACCCATGTGTATGAGTC	TTCACAAGAATTCCCAGAACCAATG	n/a	n/a	209	251
CD11c	ACTTGGCAGCTGTCTCCAAG	GCGAACATCTTCAGGTTCTG	GTCAGTCGAGTGCACAGTTT	CAAATGTTGCTTGTCTGGTG	200	313
LysM	CCCAGAAATGCCAGATTACG	CTTGGGCTGCCAGAATTTCTC	TTACAGTCGGCCAGGCTGAC	n/a	350	700
CD64	GCGATGGCGTGTATGAAGAA	AACATTCGACAACCCCCGC	CCGCCTTTGCAGGTGTATCTT	n/a	320	499

Table 2.1: Mice genotyping primer sequences.

2.2 CD11c$^+$ MACS enrichment

The CD11c MicroBeads from Miltenyi (130-125-835) were used to selectively enrich CD11c$^+$ DCs from mouse spleens primarily but also from processed tumors, as discussed later, per the manufacturer's protocol. Mice were euthanized via incubation in the CO_2 chamber for 5 minutes and underwent cervical dislocation as a secondary method. The spleens of euthanized mice were collected into 1mL of un-supplemented RPMI media on ice and chopped finely with scissors. Chopped spleens were then passed through a 70μM cell strainer (Corning, 352350) and washed with ice-cold PBS. The 20mL cell suspensions were then centrifuged at 400g for 5 minutes. Cell pellets were resuspended in 400μL of MACS Buffer (PBS with 2mM EDTA and 1% FBS) with 100μL of MACS CD11c MicroBeads and incubated at 4°C in the dark for 30 minutes. Cells were then washed with ice-cold MACS Buffer, centrifuged, and resuspended in 500μL of MACs Buffer thoroughly. LS columns (Miltenyi, 130-042-401) mounted on QuadroMacs magnets (Miltenyi, 130-091-051) and primed with 3mLs of MACS Buffer. After priming the columns, the 500μL cell suspension was then loaded and allowed to pass through. Columns were washed with 9mLs total of ice-cold MACS buffer in three rounds, and selected CD11c$^+$ cells were collected by plunging 5mLs of MACS buffer into a collection tube. These cells represented CD11c$^+$ DCs that can be used for downstream experiments and analysis.

2.3 RNA isolation for quantitative, real-time PCR

In order to verify the conditional KO (cKO) of PTPN22, $CD11c^{+}$ cells were isolated as described above, utilizing the CD11c MicroBeads for MACS purification. Following the manufacturer's protocol, RNA was isolated using a Qiagen RNeasy Plus Micro Kit (74034) and subsequently quantified on a NanoDrop One (Fisher Scientific, 13-400-525).

2.4 qRT-PCR for confirming genotype

cDNA was generated from isolated RNA using the High-Capacity cDNA Reverse Transcription Kit (Fisher, 4368814), resuspended to a final volume of 200μL and 5μL used for qRT-PCR reactions in a final volume of 25μL per reaction. The quantification of mRNA was conducted using the TaqMan gene expression master mix (Fisher, 4369514) on a StepOnePlus Real-Time PCR System (Applied Biosystems,4376600) in MicroAmp Fast Optical 96-Well reaction plates (Applied Biosystems, 434907). Each sample was run in triplicate wells and the CT of those wells was averaged before expression levels were calculated by the following formula: DCT = CT_{Gapdh} – CT_{Gene} of interest; expression level = 2^{DCT}. Forward and reverse mRNA-specific primers were used along with Roche's Universal Probe noted below.

Target	Primer 1	Primer 2	Probe
GAPDH	agcttgtcatcaacgggaag	tttgatgttagtggggtctcg	9
PTPN22	cattgtcatggcatgtatgga	ggatatagaaaaggggccaaa	2

Table 2.2: Primers for PTPN22 qPCR.

2.5 Tumor models and inoculation

Tumor models consisted of murine cancer cell lines syngeneic to the C57BL/6 background. Specifically, our lab has engineered the murine melanoma cell line B16F10 to express the model antigen SIY linked to a dsRed fluorophore, as well as the murine colorectal cancer

cell line MC38 to express the model antigen linked to a GFP fluorophore. These will be referred to as B16.SIY and MC38.SIY, respectively, moving forward. Using the respective fluorophores, these cell lines were routinely checked and sorted via fluorescence-activated cell sorting (FACS) to ensure uniform expression of the model antigen to achieve desired immunogenicity. More information is provided in the original publication [138].

Both cell lines were cultured in Dulbecco's Modified Eagle Medium (DMEM) high in glucose and pyruvate (ThermoFisher, 11995073) supplemented with 5% FBS and 1% MOPS buffer, MEM Non-Essential Amino Acids (ThermoFisher, 11140050), and Penicillin-Streptomycin (ThermoFisher, 15140122). Cells were grown in incubators at 37°C and 8% CO_2 and trypsinized with Trypsin-EDTA 0.25% (ThermoFisher, 25200072) for 2-3 minutes at 37°C for harvesting and passaging. Cells were never passaged more than twice prior to injection to prevent the accumulation of novel mutations. The parental B16F10 and MC38 cell lines were cultured in the same way as their derivatives.

For tumor inoculation, tumor cell lines were harvested and resuspended at a concentration of 10 - 20 million cells per mL in PBS, depending on the experiment. Cell suspensions were mixed thoroughly, with care to avoid bubbles, and loaded into 1mL 28G syringes (Fisher, 14-841-31). The fur of the mice was separated using small amounts of 70% EtOH to sterilize the area and create a clear window for injection into the lateral flanks of the mice. Each mouse was injected with 100μL of cell suspension, resulting in the injection of 1 - 2 million cells, depending on the experiment. B16.SIY cells were injected intradermally or subcutaneously and MC38.SIY and MC38 cells were exclusively injected subcutaneously. Tumor measurements began on day 10 post-inoculation and were measured using calipers three times a week until the end of the experiment. Tumor volume was calculated by the following formula: Width x Height x Length = Volume (cm^3).

2.6 Tumor and tissue processing for immune cell enrichment

Tumor-bearing mice were euthanized as previously described using CO_2 chambers and cervical dislocation. The desired organs were carefully removed and placed on PBS on ice. For B16.SIY tumors, care was taken so as not to compromise the integrity of the tumor (not an issue with MC38 type tumors). If tumors were injected intradermally, it was necessary to trim as much of the scabbing/ulceration and fur as possible. Tumors were then weighed prior to being put on PBS on ice. Extreme care was also taken to avoid the tumor-draining lymph nodes (tdLNs) when removing the tumors. Depending on the experiment, the spleen and tdLNs were also removed and placed on PBS on ice. Once the tissues/organs of all the mice had been collected, they were moved to new receptacles containing 1X digestion buffer prepared in un-supplemented RPMI media. For the digestion buffer, 10X aliquots were made up of 10mg Collagenase IV (Sigma, C5138-1G), 1mg Hyaluranidase V (Sigma, H6254-500MG), and 200U DNAse I Type IV (Sigma, D5025-150KU) Hyaluranidase and DNAse stock solutions were dissolved in HBSS with no calcium, magnesium or phenol red (ThermoFisher, 14175095).

Tumors in 1X digestion buffer were cut up thoroughly using scissors quickly vortexed, and returned back to ice until all samples were ready. Spleens and tdLNs in 1X digestion buffer were processed by using syringes to inject digestion buffer into the organs and to tear the tissues apart. Once all tissues had been processed in 1X digestion buffer, they were incubated at 37°C while shaking for 30 minutes. Following the incubation, all tissues were returned to ice, passed through a 70μM filter, and washed with ice-cold PBS up to 40mLs for tumors, 25mLs for spleens, and 10 mLs for tdLNs. Cell suspensions were then centrifuged at 400g for 5 minutes. At this point, tdLNs were ready for staining and were left at 4°C until needed. Spleens undergo RBC lysis by being placed in 1X RBC lysis (BD, 555899) buffer for 10 minutes per the manufacturer's protocol. Spleens were washed with ice-cold PBS, centrifuged, resuspended in ice-cold PBS, and left at 4°C until ready for further use.

Following centrifugation, tumor cell suspensions were resuspended in 20mLs of ice-cold PBS and vortexed thoroughly before slowly adding 6mLs of Ficoll-Paque (Fisher, 17144003) to the bottom of each sample and spun at 400g for 30 minutes without breaks. Tumor samples were handled carefully so as not to disturb phase separation, and the buffy coat containing immune cells was removed and washed with ice-cold PBS. At this point, all tissues were now in single-cell suspensions and ready for downstream experimentation.

2.7 Cellular staining and flow cytometry analysis of immune cells

Cellular staining is performed only on single-cell suspensions, such as those generated in the procedures mentioned above. Samples were resuspended 100-500μ and moved to either 96-well U-bottom plates (ThermoFisher, 163320) or cluster tubes (Corning, 4401). Samples were then centrifuged at 400g for 5 minutes and were now ready to be stained. In the case of SIY-pentamer staining, samples were first incubated with Fc Block (BioLegend, 101302) and SIY-pentamer (ProImmune, F1803-2B - 150 test R-PE) in Brilliant Stain Buffer Plus (BD, 566385) diluted 1:3 in PBS for 30 minutes in the dark. The master mix was then added on top of this solution and samples were incubated for an additional 30 minutes. Following incubation, samples were washed with PBS and centrifuged at 400g for 5 minutes. If no intracellular staining was needed, cells were resuspended in PBS and were ready for flow cytometry. Cells were fixed and permeabilized for intracellular staining with the FOXP3 Transcription Factor Staining Set (ThermoFisher, 00-5523-00). Cells were then stained with the intracellular master mix in the dark, overnight, and at 4°C. The next morning, cells are washed with Fix/Perm Buffer, centrifuged, and resuspended in 100μL for flow cytometry. FACS buffer was not used to avoid autofluorescence issues during flow cytometry. Single stain controls were prepared with UltraComp ebeads (ThermoFisher, 01-3333-42). The panel used for primary immune profiling of mice is listed below.

Flow cytometry was run on 5L Cytek Aurora machines. Experiments ran in 96-well,

Marker	Fluorophore	Clone	Dilution	Vendor	Cat. No.
PD1	BUV395	J43	1:200	BD	744549
CD86	BUV 496	PO3	1:200	BD	750437
CD69	BUV563	H12F3	1:200	BD	741234
Ly6G	BUV661	1A8	1:200	BD	741587
CD103	BV421	2E7	1:200	BioLegend	121422
I-A/I-E	Pacific Blue	M5/114.15.2	1:400	BioLegend	107620
CD19	BV510	6D5	1:200	BioLegend	115546
CD11b	BV570	M1/70	1:200	BioLegend	115546
CD206	BV605	C068C2	1:200	BioLegend	141721
CD317	BV650	927	1:200	BioLegend	127019
Ki67	BV711	B56	1:100	BD	563755
CD4	Spark NIR 685	GK1.5	1:200	BBioLegendD	100476
Ly6C	BV785	HK1.4	1:200	BioLegend	128041
CD44	FITC	IM7	1:200	BioLegend	103006
CD45	AF532	30-F11	1:400	Invitrogen	58-0451-82
F4/80	PerCP/Cy5.5	BM8	1:200	eBio	45-4801-80
CD8a	PerCP-ef710	53-6.7	1:200	eBio	46-0081-82
SIY	PE	n/a	1:25	ProImmune	F1803-2B
CD80	PE-Dazzle 594	16-10A1	1:200	BioLegend	104738
CD62L	PE-Cy7	MEL-14	1:200	eBio	25-0621-82
CD11c	AF647	N418	1:200	BioLegend	117312
Foxp3	APC	FJK-16s	1:75	eBio	17-5773-82
CD3	AF700	17A2	1:200	BioLegend	100216
NK1.1	APC-Cy7	PK136	1:200	BioLegend	108724
Tumor	dsRed/GFP	n/a	1:200	n/a	n/a
LD	Zombie NIR	n/a	1:400	BioLegend	423106
Fc Block	N/A	93	1:200	BioLegend	101302

Table 2.3: Flow cytometry panel for general immune profiling.

flat bottom plates or cluster tubes. The machine was calibrated daily for QC, and stock parameters and voltages were used. Forward scatter (FSC) was set to 40, and side scatter (SSC) was set to 10 for every experiment. Reference controls comprised of single stain samples were run first, followed by experimental samples. Samples were Unmixed without autofluorescence extraction and checked for compensation issues with NxN plots and manual adjustment based on controls as needed. FCS files were exported and analyzed through the FlowJo software Version 10.9.0. Exported data was cleaned using either RStudio Version

2022.07.0 and R 4.2.1 (2022-06-23) or in Microsoft Excel. Data was visualized and analyzed in GraphPad Prism 10, described elsewhere.

2.8 Gating strategies for flow cytometry

As previously mentioned, all flow cytometry experiments were run on 5L Cytek Aurora machines, and data was unmixed and prepared for analysis on SpectroFlo software. Gating was performed in FlowJo FlowJo v10.9.0. General population gates were determined by conventional immunology knowledge and validated gating strategies. The gating of activation markers was all based on the lack of expression on fluorescence minus one (FMO) controls. Each cell population had its own FMO, resulting in potentially different gating for the same activation marker on different cell types. This is important as different cell types have varying levels of autofluorescence as a result of cell shape and size, also causing variance in how each cell type is stained by the master mix applied to all cells. For experiments assaying for tumor-derived material represented by dsRed, B16F10 tumors lacking expression of SIY and dsRed were used as FMOs. Below are the gating strategies used for different experiments as specified accordingly. In all cases, PTPN22$^{fl/fl}$ x Cre^{+} mice (PTPN22 cKO) are shown in red, while PTPN22$^{fl/fl}$ x Cre^{-} mice (WT) are shown in black.

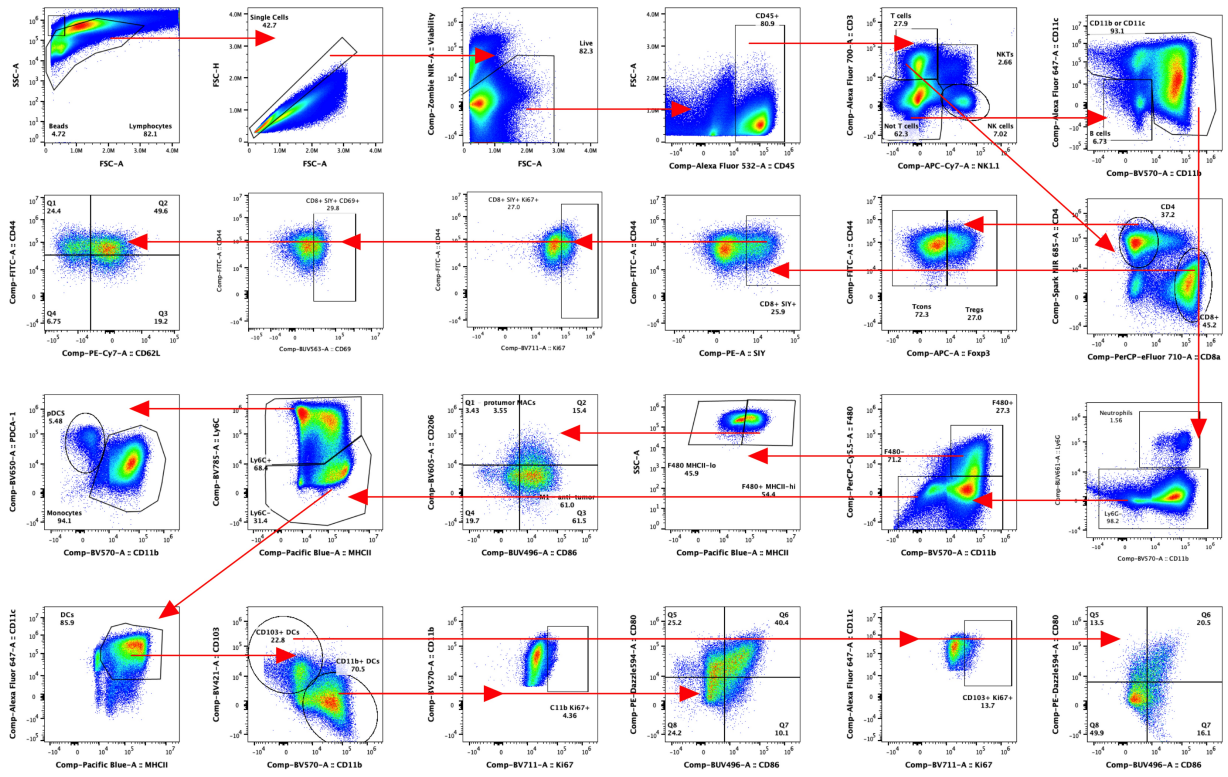

Figure 2.1: General gating strategy for B16.SIY tumors at endpoint for immune profiling. Tumors from PTPN22$^{fl/fl}$ x Cre^{+} and Cre^{-} and mice were collected at endpoint, and immune cells were isolated. Single-cell suspensions were stained and analyzed by flow cytometry.

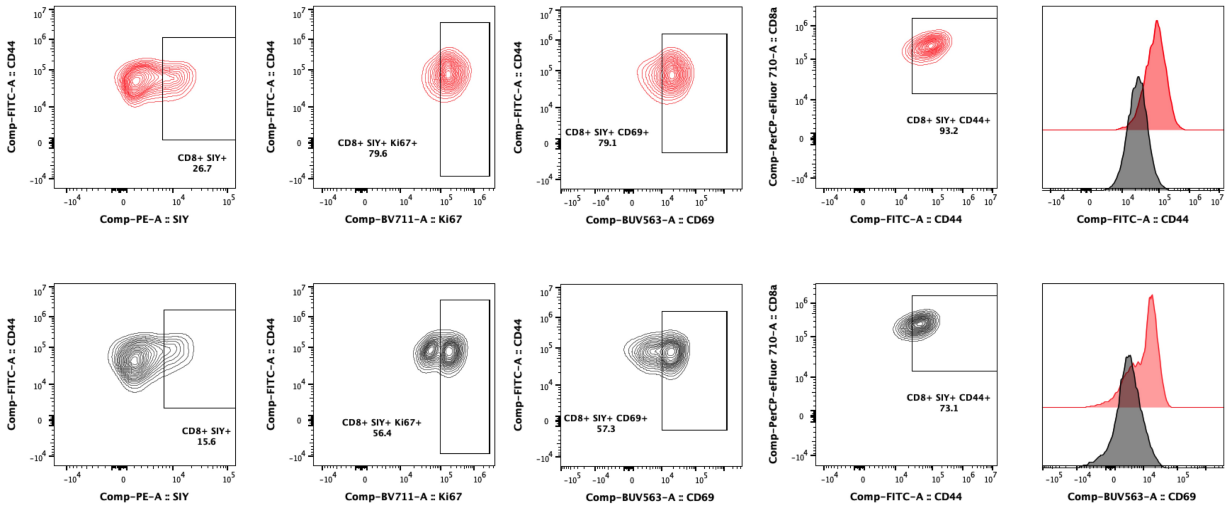

Figure 2.2: CD8$^+$ SIY$^+$ activation in B16.SIY endpoint tumors. Tumors from PTPN22$^{fl/fl}$ x Cre$^+$ and Cre$^-$ and mice were collected at endpoint, and immune cells were isolated. CD8$^+$ SIY$^+$ T cells are determined by SIY pentamer staining. Single-cell suspensions were stained and analyzed by flow cytometry. PTPN22 cKO mice are represented in red, and WT mice are represented in black.

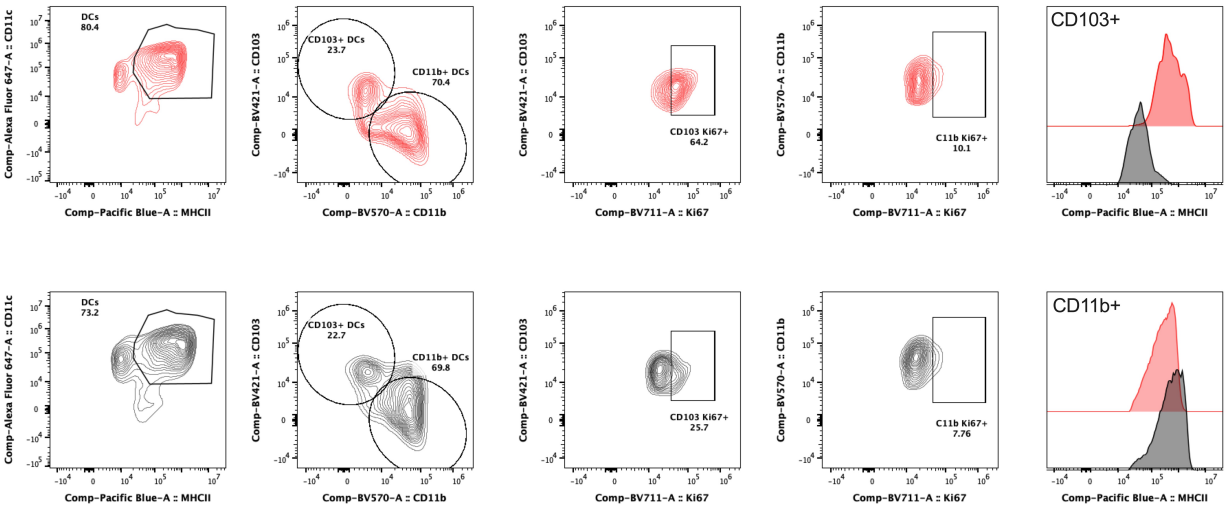

Figure 2.3: DCs activation in B16.SIY endpoint tumors. Tumors from PTPN22$^{fl/fl}$ x Cre$^+$ and Cre$^-$ and mice were collected at endpoint, and immune cells were isolated. Single-cell suspensions were stained and analyzed by flow cytometry. PTPN22 cKO mice are represented in red and WT mice are represented in black.

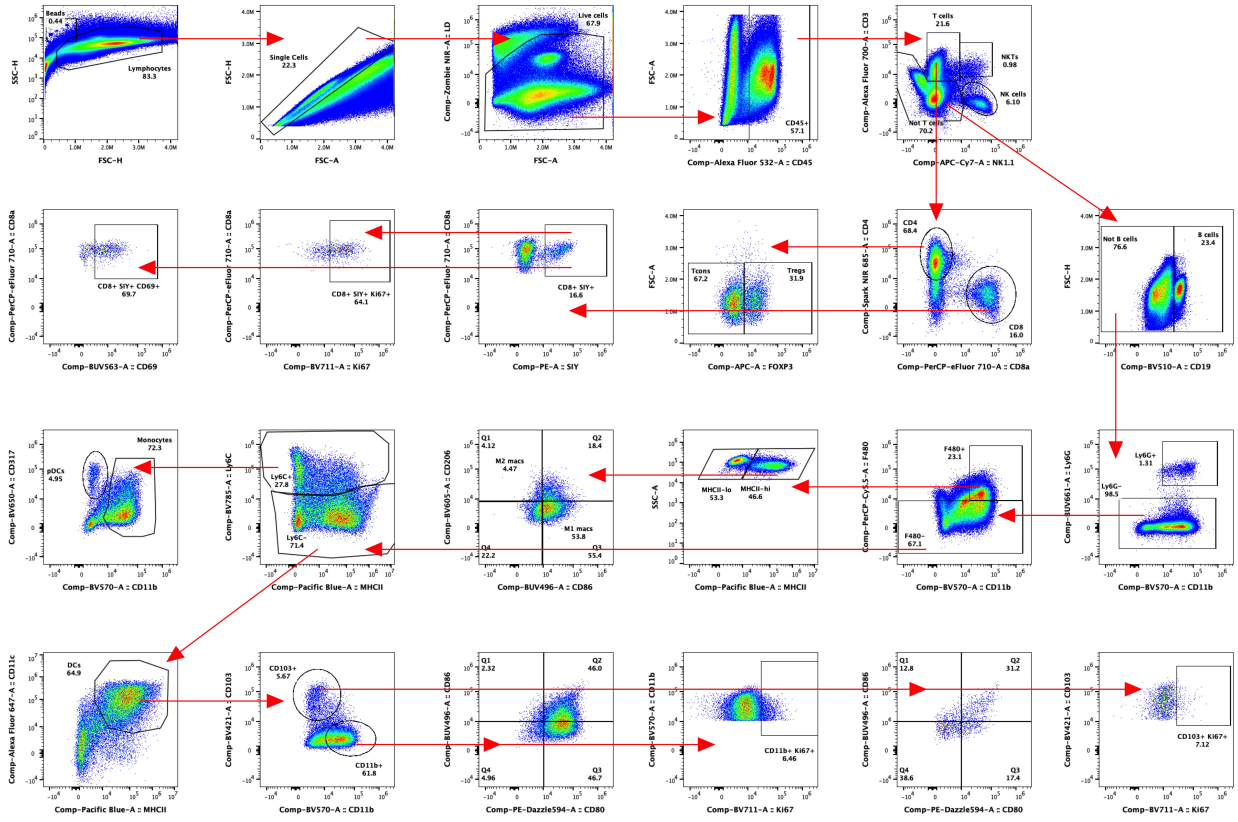

Figure 2.4: General gating strategy for MC38.SIY tumors at endpoint for immune profiling. Tumors from PTPN22$^{fl/fl}$ x Cre^{+} and Cre^{-} and mice were collected at endpoint, and immune cells were isolated. Single-cell suspensions were stained and analyzed by flow cytometry.

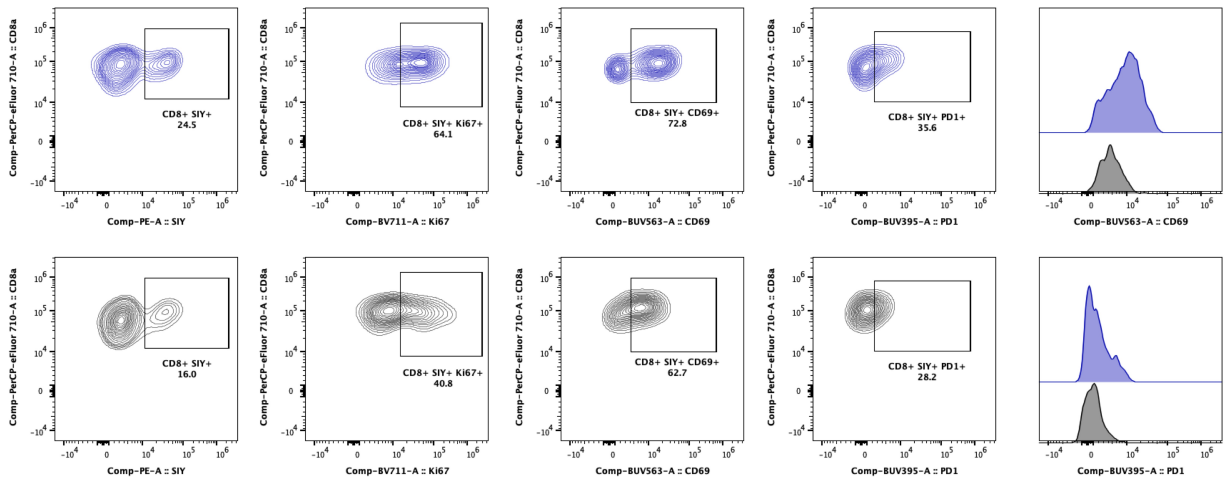

Figure 2.5: CD8$^+$ SIY$^+$ activation in MC38.SIY endpoint tumors. Tumors from PTPN22$^{fl/fl}$ x Cre$^+$ and Cre$^-$ and mice were collected at endpoint, and immune cells were isolated. CD8$^+$ SIY$^+$ T cells are determined by SIY pentamer staining. Single-cell suspensions were stained and analyzed by flow cytometry. PTPN22 cKO mice are represented in red and WT mice are represented in black.

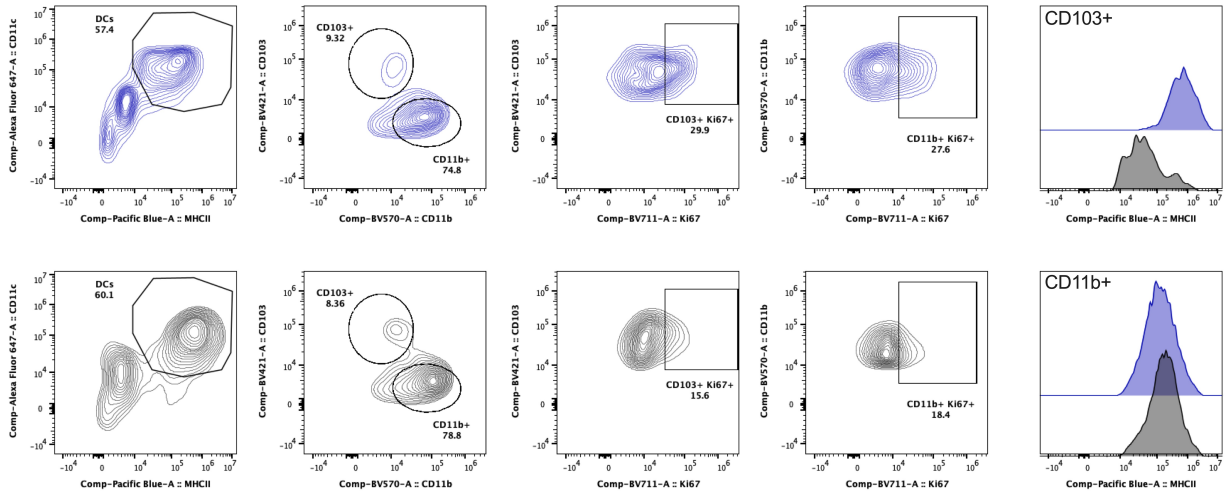

Figure 2.6: DCs activation in MC38.SIY endpoint tumors. Tumors from PTPN22$^{fl/fl}$ x Cre$^+$ and Cre$^-$ and mice were collected at endpoint, and immune cells were isolated. Single-cell suspensions were stained and analyzed by flow cytometry. PTPN22 cKO mice are represented in red and WT mice are represented in black.

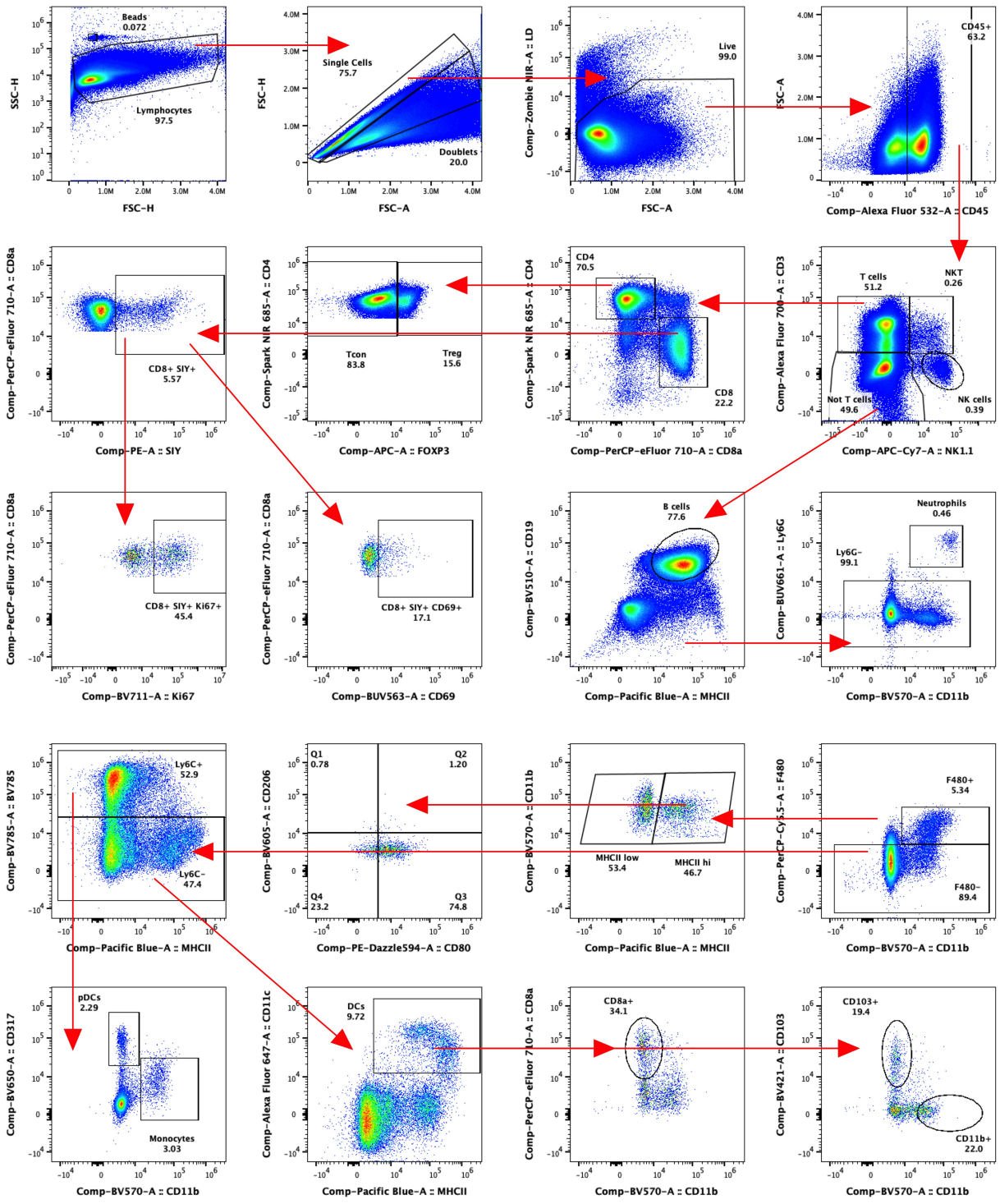

Figure 2.7: General gating strategy for tdLNS of day 7 B16.SIY tumor-bearing mice for immune profiling. Tumor draining lymph nodes (tdLNs) from PTPN22$^{fl/fl}$ x Cre^{+} and Cre^{-} and mice were collected on day 7, and immune cells were isolated. Single-cell suspensions were stained and analyzed by flow cytometry.

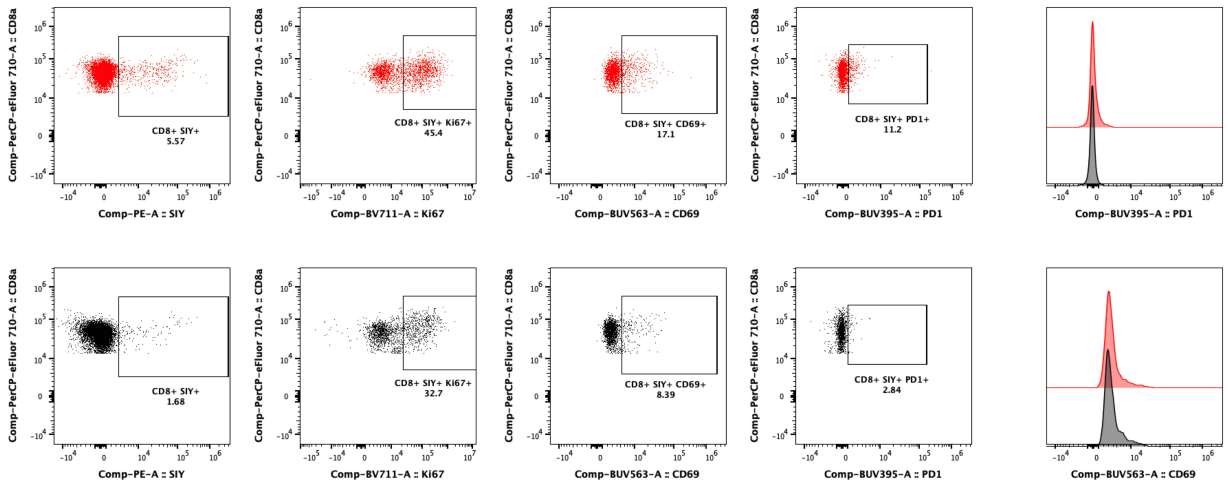

Figure 2.8: CD8$^+$ SIY$^+$ activation in tdLNs of day 7 B16.SIY tumor-bearing mcie. Tumor draining lymph nodes (tdLNs) from PTPN22$^{fl/fl}$ x Cre$^+$ and Cre$^-$ and mice were collected on day 7, and immune cells were isolated. CD8$^+$ SIY$^+$ T cells are determined by SIY pentamer staining. Single-cell suspensions were stained and analyzed by flow cytometry. PTPN22 cKO mice are represented in red and WT mice are represented in black.

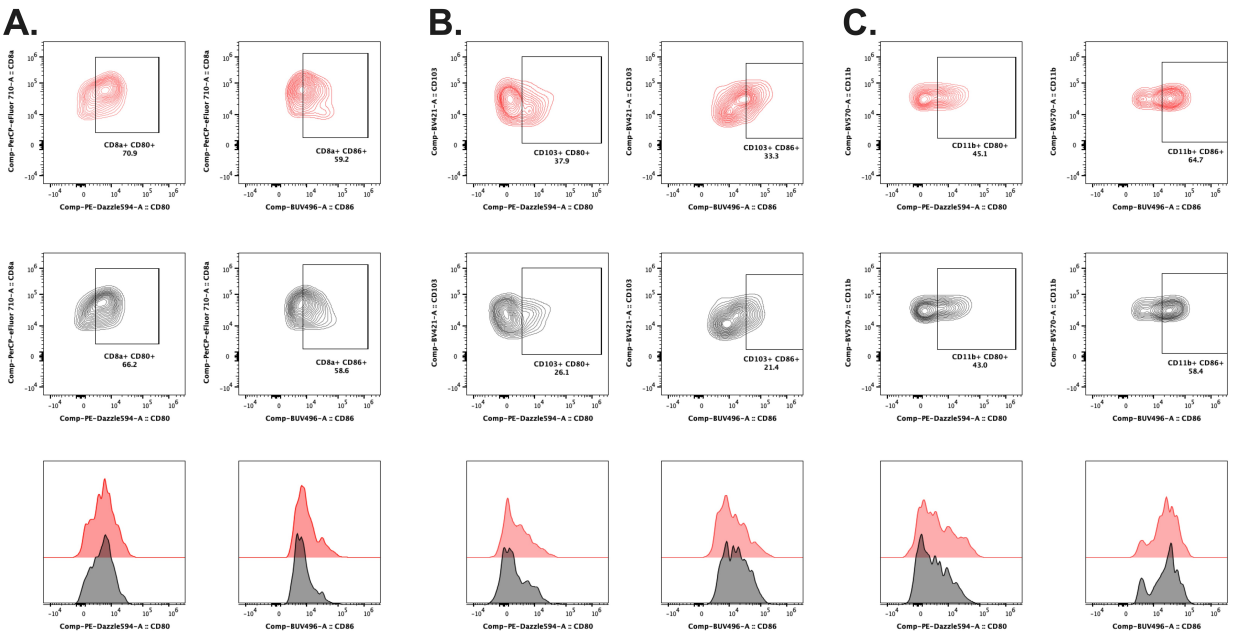

Figure 2.9: DCs activation in tdLNS of day 7 B16.SIY tumor-bearing mice for immune profiling. Tumor draining lymph nodes (tdLNs) from PTPN22$^{fl/fl}$ x Cre$^+$ and Cre$^-$ and mice were collected on day 7 and immune cells were isolated. Dcs were subtypes into **(A)** CD8α^+ **(B)** CD103$^+$ and **(C)** CD11b$^+$ DCs. Single-cell suspensions were stained and analyzed by flow cytometry. PTPN22 cKO mice are represented in red and WT mice are represented in black.

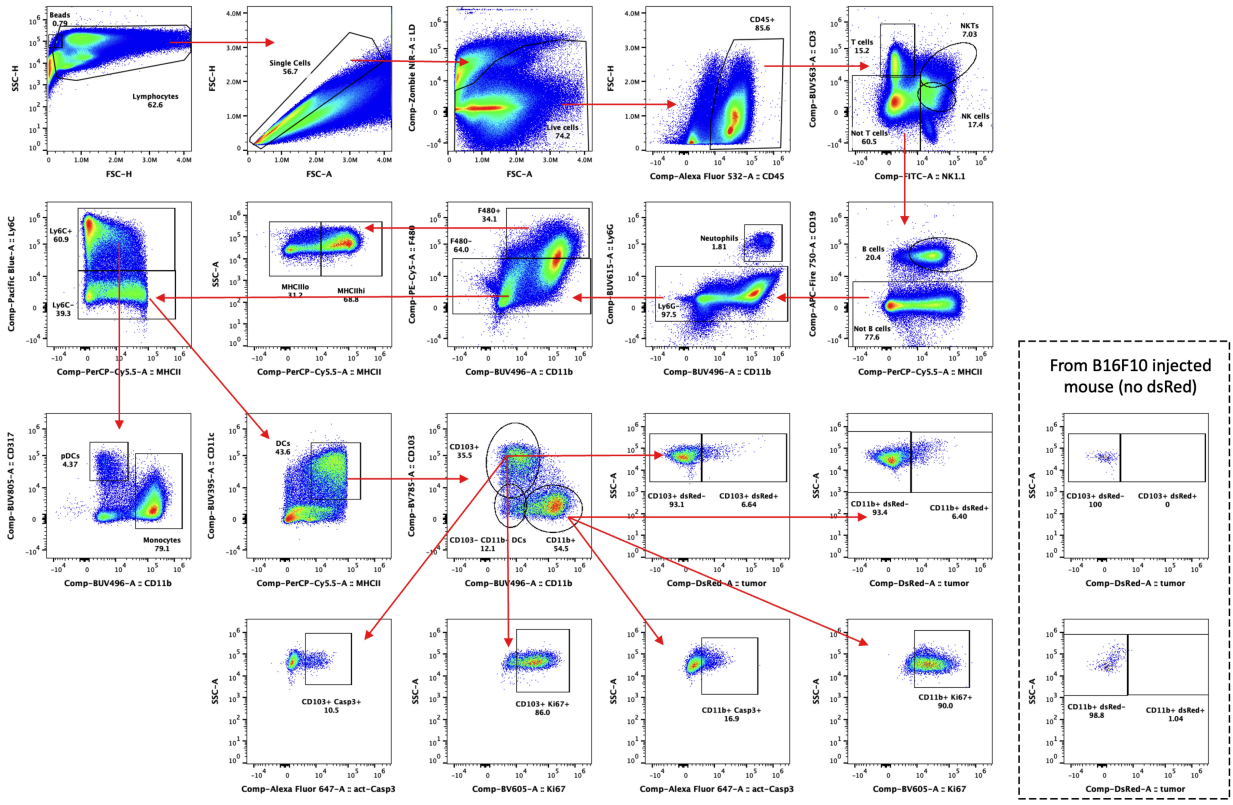

Figure 2.10: General gating strategy for B16.SIY tumors on day 20. Tumors from PTPN22$^{fl/fl}$ x Cre^{+} and Cre^{-} and mice were collected on day 20, and immune cells were isolated. Single-cell suspensions were stained and analyzed by flow cytometry.

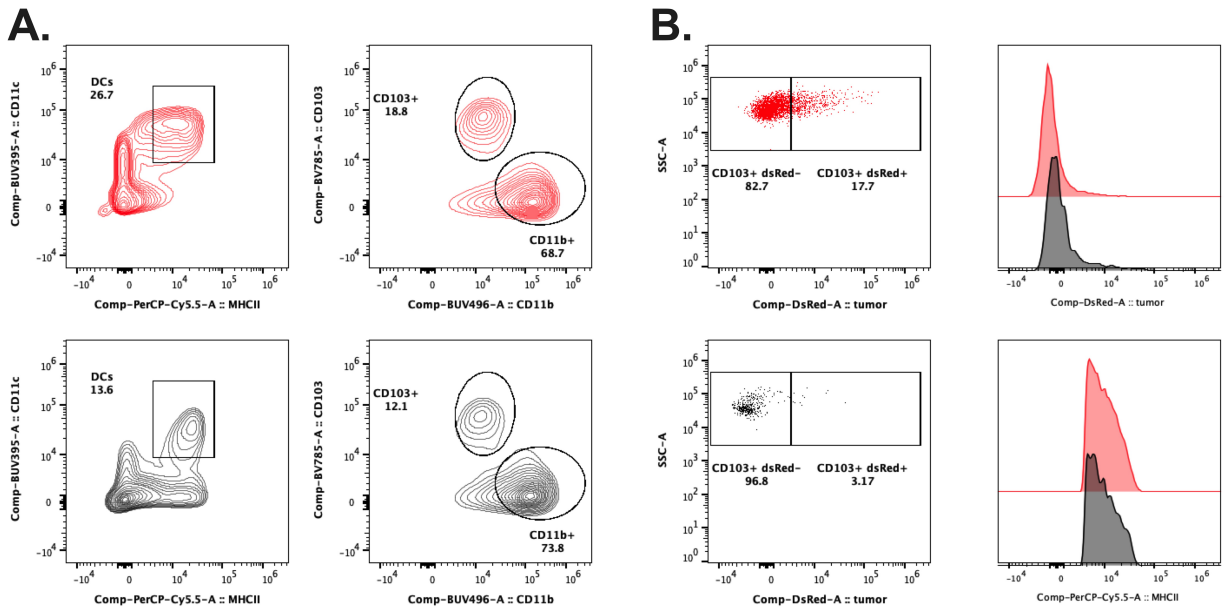

Figure 2.11: Indentification of dsRed$^+$ DCs from day 20 B16.SIY tumors. Tumors from PTPN22$^{fl/fl}$ x Cre$^+$ and Cre$^-$ and mice were collected on day 20, and immune cells were isolated. B16F10 tumors lacking SIY and dsRed were used as controls to identify cells positive for dsRed acquisition. Gating for **(A)** DCs and their subtypes are shown as well as gating for **(B)** dsRed in C103$^+$ and CD11b$^+$ DCs along with the MFI. PTPN22 cKO mice are represented in red and WT mice are represented in black.

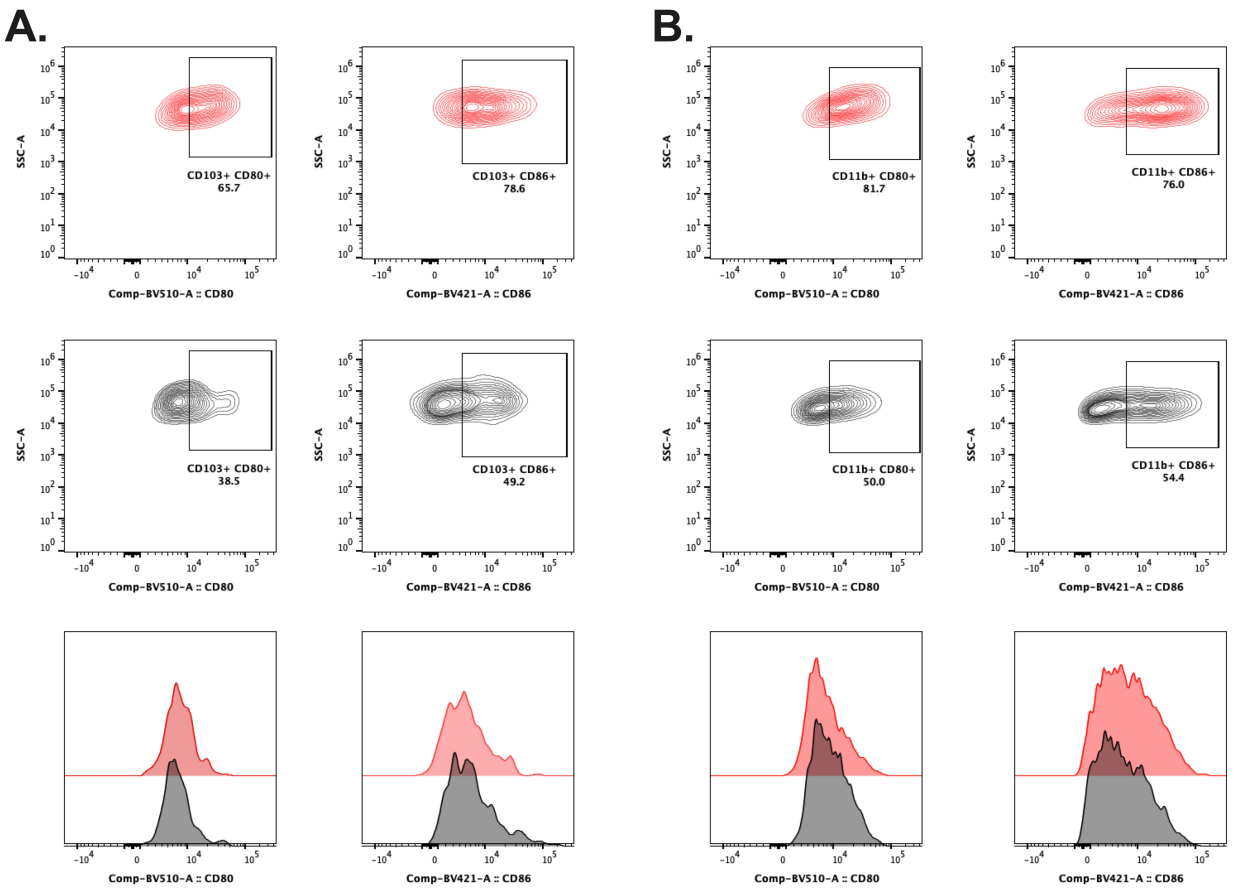

Figure 2.12: Activation profile of dsRed^{+} DCs from day 20 B16.SIY tumors. Tumors from PTPN22$^{fl/fl}$ x Cre^{+} and Cre^{-} and mice were collected on day 20, and immune cells were isolated. B16F10 tumors lacking SIY and dsRed were used as controls to identify cells positive for dsRed acquisition. CD80 and CD86, along with their MFIs, are shown for **(A)** CD103^{+} and **(B)** CD11b^{+} DCs. PTPN22 cKO mice are represented in red and WT mice are represented in black.

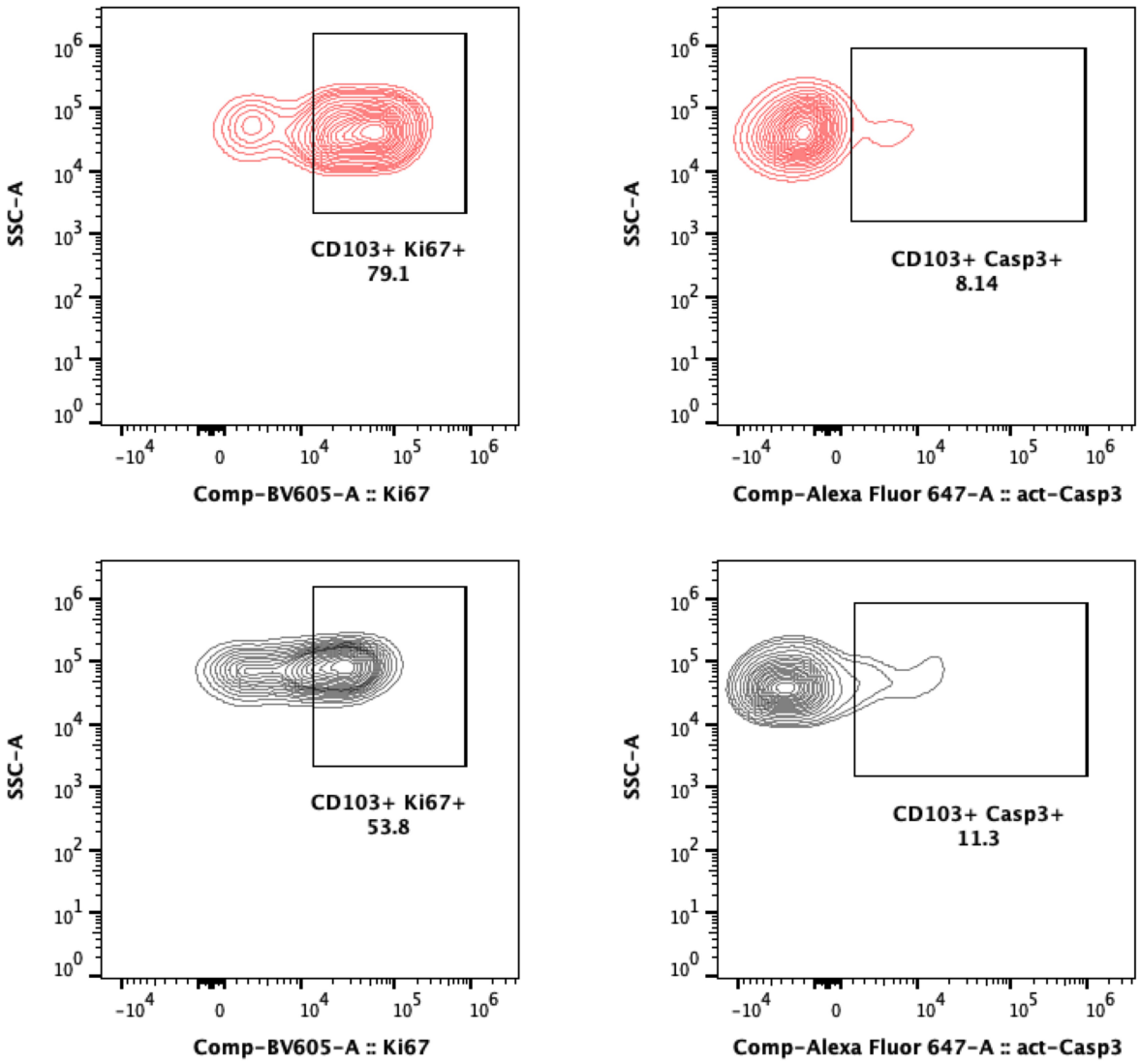

Figure 2.13: Proliferation and apoptosis of dsRed^{+} DCs from day 20 B16.SIY tumors. Tumors from PTPN22$^{fl/fl}$ x Cre^{+} and Cre^{-} and mice were collected on day 20, and immune cells were isolated. B16F10 tumors lacking SIY and dsRed were used as controls to identify cells positive for dsRed acquisition. Single-cell suspensions were stained and analyzed by flow cytometry. PTPN22 cKO mice are represented in red and WT mice are represented in black.

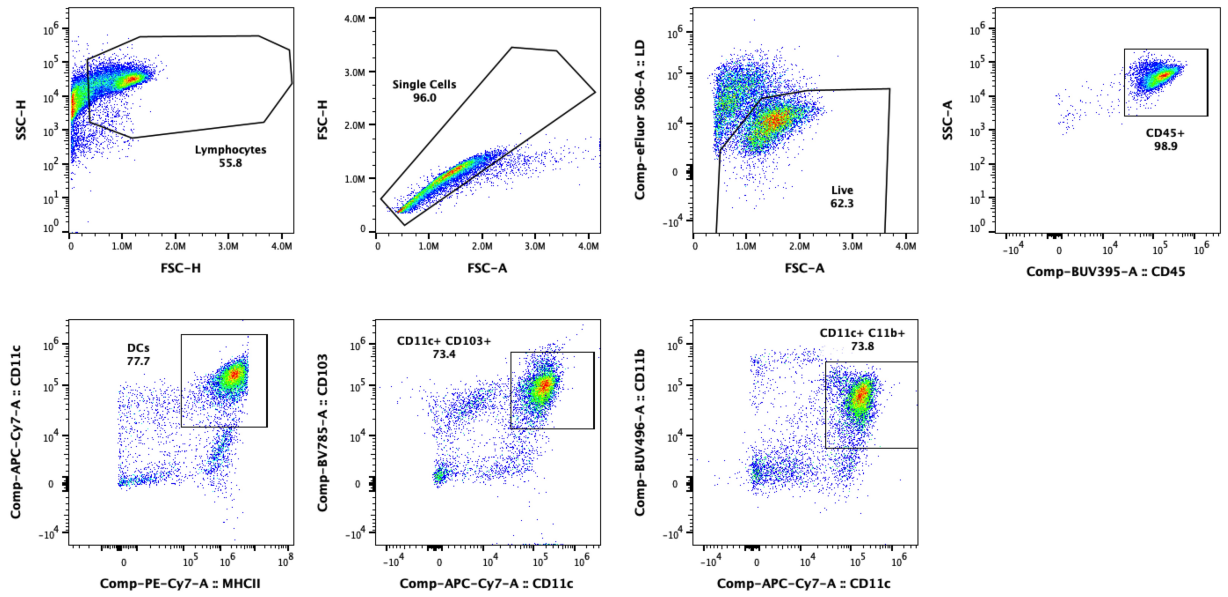

Figure 2.14: General gating strategy for CD11c$^+$ cells enriched from spleens cultured in vitro with OVA substrates. CD11c$^+$ cells were enriched from spleens of naive PTPN22$^{fl/fl}$ x Cre$^+$ and Cre$^-$ mice and cultured in U-bottom well plates for 2-3 hours at 37°C with OVA substrates.

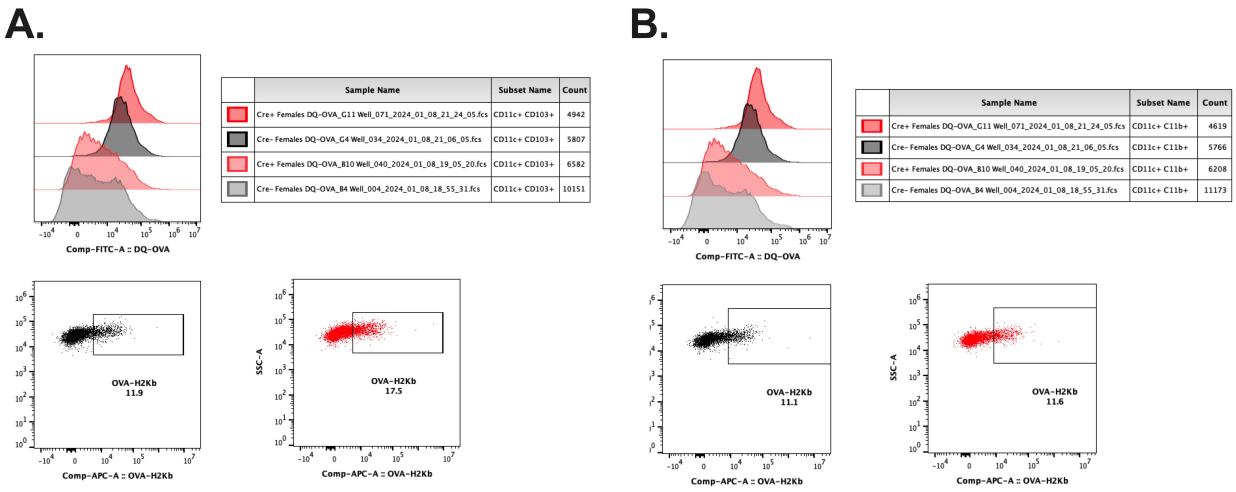

Figure 2.15: Antigen processing and presentation of CD11c$^+$ cells in vitro. CD11c$^+$ cells were enriched from spleens of naive PTPN22$^{fl/fl}$ x Cre$^+$ and Cre$^-$ mice and cultured in U-bottom well plates for 2-3 hours at 37°C with OVA substrates The MFIs of DQ-OVA are shown from untreated (light colored) and high dose (darker colored) along with the gating for OVA-H2Kb for **(A)** CD103$^+$ and **(B)** CD11b$^+$ DCs. PTPN22 cKO mice are represented in red and WT mice are represented in black.

2.9 IFN-γ Enzyme-Linked Immunospot (ELISPOT) assay

IFN-γ ELISPOT assays were used to probe the priming of tumor antigen-specific $CD8^+$ T cells from day 7 tumor-bearing mice. Mice were injected with 2 million B16.SIY cells in the flank subcutaneously, as previously described. On day 7, mice were euthanized, and both spleens and tdLNs were collected and processed as previously described. Single-cell suspensions of spleens were counted and prepared to be plated at 1 million cells per well in triplicate. The night before, ELISPOT 96 well-plate (Millipore, MAIPS4510) was coated with capture antibody (BD, 51-2525KZ) in a 1:200 dilution and incubated at 4°C. The plate was washed twice with supplemented DMEM media and blocked for at least 2 hours at room temperature with the same media. Supplemented DMEM media was made by adding 2-Mercaptoethanol l (Millipore, ES-007-E) to a final concentration of 50μM and 1X of a house-made nutrient supplement solution (yellow mix). This media will be referred to as complete DMEM media (cDMEM). After blocking, cells were seeded and stimulated with a serial dilution of SIY peptide (SIYRYYGL) up to 160nM. Positive controls were stimulated with 50ng/mL PMA (Fisher, 52-440-01MG) and 500ng/mL Ionomycin (Millipore, I0634-1MG), while negative controls were exposed to an irrelevant OVA peptide (SIINFEKL). Cells were incubated at 37°C overnight, taking care not to shake or move the plates throughout incubation to avoid spot smudges. At this time, the tdLNS were stained for flow cytometry.

The next day, the cell suspension media was removed (avoiding cells at the bottom of each well) and placed into a new well plate with the remainder of the cell suspension being aspirated, and plates were washed thoroughly with DI H_2O twice (including between the membrane and the plate), followed by washing with Well Buffer (PBS with 0.05% Tween 20) twice more. The conditioned media from the plate was sealed and kept at 4°C for short-term storage for later use. For IFN-γ spot detection, the plate was incubated with a 1:2,000 dilution of a biotinylated detection antibody (BD, 51-1818KA) diluted in PBS with 10% FBS for 1-2 hours at room temperature. The plate was then washed with Well Buffer and

dabbed dry onto a paper towel before incubating with streptavidin-HRP at 1:100 in PBS with 10% FBS for 1 hour at room temperature. The plate was washed 4x with Well Buffer and soaked for 1-2 minutes per wash and with PBS x2 soaking for 5 minutes per wash before being developed with AEC substrate (BD, 551951) at a concentration of 1 drop per mL for 6-7 minutes, or until dots became visible without overexposing (evident by halo-ing around individual spots). The membrane was separated from the plate and let dry for 1-2 days. The membranes were imaged utilizing an Immunospot Series 3 Analyzer and ImmunoSpot software (Cellular Technology) in order to quantify the spot number and size. Data were processed in Microsoft Excel and plotted using GraphPad Prism 10.

2.10 IL-2 enzyme-linked immunosorbent assay (ELISA)

Conditioned media collected from IFN-γ ELISPOT assays were used to probe for the secretion of IL-2 via ELISA. The conditioned media was sealed with paraffin in a 96-well plate and kept at 4°C until ready for assay. The assay was performed using the IL-2 Mouse Uncoated ELISA Kit (ThermoFisher, 88-7024-88) per the manufacturer's protocol. Plates were read using a BioTek Cytation 1 imaging reader with the Gen5 software, and data were processed and visualized as previously described.

2.11 Antibody administration and treatments

Mice were treated with monoclonal antibodies (mAbs) for different experiments. In all cases, mAbs were diluted in PBS and injected intraperitoneally with 100μL of mAbs. Checkpoint blockade therapy was carried out by injecting tumor-bearing mice with 100μg of anti-PD-L1 (BioXcell, BE0101) four times with two days between every treatment. Depending on the experiment, treatment regimens began on days 7, 9, or 12. The treatment schema is noted as needed.

For $CD8^+$ T cell depletion, mice were injected with 200μg one day prior to tumor inoculation and once weekly thereafter until the end of the experiment. Retro-orbital blood collection was used to ensure cell depletion. Briefly, blood was washed in PBS and RBC lysed, as previously discussed, and stained with the panel below for flow cytometry.

Marker	Fluorophore	Clone	Dilution	Vendor	Cat. No.
CD45	APC	30-F11	1:200	BioLegend	10311 1
CD3	BV421	17A2	1:200	BioLegend	100228
CD4	PE	GK1.5	1:200	eBio	12-0041-81
CD8	FITC	53-6.7	1:200	BD	553031

Table 2.4: Flow cytometry panel check for $CD8^+$ T cell depletion.

2.12 In vivo proliferation, apoptosis, and antigen uptake analysis

The proliferation, apoptosis, and tumor-derived material uptake of intratumoral DCs was measured via flow cytometry. Mice were injected with 1 million B16.SIY cells subcutaneously and euthanized on days 20-25, prior to the endpoint. Two additional mice were injected with the parental B16F10 cell line for controls. Tumors were processed, and the immune infiltrate was collected into single-cell suspensions. Tumor-infiltrating immune cells were then prepared and stained for flow cytometry. Probing for proliferation and apoptosis was achieved through the use of intracellular Ki67 and activated Caspase-3 staining. Mice injected with B16F10 were used as controls for tumor-derived material defined by dsRed expression (linked to SIY expression on B16.SIY cells). The flow cytometry panel is listed below.

2.13 Ex vivo antigen uptake and processing by $CD11c^+$ cells

$CD11c^+$ were tested for their ability to take up and process antigens in vitro. Naive mice were euthanized, and their spleens were collected as described above. However, spleens

Marker	Fluorophore	Clone	Dilution	Vendor	Cat. No.
CD11c	BUV395	N418	1:200	BD	744180
CD11b	BUV496	M1/70	1:200	BD	749864
CD3	BUV563	17A2	1:200	BD	741319
Ly6G	BUV615	51A8	1:200	BD	751263
CD317	BUV805	927	1:200	BD	749271
CD86	BV421	GL-1	1:200	BioLegend	105032
Ly6C	PacBlue	HK1.5	1:200	BioLegend	128013
CD80	BV510	16-1OA1	1:200	BD	740130
Ki67	BV605	16A8	1:200	BioLegend	652413
CD103	BV785	2E7	1:200	BioLegend	121439
NK1.1	FITC	PK136	1:200	BioLegend	108706
CD45	AF532	30-F11	1:400	Invitrogen	58-0451-82
I-A/I-E	PerCP/Cy5.5	M5/114.15.2	1:400	BioLegend	107626
Tumor	dsRed	n/a	1:200	n/a	n/a
F4/80	PE-Cy5	BM8	1:200	Invitrogen	15-4801-82
act-Casp3	AF647	C92-605	1:200	BD	560626
LD	Zombie NIR	n/a	1:400	BioLegend	423106
CD19	APC-Fire 750	6D5	1:200	BioLegend	115558
Fc Block	N/A	93	1:200	BioLegend	101302

Table 2.5: Flow cytometry panel for proliferation, apoptosis, and antigen take up intratumoral $CD11c^+$ cells.

were not digested with digestion buffer. For experiments utilizing non-tumor-bearing mice, organs were cut and passed through a filter right away. Single-cell suspensions from spleens were then enriched for $CD11c^+$ with the CD11c MACS kit. Cells were counted and plated in triplicate at 150K cells per well. Cells were pulsed with either DQ-OVA (ThermoFisher, D12053) for antigen processing or with OVA-AF647 (ThermoFisher, O34784) for antigen uptake. Both treatments were plated as serial dilutions spanning from 320μg/mL down to 0.313μg/mL. Plates were incubated for 2-3 hours at 37°C. Following incubation, cells were centrifuged at 400g for 5 minutes, washed with ice-cold PBS, and stained for flow cytometry analysis per the panel below. Experiments were replicated in both male and female mice.

Marker	Fluorophore	Clone	Dilution	Vendor	Cat. No.
CD45	BUV395	30-F11	1:200	BD	564279
CD103	BV785	2E7	1:200	BioLegend	121439
CD11c	APC-Cy7	N418	1:200	BioLegend	117324
I-A/I-E	PE-Cy7	M5/114.15.2	1:500	BioLegend	107630
CD11b	BUV496	M1/70	1:200	BD	749864
LD	ef506	GL-1	1:500	eBio	65-0866-14
H2-Kb-OVA	APC	25-D1.16	1:100	eBio	17-5743-82
DQ-OVA	FITC	n/a	n/a	ThermoFisher	D12053
OVA-AF647	AF647	n/a	n/a	ThermoFisher	O34784

Table 2.6: Flow cytometry panel for in vitro OVA experiments on CD11c$^+$ cells.

2.14 Ex vivo FLT3L stimulation of CD11c$^+$ cells

CD11c$^+$ DCs were tested for their ability to respond to FLT3L stimulation in vitro. Organs were processed as before, with the addition of inguinal and axillary lymph nodes (LNs) taken along with spleens for the purification of CD11c$^+$ cells by MACS. CD11c$^+$ cells from spleens and LNs were cultured at 37°C for 48 hours with 100 ng/mL of recombinant Flt3L and analyzed by flow cytometry.

Marker	Fluorophore	Clone	Dilution	Vendor	Cat. No.
CD45	BUV395	30-F11	1:200	BD	564279
CD11c	PE	N418	1:200	BioLegend	117307
I-A/I-E	BV605	M5/114.15.2	1:500	BioLegend	107639
LD	ef506	GL-1	1:500	eBio	65-0866-14

Table 2.7: Flow cytometry panel for in vitro FLT3L experiments on CD11c$^+$ cells.

2.15 CD11c$^+$ enrichment for bulk RNA sequencing

Dendritic cells (DCs) are a rare subset of immune cells. These cells are even more rare within tumors. In order to achieve a sufficient number of intratumoral CD11c$^+$ DCs, 3-4 mice were pooled together, and these batches were repeated three times, resulting in a total of 43 mice and 14 samples submitted for bulk RNA sequencing. Each batch of experiments

was repeated in the exact same way. Mice were injected with 1.5 million B16.SIY cell subcutaneously and euthanized at day 20 to collect tumors. Tumors were processed as usual, and single-cell suspensions of immune infiltrates were then enriched for $CD11c^+$ through CD11c MACs. Enriched $CD11c^+$ fractions were then pooled together (2-4 mice depending on the tumor size) and sorted on a BD FACSAria-III 3-14 Cell Sorter with the panel listed in the table below. Sorted samples were resuspended in 1mL TRIzol (ThermoFisher, 15596026) and frozen at -80C until all samples were obtained.

Marker	**Fluorophore**	**Clone**	**Dilution**	**Vendor**	**Cat. No.**
CD45	APC	30-F11	1:200	BD	564279
CD11c	PE	N418	1:200	BioLegend	117307
CD3	FITC	145-2C11	1:200	BD	553062
LD	Zombie NIR	n/a	1:400	BioLegend	423106

Table 2.8: Flow cytometry panel for sorting of enriched intratumoral $CD11c^+$.

2.16 RNA isolation for bulk RNAseq

Once all samples were obtained, RNA was isolated utilizing a Qiagen RNeasy Micro Kit (74004) with a modified protocol. Frozen samples were allowed to thaw and sit at room temperature for 5 minutes while vortexing nearly every minute before adding 200μL of Chloroform to each sample and vortexing vigorously. Samples were allowed to rest at room temperature for 1 minute, vortexed again, and centrifuged at 15,000g for 10 minutes. The upper clear layer was transferred into a new tube and proceeded per the manufacturer's protocol, beginning with Step 4. Steps 7-9 were also skipped. RNA was eluted in 15μL of RNase-free water utilizing 1μL to measure RNA concentration with a NaNoDrop One as described above. Samples were placed at 4°C and left for QC and subsequent RNAseq.

2.17 Bulk RNAseq of intratumoral CD11c$^+$ cells

RNA was purified from intratumoral CD11c$^+$ cells as previously described and submitted for bulk RNA sequencing in an Illumina NovaSeqX at the Genomics Facility at the University of Chicago. An oligo-dT mRNA directional library was prepared for sequencing in 30M PE100 clusters. Raw reads were processed with the help of Drs. Jason Shapiro and David Tieri. Briefly, processing was performed with a variety of R packages, but all graphics and data wrangling was carried out using the tidyverse suite of packages. Mapping of the reads to the mouse reference genome GRCm38 was carried out with START, version 2.6.1d. with quality reports being generated using fastqc and multiqc. The raw reads were mapped to the *Mus musculus* transcriptome with Salmon, version 1.10.1, and were read into R using txtimport. Non-protein coding regions and genes with low expression were removed, and counts were normalized. Normalized counts were used for downstream analysis.

2.18 scRNAseq of MC38.SIY tumors

Single-cell RNA sequencing (scRNAseq) of MC38.SIY tumors was performed and analyzed by Ruxandra Tonea from our laboratory. Briefly, mice were injected subcutaneously with MC38.SIY-GFP cells (2 x 10^6), and tumors were harvested from two different mice at day 21. Single-cell suspensions of the tumor immune infiltrate were stained, and live CD45+ cells were sorted on a MACSQuant Tyto Cell Sorter using two regular speed cartridges. 10000 cells from each biological replicate were loaded into the 10x Genomics Sequencer and sequencing was performed by the 10x Genomics Core at UChicago. Reads were aligned, and feature-barcode matrices were generated using the 10x Genomics Cell Ranger software. Cells expressing a high percentage of mitochondrial RNA and lowly expressed genes were excluded. Data was normalized using Seurat's SCTransform function. Principal component analysis (PCA) was performed first, followed by dimensionality reduction using RunUMAP

on the top 30 principal components (PCs). The k-nearest neighbors were calculated, and the SNN graph was constructed using Seurat's FindNeighbors function. Pseudo-bulk differential expression via DESeq2-LRT method was performed to identify the top differentially expressed genes in each cluster. Based on the top differentially expressed genes, each cluster was annotated, as noted in **Figure 4.21**.

2.19 Graphical figures

All of the figures presented here were made by the author. For data-driven figures, GraphPad Prism v10 was used for consolidation and organization of figures. Graphical representations were created using BioRender.com.

2.20 Statistical analysis

Except for bulk RNAseq data, all of the data was managed and processed utilizing Microsoft Excel or R, as previously described, and statistical analysis was performed using GraphPad Prism 10. Tumor growth curves were analyzed by two-way ANOVA, utilizing Sidak's Multiple Comparisons tests when appropriate, and are plotted as mean +/- S.E.M. Survival curves were analyzed by Kaplan-Meier survival analysis with p values for Gehan-Brewslow- Wilcoxon test reported. Violin plots were similarly analyzed by two-way ANOVA and Sidak's Multiple Comparisons test and by calculating the area under the curve and comparing it with an unpaired, two-tailed student's t-test. Bar graph comparisons were analyzed by unpaired, two-tailed student's t-test (parametric) or Wilcoxon-Mann-Whitney test (non-parametric) depending on normality. Spearman's correlations were used for multivariable analysis. Raw FCS files were unmixed using Cytke's SpectroFlo software. For processed flow cytometry data, all counts, percentages, and mean fluorescence intensities (MFI) were calculated using FlowJo.

CHAPTER 3

DELETION OF PTPN22 IN DENDRITIC CELLS AUGMENTS ANTI-TUMOR IMMUNITY

3.1 Introduction

Within the past decade, immunotherapies have been developed targeting immune checkpoints that normally are inhibitory for T cell function. As previously discussed in detail, the best characterized to date are cytotoxic T lymphocyte antigen 4 (CTLA-4), programmed cell death 1 (PD-1), and its ligand PD-L1 [139, 56]. Antibodies blocking the engagement of these inhibitory receptors, or immune checkpoint blockade (ICB) therapy, have become successful therapeutic agents in a broad array of cancers in the clinic. These include head and neck cancer, melanoma, non-small cell lung cancer, Hodgkin lymphoma, hepatocellular carcinoma, and others. ICB has been key in providing prolonged survival in patients with normally fatal cancers. For example, about 20% of melanoma patients treated with anti-PD1 achieve a complete response that is often durable.

While ICB results in cures for some, the overall percentage of patients across all cancers that respond to therapy remains low, making it critical to elucidate the mechanisms of resistance against ICB. It is similarly important to identify new ways of activating the immune system in order to elicit more effective anti-tumor responses. One major area of interest is host germline genetic differences in immune regulatory genes. Given the association of the PTPN22 SNP in autoimmunity, universal knock-out (KO) animals were generated, highlighting its role as a negative regulator of immunity. While PTPN22 KO animals display heightened anti-tumor immunity, this does not seem to be mediated exclusively by T cells as previously thought, underscoring to need to understand the role of PTPN22 in other immune compartments. As key mediators of immunity, this work thus set out to understand the role of PTPN22 in regulating myeloid cells in the context of anti-tumor immunity.

3.2 Results

3.2.1 Characterization of PTPN22 conditional knock out CD11c$^+$ mice

Previously published work has relied on either a universal KO mouse or a knock-in mouse bearing the autoimmune-associated variant of PTPN22, R620W [118, 140, 135, 137]. While the R620W knock-in model might recapitulate human pathology more faithfully, discrepancies between mice and humans have resulted in contradictory results of this model. Chiefly, it has been shown that this variant is 50% more catalytic but at the same time displays decreased protein stability [115, 141]. The PTPN22 KO mouse model thus represents a more reliable tool for characterizing PTPN22 regulation of the immune system. However, this universal KO model cannot optimally distinguish effects intrinsic to specific cell subpopulations. To address this, we generated a novel PTPN22$^{\mathrm{fl/fl}}$ mouse, allowing us to study its role in different immune compartments efficiently and selectively. Here, the use of this model to selectively knock out PTPN22 in CD11c$^+$ dendritic cells and macrophage-lineage cells is described.

The generation of a PTPN22 conditional knockout (cKO) mouse model was achieved by the insertion of loxP sites flanking exons 2 and 8 in the PTPN22 gene. Under the expression of Cre recombinase, these exons are excised, resulting in the loss of the expression of wild-type (WT) PTPN22 expression (**Figure 3.1**). Real-time qPCR of CD11c$^+$ cells from the spleens of cKO and WT mice confirm the conditional deletion of PTPN22 only in CD11c$^+$ of Cre$^+$ mice. PTPN22 global KO animals develop splenomegaly with age, attributed to an accumulation of CD44$^+$ CD8$^+$ T cells [118]. In order to further characterize our novel PTPN22 cKO, immune profiling of animals was carried out in both young (6.5 weeks) and aged (20 months) mice, analyzing both the spleen and inguinal lymph nodes. No gross differences were observed in young, naive mice. Further, immune-profiling did not reveal any differences in the percentage of DCs and T cells or any of their subtypes, as well as B cells,

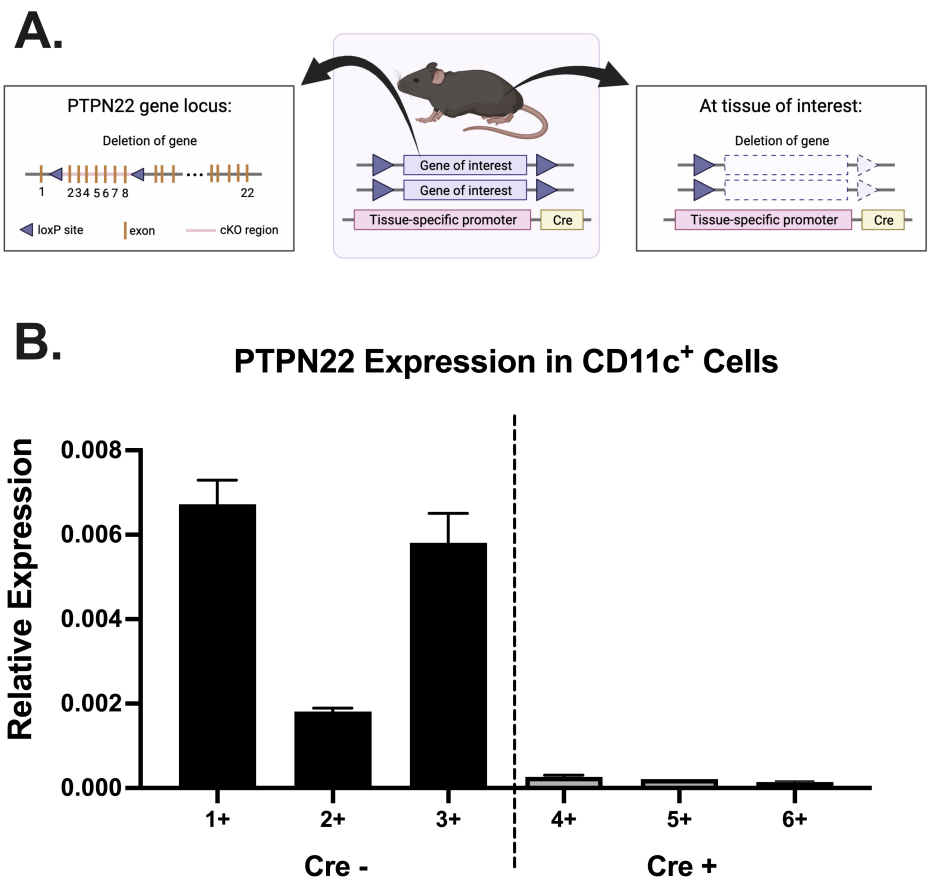

Figure 3.1: Generation and validation of PTPN22 cKO in CD11c^{+} compartment. **(A)** Schematic of the PTPN22 conditional knockout (cKO) mouse model. **(B)** Spleens were collected from PTPN22$^{fl/fl}$ Cre^{+} and Cre^{-} and CD11c^{+} were isolated through CD11c MACS enrichment. RNA was isolated to generate cDNA for qPCR in order to quantify the relative expression of PTPN22.

natural killers (NK) cells, macrophages, monocytes, and neutrophils (**Figure 3.2**). Given the accumulation of lymphocytes in aged (6-month) mice in the global PTPN22 KO, cKO mice were aged to 20 months in order to identify any potential differences that may arise with age. Similarly to young mice, aged PTPN22 cKO mice displayed no gross differences, evidenced by a lack of difference between body and spleen weights. Immune-profiling of the spleens and inguinal lymph nodes further confirmed no differences in any immune compartment, in stark comparison to the accumulations seen in aged, global PTPN22 KO mice (**Figure 3.3**). Thus, validated conditional knockout of PTPN22 in the CD11c^{+} compartment does

not have any baseline effects on the immune profiles of naive mice, regardless of age.

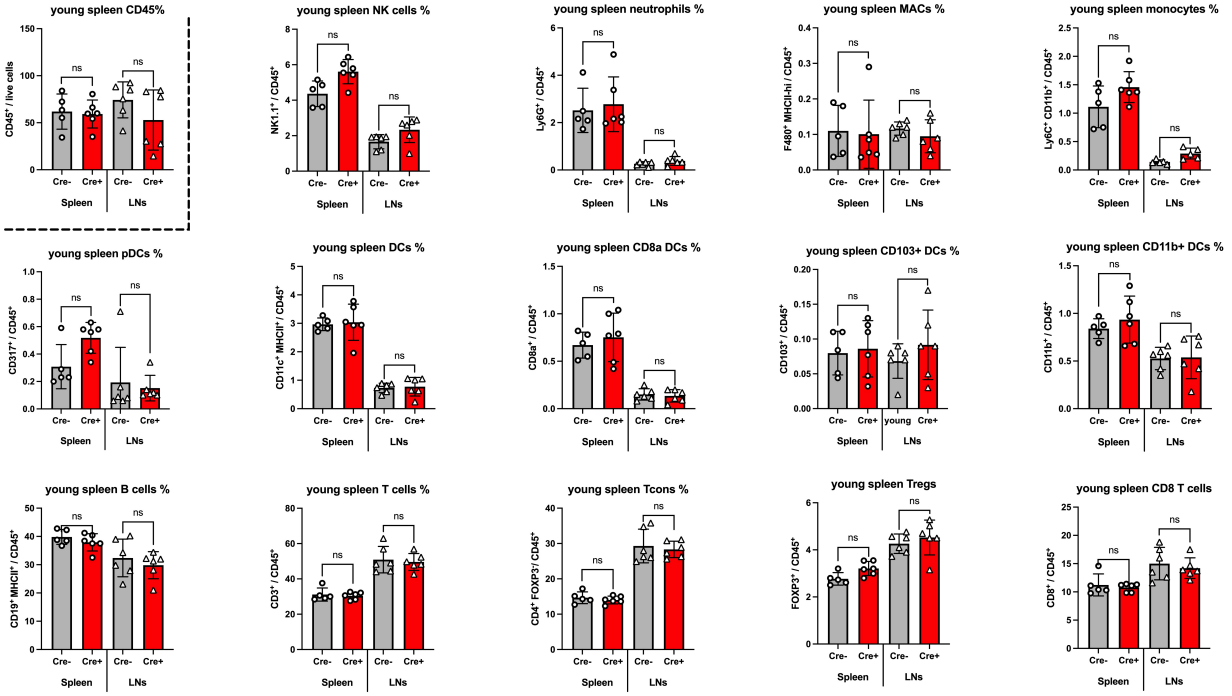

Figure 3.2: Immune-profiling of young PTPN22 cKO mice. Spleens and inguinal lymph nodes were collected from PTPN22$^{fl/fl}$ Cre^{+} and Cre^{-} and CD11c^{+} mice. Single-cell suspensions were stained and analyzed by flow cytometry. Young, female mice had an average age of 6.5 weeks. N $\geq$ 5 per group. Student's t-tests were used to test for significance between the experimental and control groups in either spleen or LNs. Data are plotted as the percentages of the CD45^{+} population.

3.2.2 PTPN22 cKO in CD11c^{+} cells improves anti-tumor immunity in multiple tumor models

Despite no differences being observed in the baseline immune profiles of naive PTPN22 cKO mice, we went on to investigate their ability to control syngeneic tumors, given the critical role of DCs in mounting an effective anti-tumor immune response [142, 143, 144, 145]. To achieve this, we first utilized a syngeneic, orthotopic cancer model: aged-matched litter-mates were injected intradermally with 1 million B16.SIY cells in the lateral flank. Indeed, PTPN22 CD11c-Cre cKO showed improved spontaneous tumor control compared to

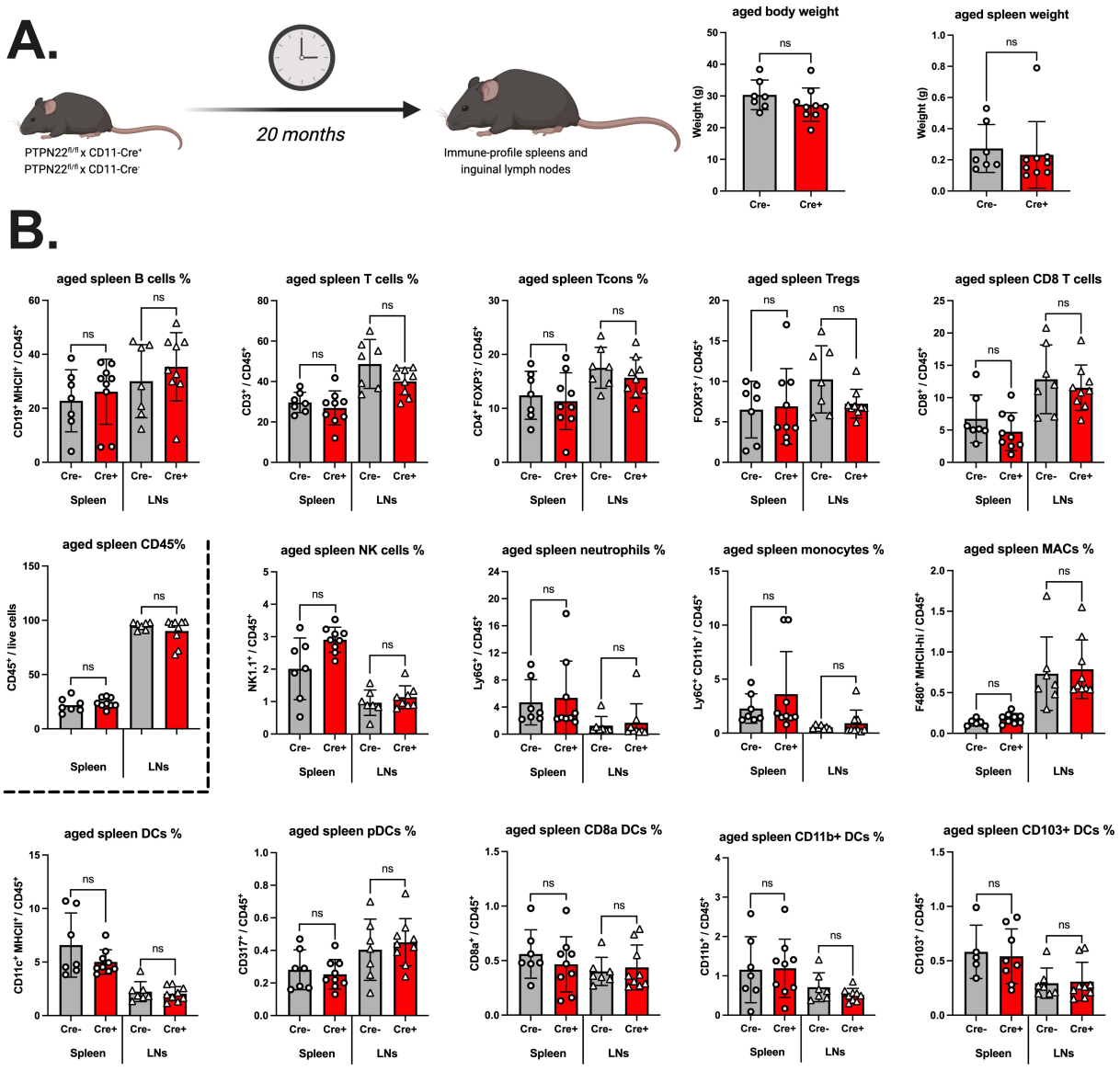

Figure 3.3: Immune-profiling of aged PTPN22 cKO mice. Spleens and inguinal lymph nodes were collected from PTPN22$^{fl/fl}$ Cre^{+} and Cre^{-} and CD11c^{+} mice. Single-cell suspensions were stained and analyzed by flow cytometry. Aged mice had an average age of 20 months.

wildtype, Cre-negative mice. These mice showed increased survival compared to controls and had smaller tumors by weight at endpoint (**Figure 3.4 A**). Similar results were seen in both the N1H7 and N2B5 founder clones of PTPN22$^{fl/fl}$ x CD11c-Cre^{+} mice. The N1H7 clone was selected for subsequent experiments. The murine colorectal cancer cell line expressing

the model antigen SIY was as a confirmatory model, in this case, implanted subcutaneously. PTPN22 cKO mice similarly displayed increased tumor control in the MC38.SIY model as well as improved survival and decreased overall tumor weight at endpoint (**Figure 3.4 B**).

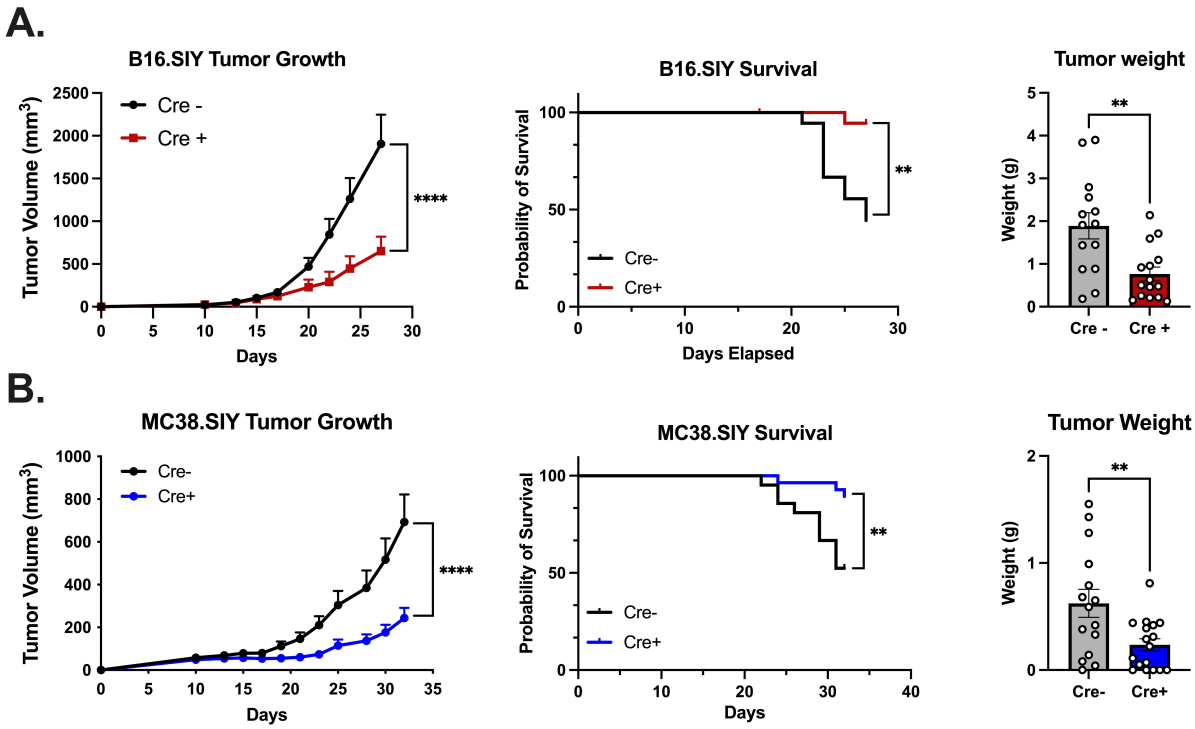

Figure 3.4: PTPN22 cKO mice display improved tumor control. PTPN22$^{fl/fl}$ Cre^{+} and Cre^{-} aged-matched litter-mates were tested for their ability to control syngeneic tumor models. **(A)** Female mice were injected intradermally with 1 million B16.SIY and **(B)** male and female mice were injected subcutaneously with 1 million MC38.SIY cells and allowed to grow until endpoint. For B16.SIY, both N1H7 and N2B5 clones of the PTPN22$^{fl/fl}$ x CD11c-Cre^{+} mice were used with N $\geq$ 15 per group). For MC38.SIY, only the N1H7 clone of the PTPN22$^{fl/fl}$ x CD11c-Cre^{+} mice were used with N $\geq$ 12 per group). Pooled data from independent experiments are plotted for B16.SIY (N = 3) and MC38.SIY (N =2). PTPN22$^{fl/fl}$ x Cre^{+} mice are presented as red in B16.SIY experiments and blue in MC38.SIY experiments with PTPN22$^{fl/fl}$ x Cre^{-} controls always presented as gray.

Because PTPN22 is exclusively being deleted in the CD11c^{+} immune compartment, we hypothesized that improved tumor control must be mediated by the immune system. B16.SIY tumors were collected and processed at endpoint in order to extract the immune infiltrate for immune profiling by flow cytometry. PTPN22 cKO mice displayed an increase

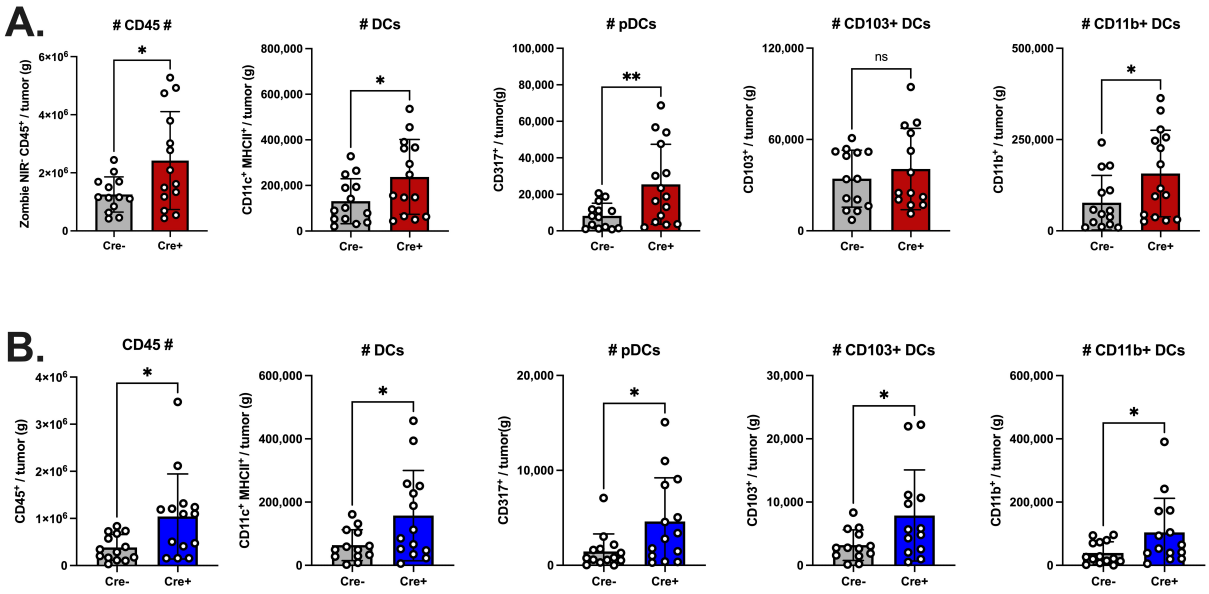

Figure 3.5: PTPN22 cKO mice have an increase of tumor-infiltrating DCs. Tumors from PTPN22$^{fl/fl}$ x Cre^{+} and Cre^{-} aged-matched litter-mates were isolated for immune-profiling. DC subsets of **(A)** B16.SIY (N $\geq$ 15) and **(B)** MC38.SIY (N $\geq$ 12) tumors are shown as the number per gram of tumor and the percentage of all CD45^{+} cells. The gating strategy is outlined in the **Materials and Methods**.

in the overall number of tumor-infiltrating CD45^{+} immune cells per gram of tumor.

A more detailed analysis of the DC compartment revealed an increased number per gram of tumors of DCs. Subset analysis revealed an increase in conventional DC (cDC) subsets of CD103^{+} and CD11b^{+} DCs (**Figure 3.5 A**). Plasmacytoid DCs (pDCs) were also increased despite their lower levels of CD11c expression [146]. The lack of a significant increase in CD103^{+} DCs in this model could be attributed to the fact that DCs may be subject to CD8^{+} T cell-mediated cytotoxicity at late time points[147]. The immune profiles of tumor infiltrates in the MC38.SIY model showed an overall similar pattern, including a significant increase in the CD103^{+} DCs compartment (**Figure 3.5 B**).

The changes in the DC compartment led us to investigate whether further qualitative differences in these subsets were present. MHC II is used as a defining marker for myeloid cells and DCs, but within the conventional DC (cDC) subsets, its level of expression can also serve as an indication of maturity and activation [148, 149]. The mean fluorescence intensity

(MFI) of MHC II was used to quantify maturity/activation in the cD103$^+$ and CD11b$^+$ subsets. In the B16.SIY model, CD103$^+$ DCs but not CD11b$^+$ DCs display a significant increase in the MFI of MHC II in PTPN22 cKO animals (**Figure 3.6 A**). Accordingly, the same pattern was observed in the MC38.SIY model where the MFI of MHC II was greater in CD103$^+$ DCs of PTPN22 cKO mice (**Figure 3.6 B**).

DCs contribute to endogenous anti-tumor immunity by activating and maintaining T cells, which are ultimately the major effector cells involved in anti-tumor immunity, and prior work from our lab has established them as the main effector cells in the B16.SIY and MC38.SIY models. PTPN22 cKO mice had an increase in the total number of tumor-infiltrating lymphocytes (TILs) per gram of tumor in comparison to control animals. In the B16.SIY model, this increase was primarily driven by an expansion of CD8$^+$ T cells, with no changes observed in the CD4$^+$ FOXP3$^-$ conventional T cells (Tcons) or CD4$^+$ FOXP3$^+$ regulatory T cells (Tregs) as shown in **Figure 3.7 A**. Similar results were observed in the MC38.SIY model; however, in this model, all T cell subsets were significantly increased, representative of the increased immunogenic nature of the MC38 model (**Figure 3.7 B**). Together, these results highlight the positive impact of deleting PTPN22 in the CD11c compartment on the anti-tumor response as a whole.

3.2.3 Tumor antigen-specific, intratumoral T cells are increased in PTPN22 cKO animals

T cells represent the main effector cell type in the B16.SIY and MC38.SIY tumors. Specifically, tumor antigen-specific CD8$^+$ T cells are responsible for the recognition and killing of tumor cells. The use of cancer cell lines expressing the model antigen SIY allows for the identification and characterization of endogenous tumor antigen-specific CD8$^+$ T cells through the use of SIY-K^b pentamer staining. In accordance with the increased tumor control observed in B16.SIY tumors, CD8$^+$ SIY$^+$ T cells were more numerous per gram

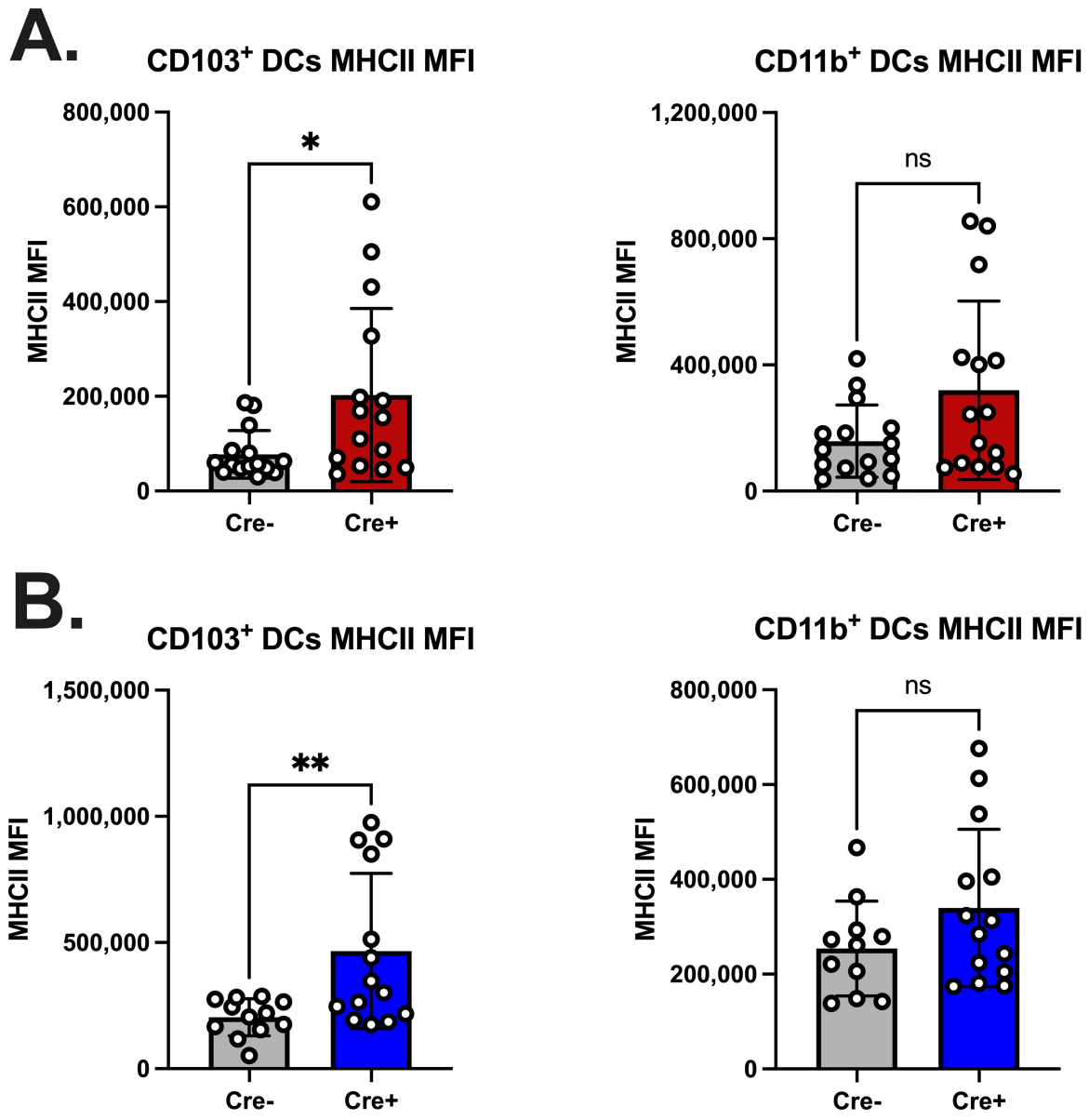

Figure 3.6: Intratumoral DCs lacking PTPN22 result in more mature CD103$^+$ DCs. Intratumoral DCs defined as CD11c$^+$ MHC II$^+$ from PTPN22$^{fl/fl}$ x Cre$^+$ and Cre$^-$ mice bearing B16.SIY (N $\geq$ 15) and MC38.SIY (N $\geq$ 12) tumors were sub-categorized as CD103$^+$ CD11b$^-$ and CD11b$^+$ CD103$^-$. The mean fluorescence intensity (MFI) of MHC II is shown for both subsets in **(A)** B16.SIY (red) and **(B)** MC38.SIY (blue) tumors.

of tumor. The increase in CD8$^+$ SIY$^+$ T cells seemed to be mediated by an increase in proliferation as indicated by a higher percentage of CD8$^+$ SIY$^+$ Ki67$^+$ T cells. These cells also expressed a greater percentage of the activation markers CD44 and CD69 (**Figure 3.8**

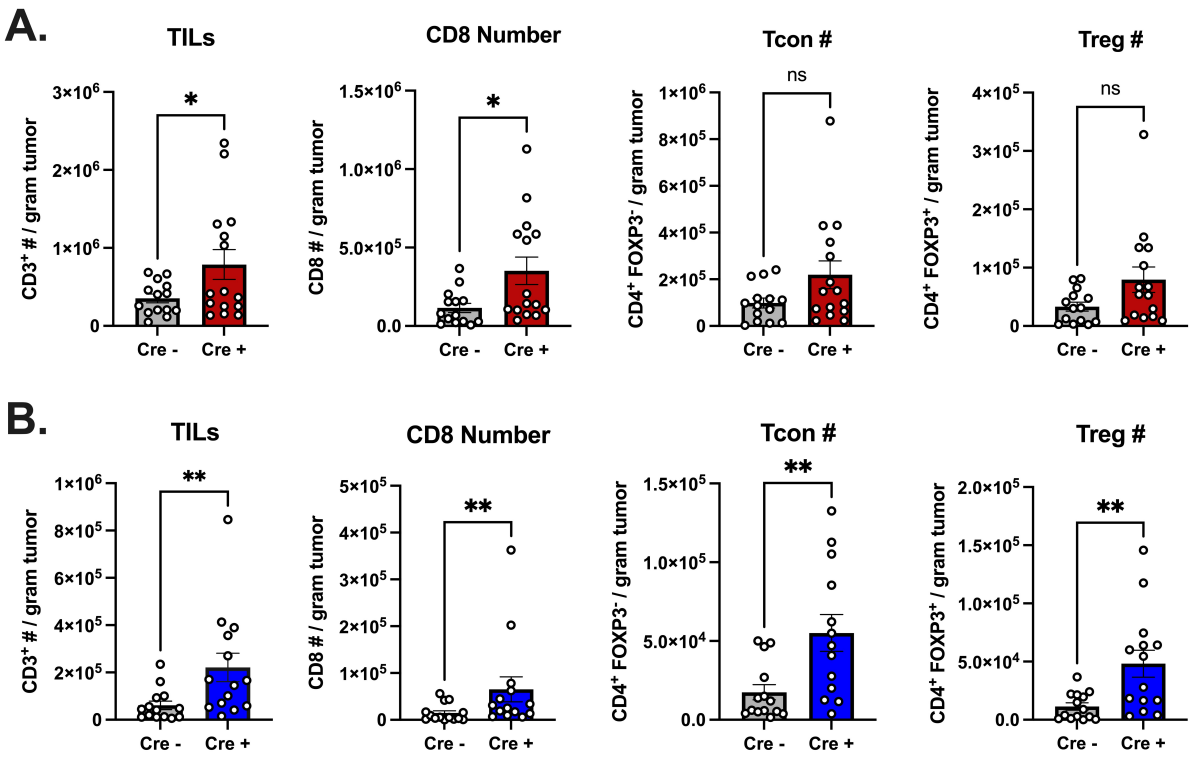

Figure 3.7: PTPN22 cKO mice have increased tumor-infiltrating T cells. Intratumoral T cells defined as $CD3^+$ $NK1.1^-$ from $PTPN22^{fl/fl}$ x Cre^+ and Cre^- mice bearing **(A)** B16.SIY (N $\geq$ 15) and **(B)** MC38.SIY (N $\geq$ 12) tumors were sub-categorized as $CD8^+$ $CD4^-$ and $CD4^+$ $CD8^-$ $CD4^+$ $CD8^-$ T cells were further subtyped as $FOXP3^+$ (T regulatory cells; Tregs) and $FOXP3^-$ (T conventional cells; Tcons) .

A). $CD8^+$ SIY^+ T cells represent the cytotoxic anti-tumor arm of the immune system in this context. $CD8^+$ T cells also secrete chemokines for the recruitment of Tregs, which provide a counter-regulation to control ongoing immune response [150]. Therefore, we analyzed the ratio of the number of $CD8^+$ SIY^+ T cells to Tregs per gram of tumor [151, 152, 153]. In the B16.SIY model, the $CD8^+$ SIY^+ T cell/Treg ratio was increased in PTPN22 cKO mice, indicative of a shift towards an anti-tumor TME (**Figure 3.8 A** far right). In the MC38.SIY model, $CD8^+$ SIY^+ T cells were similarly increased in quantity and in the percentage of proliferating $Ki67^+$ cells. The activation profile of these cells in the MC38.SIY model also displayed an increased percentage of cells expressing the activation markers CD69 and PD-1. In this model, the $CD8^+$ SIY^+ T cell/Treg ratio showed a positive trend (**Figure 3.8 B**).

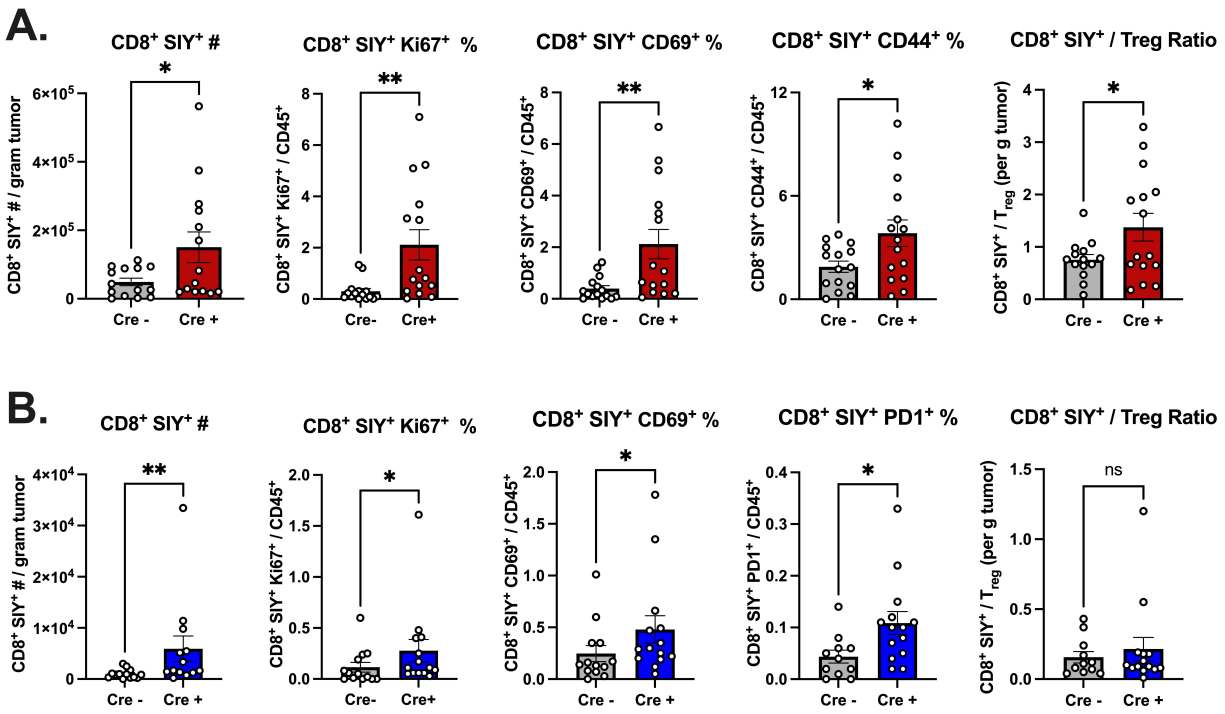

Figure 3.8: Tumor-infiltrating, tumor antigen-specific CD8$^+$ T cells are more numerous and activated in PTPN22 cKO mice. Intratumoral tumor antigen-specific CD8$^+$ T cells defined as SIY$^+$ from PTPN22$^{fl/fl}$ x Cre$^+$ and Cre$^-$ mice bearing **(A)** B16.SIY (N $\geq$ 15) and **(B)** MC38.SIY (N $\geq$ 12) tumors were profiled for markers of proliferation and activation. The CD8$^+$ SIY$^+$ / Treg ratio was defined by diving the number of CD8$^+$ SIY$^+$ per gram of tumor by the number of Tregs per gram of tumor.

In addition to an increase in DCs and T cells, we also observed an increased number per gram of tumors of NK cells, natural killer T cells (NKTs), tumor-associated macrophages, and monocytes. Interestingly, neutrophils were the only immune compartment to not be significantly different in either model. This pattern was also consistent in MC38.SIY tumors (**Figure 3.9**) These data suggest that targeted DC modulation can have profound impacts on the TME, resulting in increases within these cellular compartments [154, 155].

Lastly, the number of CD8$^+$ SIY$^+$ and CD103$^+$ DCs per gram of tumor were strongly correlated with tumor mass, with PTPN22 cKO mice enriched for smaller tumors (**Figure 3.10**). These findings underscore the importance of these cells in anti-tumor immunity and suggest that in PTPN22 cKO mice, the increased numbers and activation status of CD103$^+$

DCs drive increased CD8$^+$ SIY$^+$ T cell responses resulting in improved tumor control.

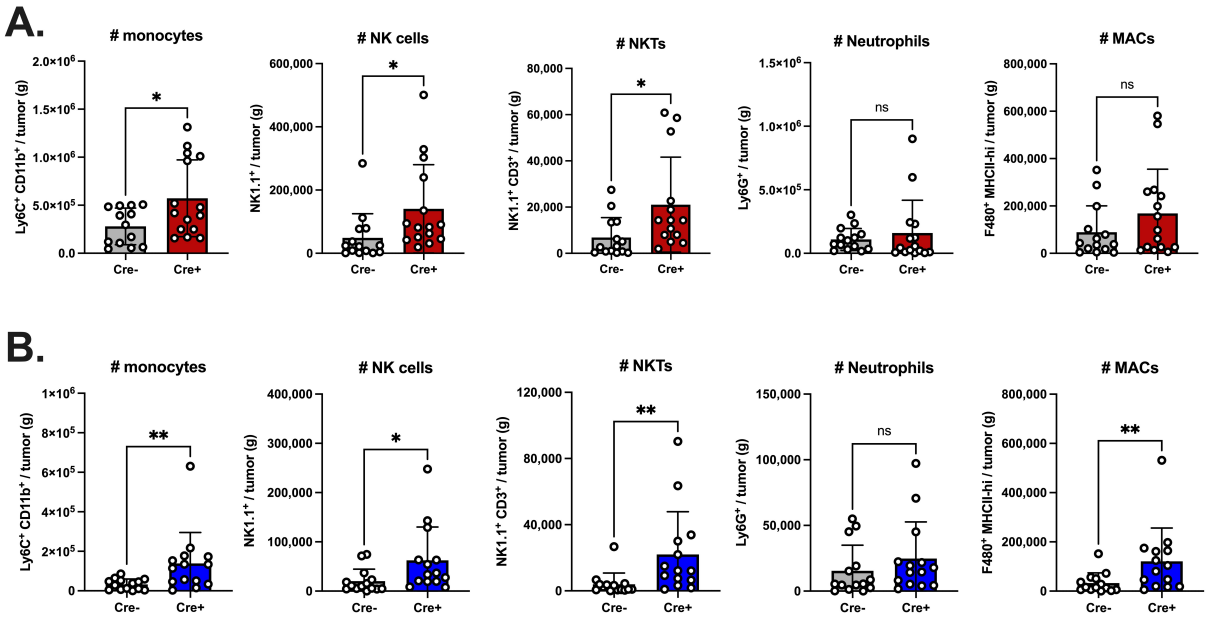

Figure 3.9: PTPN22 cKO mice have an altered tumor-infiltrating immune profile. Tumors from PTPN22$^{fl/fl}$ x Cre$^+$ and Cre$^-$ aged-matched litter-mates were isolated for immune-profiling. Immune profile of **(A)** B16.SIY (N $\geq$ 15) and **(B)** MC38.SIY (N $\geq$ 12) tumors are shown as the number per gram of tumor and the percentage of all CD45$^+$ cells. The gating strategy is outlined in the **Materials and Methods**.

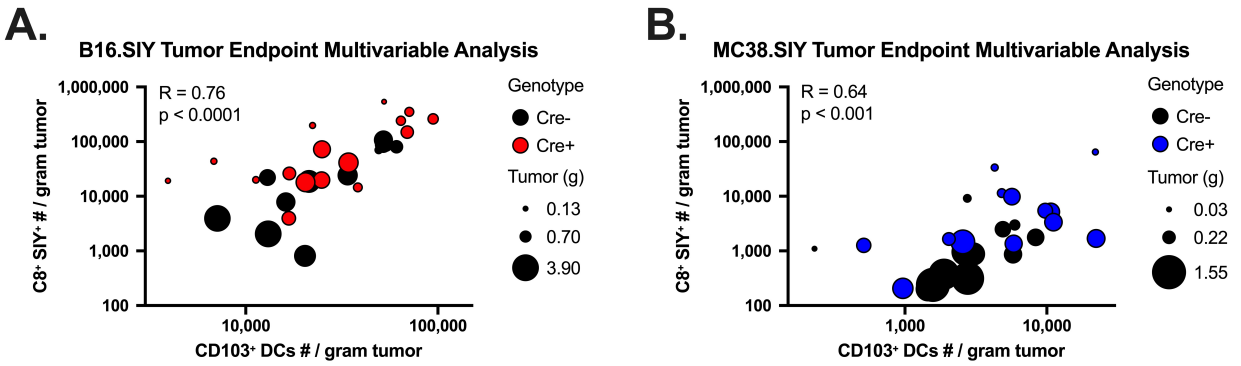

Figure 3.10: The number of CD8$^+$ SIY $^+$ T cells and CD103$^+$ DCs drive decreased tumor mass in PTPN22 cKO mice. Intratumoral CD8$^+$ SIY$^+$ T cells and CD103$^+$ DCs from PTPN22$^{fl/fl}$ x Cre$^+$ and Cre$^-$ mice bearing **(A)** B16.SIY (N $\geq$ 15) and **(B)** MC38.SIY (N $\geq$ 12) tumors were analyzed by multivariable analysis, taking into account tumor weight in grams and Cre type. Spearman R Correlation values for CD8$^+$ SIY$^+$ T cells and CD103$^+$ DCs are shown along with their p-value.

3.2.4 Improved tumor control in PTPN22 cKO animals is dependent on $CD8^+$ T cells

PTPN22 cKO mice displayed an improved anti-tumor immune response that included increased antigen-specific $CD8^+$ T cells. To determine whether $CD8^+$ T cells were required for this improved tumor control, we utilized anti-CD8β depleting antibodies. The use of this specific antibody is important as antibodies targeting CD8α would also result in the depletion of lymphoid-resident $CD8\alpha^+$ DCs. In both the B16.SIY and MC38.SIY models, depletion of $CD8^+$ T cells resulted in complete loss of tumor control in PTPN22 cKO models, while vehicle-treated animals display the same improved tumor control phenotype in PTPN22 cKO mice as previously shown (**Figure 3.11**). These results establish $CD8^+$ T cells as the dominant effector cell types mediating improved tumor control when PTPN22 is specifically deleted from DCs.

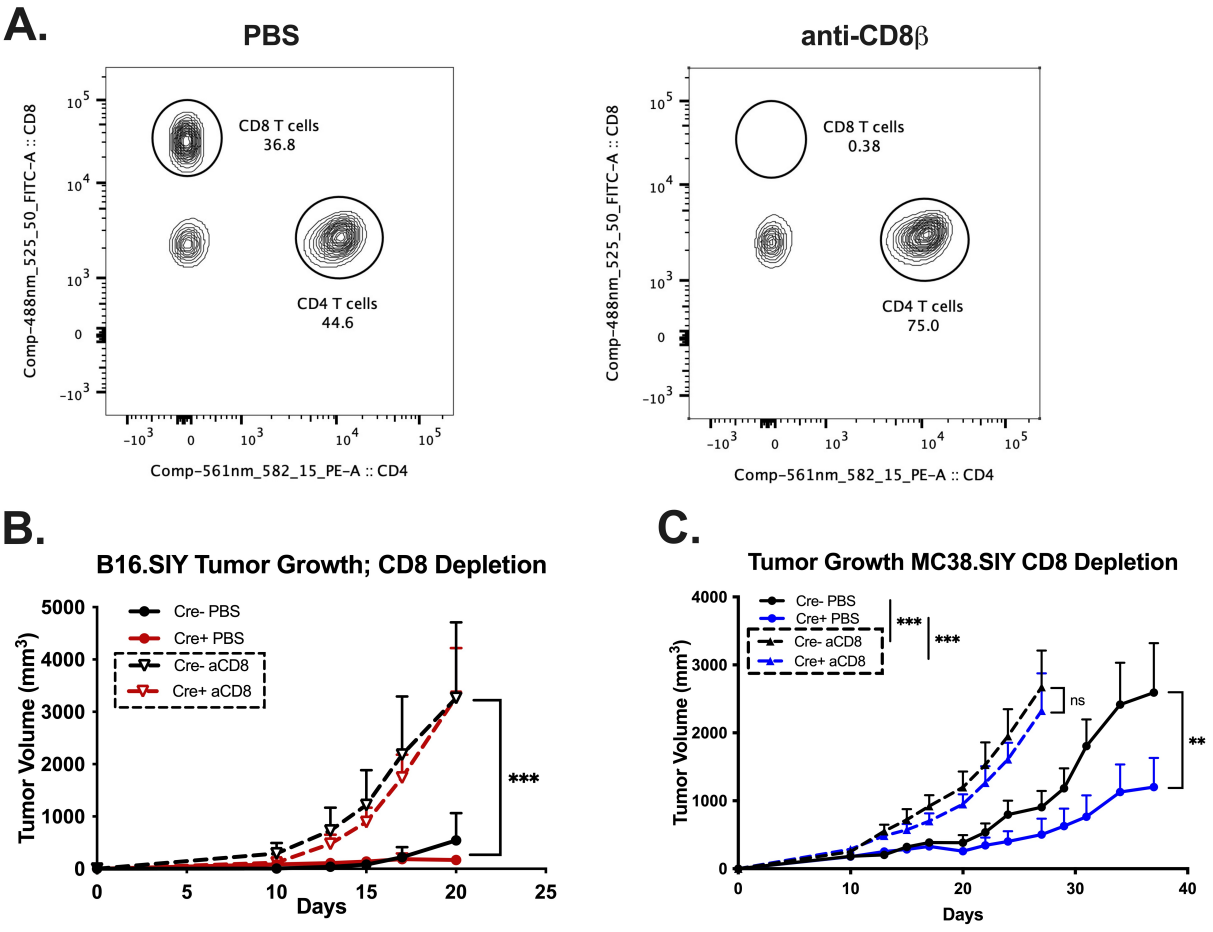

Figure 3.11: Improved tumor control in PTPN22 cKO mice is dependent on CD8$^+$ T cells. Anti-CD8β (aCD8β) antibody was used to deplete CD8$^+$ T cells. Tumor-bearing mice were injected with either 200ng of aCD8β or PBS (100μL) intraperitoneally one day prior to tumor inoculation and once a week until the end of each experiment. **(A)** Tumor-bearing mice were bled retro-orbitally to confirm depletion of CD8$^+$ T cells via flow cytometry. PTPN22$^{fl/fl}$ x Cre$^+$ and Cre$^-$ mice bearing **(A)** B16.SIY and **(B)** MC38.SIY tumors undergoing CD8$^+$ T cell depletion (solid lines with filled-in circles) or control PBS treatment (dashed lines with open triangles).

3.3 Summary of findings

The data in Chapter 3 characterize a novel mouse model for the conditional deletion of PTPN22 in $CD11c^+$ cells. Unlike PTPN22 KO mice, this conditional model of deletion only in DCs did not lead to splenomegaly with age, nor accumulation of effector $CD8^+$ T cells. Thus, autoimmunity does not seem to be triggered. Nonetheless, conditional deletion of PTPN22 in the $CD11c^+$ compartment improved anti-tumor immunity in multiple syngeneic mouse models of cancer. Immune profiling revealed increased numbers of T cells and DCs per gram of tumor, which included tumor antigen-specific $CD8^+$ T cells. Improved tumor control was dependent on the presence of $CD8^+$ T cells, as their depletion completely abrogated the observed phenotype. Intratumoral DCs in PTPN22 cKO animals also had increased expression of maturation activation and markers. These results led us to investigate more deeply the biological effects of PTPN22 deletion in $CD103^+$ DCs and the downstream effects on $CD8^+$ T cell priming.

CHAPTER 4

PTPN22 IS A NEGATIVE REGULATOR OF DENDRITIC CELL ACTIVATION AND IMPACTS THE CD103$^+$ DC - CD8$^+$ T-CELL AXIS

4.1 Introduction

The conditional deletion of PTPN22 in the CD11c$^+$ compartment drove improved CD8$^+$ T cell-dependent anti-tumor immunity. This apparently improved DC-T cell crosstalk led us to investigate more deeply the biological processes within DCs that are augmented upon PTPN22 deletion. CD103$^+$ dendritic cells (DCs) within the TME are responsible for taking up tumor-derived material and presenting it to antigen-specific CD8$^+$ T cells in the tumor-draining lymph nodes (tdLNs), driving their expansion and activation. It is these activated, antigen-specific CD8$^+$ T cells that enter the circulation and home to tumor sites, where they have the opportunity to perform their effector function and kill tumor cells. The use of the B16 and MC38 models expressing the model antigen SIY allows for the tracking of these endogenous CD8$^+$ T cells. Inasmuch as PTPN22 was conditionally and specifically deleted in the CD11c$^+$ DC compartment, we hypothesized that critical biological processes in DCs important for T cell activation might have been potentiated.

4.2 Results

4.2.1 PTPN22 deletion in the CD11c$^+$ compartment results in improved priming of CD8$^+$ T cells

We began by probing the tdLNs of day 7 tumor-bearing mice during the priming phase of the anti-tumor T cell response [156, 157, 158]. At this early stage, during the priming

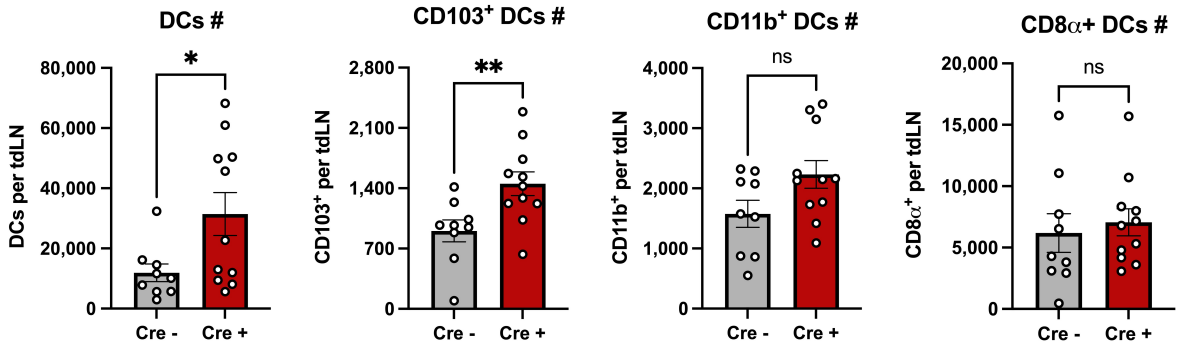

Figure 4.1: Expansion of CD103$^+$ DCs drives an increase in DCs in the tdLNs of PTPN22 cKO mice during the priming phase. PTPN22$^{fl/fl}$ x Cre$^+$ and Cre$^-$ aged-matched litter-mates were injected intradermally with 1 million B16.SIY cells. Spleens and tumor-draining lymph nodes (tdLNs) were harvested on day 7. DCs in the tdLN were quantified as the total number per tdLN and subtyped as previously done (N $\geq$ 9 per group). Pooled data are plotted from independent experiments (N = 2).

phase, tumors are not yet appreciable, but the endogenous anti-tumor response has already begun. This phase is primarily characterized by the migration of mature, tumor antigen-loaded DCs to the tdLNs, where they cross-prime (activate) antigen-specific CD8$^+$ T cells. Successful cross-priming can be assessed by the presence and expansion of activated, tumor antigen-specific CD8$^+$ in the tdLNs as well as in circulation, such as in the spleen. Moreover, in order for this to take place DCs in the tdLNs must have a mature/activated phenotype characterized by the expression of MHC II and the co-stimulatory receptors CD80 and CD86. When mounting an immune response, our laboratory has found that DCs also proliferate in response to stimuli in order to amplify the elicited immune response. Because the subcutaneous and dermal tissues differ in their make-up of immune resident cells and their lymphatic drainage, cross-priming experiments were performed using intradermally injected B16.SIY cells [159, 160, 161, 162, 163].

We first set out to evaluate how deletion of PTPN22 in CD11c$^+$ DCs affected DCs in the tdLN during an anti-tumor immune response. PTPN22 cKO resulted in an expansion of DCs in the tdLNS. This expansion was primarily due to the expansion of CD103$^+$ DCs and not CD11b$^+$ DCs or CD8α^+ DCs (**Figure 4.1**). We then characterized the activation profile

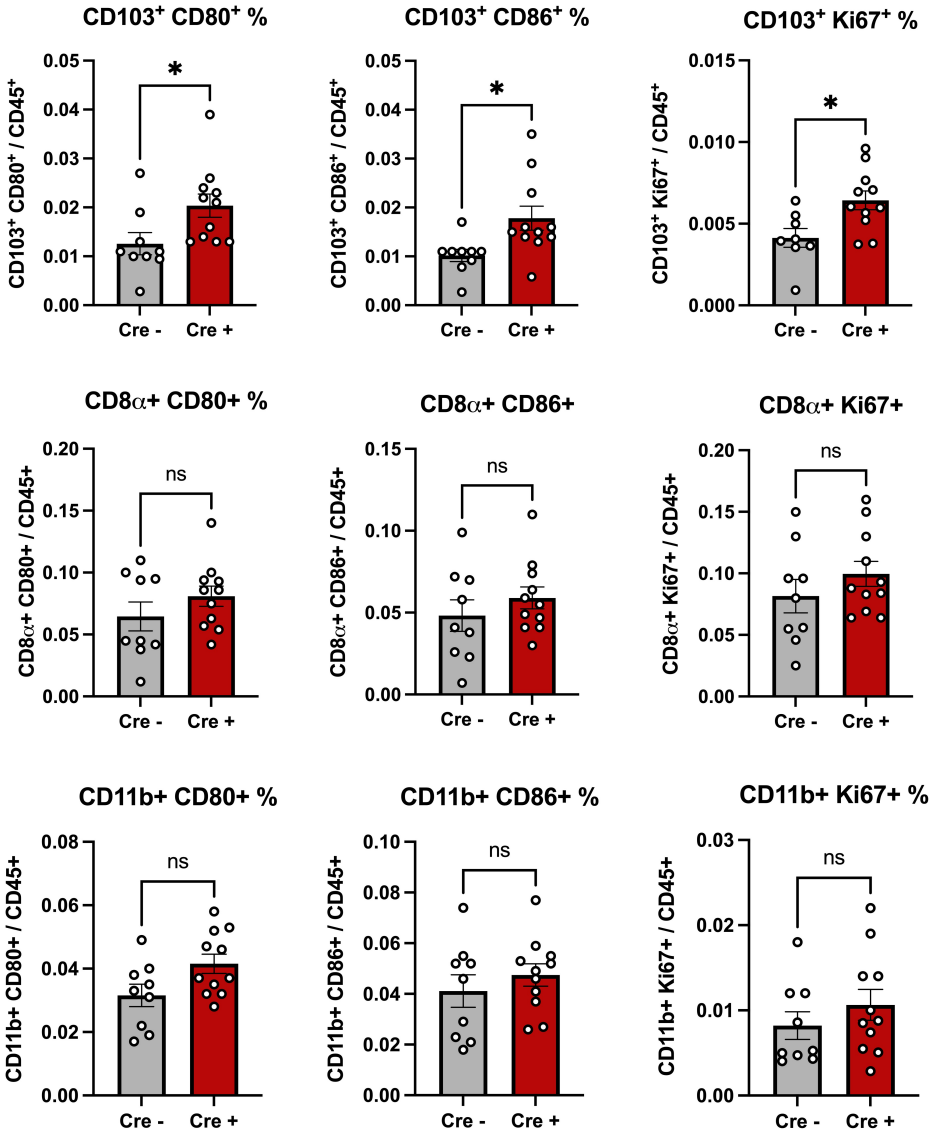

Figure 4.2: CD103$^+$ DCs from PTPN22 cKO mice have an activated phenotype in the tdLNs tumor-bearing mice in the priming phase. DCs in the tdLNs from day 7 tumor-bearing mice were subtyped and profiled for the expression of activation markers ($N \geq 9$ per group). Data are shown as the percentage of total CD45$^+$ cells. Pooled data are plotted from independent experiments ($N = 2$).

of these DCs by examining the percentage of cells positive for the co-stimulatory molecules CD80 and CD86, which are critical for CD8$^+$ T cell activation and maintenance, as well as the proliferation marker Ki67. Accordingly, the expansion of the migratory CD103$^+$ was also accompanied by an increase in the percentage of CD80 and CD86 positive cells as well

as Ki67. On the other hand, neither CD11b$^+$ DCs nor CD8α^+ DCs displayed any changes in their activation profiles or proliferation status (**Figure 4.2**). The overall increase in the number and activation profile of CD103$^+$ DCs in the tdLN is consistent with the improved anti-tumor immune response observed in these mice.

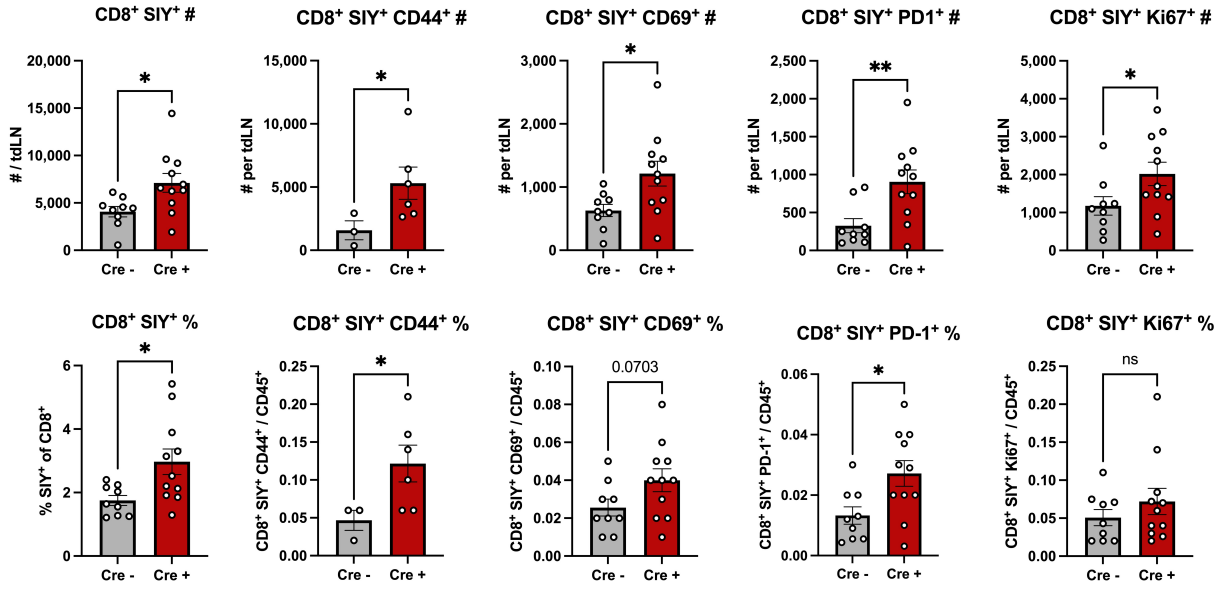

Figure 4.3: Tumor infiltrating, antigen-specific CD8$^+$ T cells from PTPN22 cKO are more numerous and active in the tdLNs during the priming phase. CD8$^+$ sIY$^+$ T cells in the tdLN were profiled for markers of activation and proliferation (N $\geq$ 9 per group). Data are shown as the total number per tdLN and the percentage of total CD45$^+$ cells. Pooled data are plotted from independent experiments (N = 2).

To assess whether this increased number and activation status of CD103$^+$ DCs would translate into increased T cell priming, antigen-specific CD8$^+$ T cells were quantified and characterized in the tdLNs of day 7 tumor-bearing mice through the use of SIY-pentamer staining. In PTPN22 cKO, we observed an increase in both the number and percentage of CD8$^+$ SIY$^+$ T cells, suggesting their preferential expansion in these mice. Moreover, profiling of their activation profile similarly displayed an increased quantity and percentage of cells expressing the activation markers CD44, CD69, and PD-1. Lastly, this expansion of activated CD8$^+$ SIY$^+$ T cells was marked by the increased expression of the proliferation marker Ki67 (**Figure 4.3**).

As a supplemental tool to probe the priming of $CD8^+$ SIY^+ T cells, we utilized the interferon-gamma (IFN-γ) ELISPOT Assay. By harvesting splenocytes from day 7 tumor-bearing mice, $CD8^+$ SIY^+ T cells that have been primed in the tdLNs and entered circulation can be assessed. We found that splenocytes from PTPN22 cKO mice generated more IFN-γ spots as compared to control animals when exposed to the antigenic peptide SIY and not with a control peptide (**Figure 4.4 A** and **B** left panel). We also used the conditioned media from these cultures to test for levels of IL-2 by ELISA. Similarly, splenocytes from PTPN22 cKO mice produced more IL-2 in response to SIY peptide (**Figure 4.4 B** right panel). These results suggest that the increased number and activation status of $CD103^+$ DCs led to a greater activation and expansion of $CD8^+$ SIY^+ T cells.

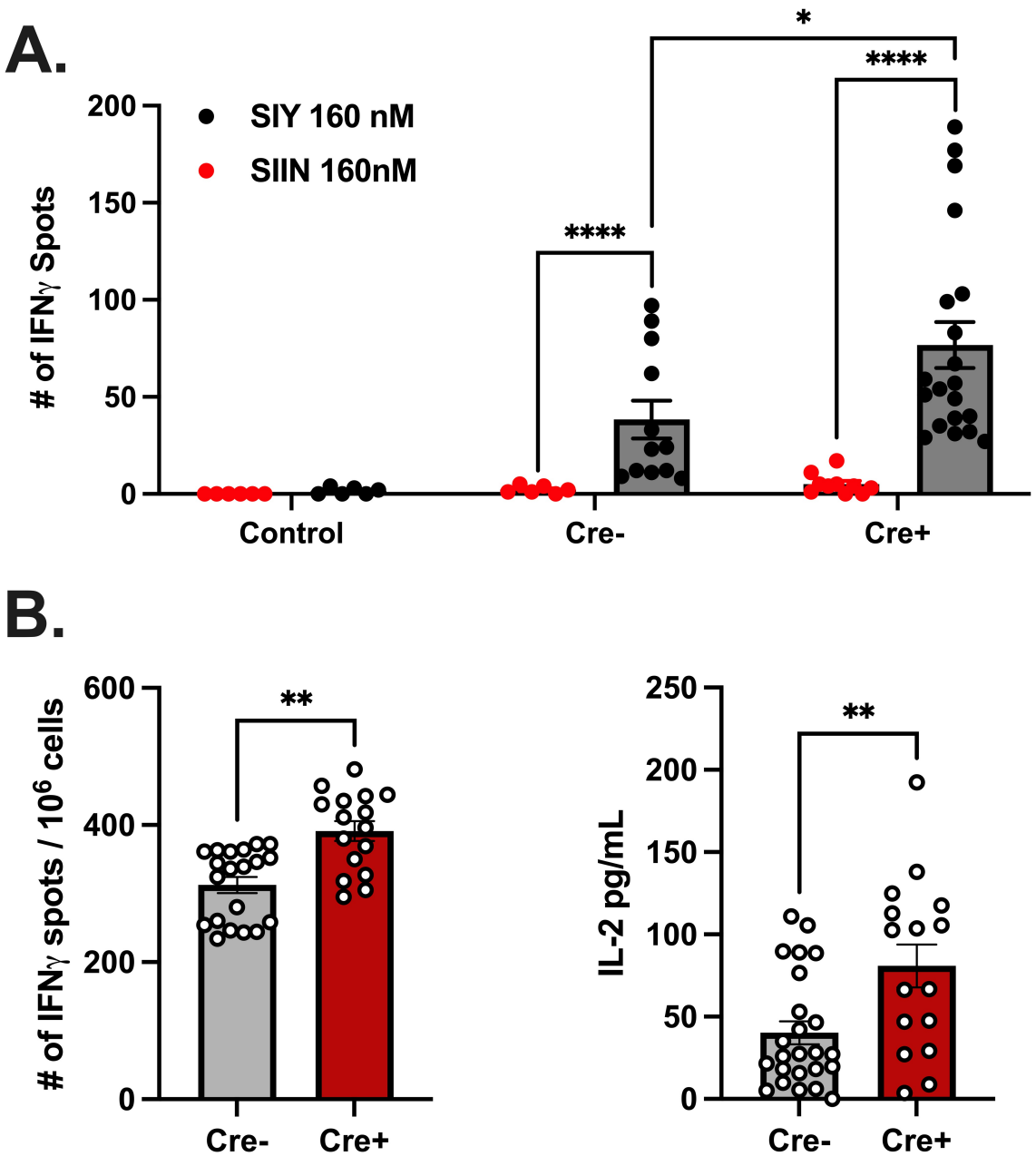

Figure 4.4: PTPN22 cKO mice have superior priming of CD8$^+$ SIY$^+$ T cells. Spleens harvested on day 7 of tumor-bearing PTPN22$^{fl/fl}$ x Cre$^+$ and Cre$^-$ aged-matched litter-mates were used for an IFNγ ELISPOT to assess priming. **(A)** The number of IFNγ spots produced by splenocytes cultured overnight with either cognate SIY peptide or an irrelevant OVA (SIINFEKL) peptide from a single experiment (N $\geq$ 6 per group. **(B)** Pulled data from two independent experiments plotted together showing the number of IFNγ spots and amount of IL-2 via ELISA from conditioned media (N $\geq$ 16 per group).

4.2.2 Bulk RNAseq analysis of intratumoral CD11c$^+$ cells reveals differences in signaling

In order to gain deeper insights into the improved activation properties of DCs upon PTPN22 deletion, RNAseq was performed. Specifically, bulk RNAseq of intratumoral CD11c$^+$ cells was chosen in order to gain more sequencing depth into this rare cellular compartment. In order to achieve this, mice were injected with 1.5 million B16.SIY cells and tumors were harvested at day 20, and CD11c$^+$ were enriched by MACS and then further purified by flow cytometric sorting. Purified intratumoral CD11c$^+$ cells were resuspended in Trizol and stored at -80°C. This was repeated 4 times four times in order to collect sufficient cells for RNAseq (**Figure 4.5**). Day 20 was chosen as the difference in tumor growth becomes appreciable at this point, signifying a biological point of differentiation underlying the observed phenotype. Sequencing was carried out at the University of Chicago Genomics Core. Despite the strong functional phenotype, transcriptional differences were modest between wildtype and PTPN22 cKO DCs (**Figure 4.6**).

Gene set enrichment analysis (GSEA) was used to further probe the data. GSEA takes into account the comparison in the distribution of ranked gene expression differences, providing insight into signaling and biological pathways. This type of analysis is especially useful in this case as it allows us to take into consideration the overall changes in gene expression profiles as opposed to single genes. The analysis focused on biologically relevant gene signatures given the vast and broad catalog of GSEA signatures available to identify meaningful pathways while painting statistical power. **Figure 4.7** shows these results, and **Table 4.1** details the normalized enrichment scores (NES) and adjusted p-values for each signaling pathway.

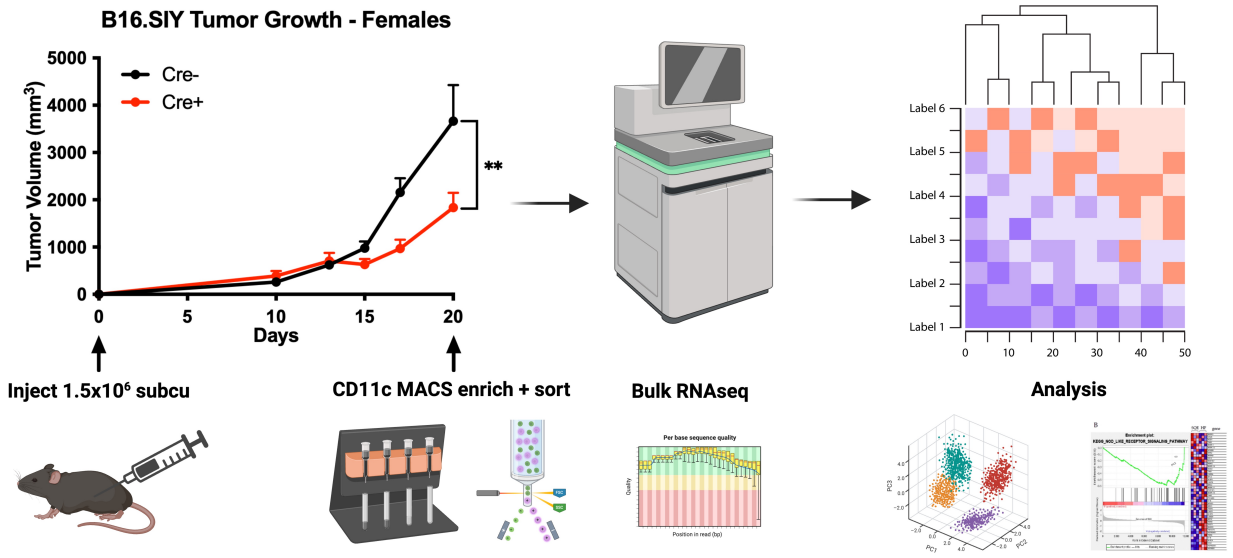

Figure 4.5: Schematic of the experimental layout for bulk RNAseq of intratumoral CD11c$^+$ DCs. Female PTPN22$^{fl/fl}$ x Cre$^+$ and Cre$^-$ aged-matched litter-mates were injected with 1.5 million B16.SIY cells and harvested on day 20. CD11c$^+$ DCs were enriched from tumors via MACS and further purified by flow cytometry sorting based on viability stain, CD45$^+$ CD3$^-$ and CD11c$^+$ MHC II$^+$. The experimental layout was repeated 4 times to obtain a sufficient amount of cells for sequencing (N $\geq$ 20 mice per group, resulting in 6 Cre$^+$ and 8 Cre$^-$ samples for sequencing).

Gene Signature Name	pAdj	NES
GOMF-CHEMOKINE-ACTIVITY	4.16E-05	1-2.2203820077A2
GOBP-LYMPHOCYTE-CHEMOTAXIS	4.16E-05	-2.119682011
GOMF-CCR-CHEMOKINE-RECEPTOR-BINDING	0.000210684	-2.061956638
GOMF-DNA-BINDING-TRANSCRIPTION-REPRESSOR-ACTIVITY	4.16E-05	1.811112123
GOMF-PROTEIN-PHOSPHATASE-BINDING	0.000402824	1.679608323
GOBP-TRANSMEMBRANE-RECEPTOR-PROTEIN-TYROSINE-KINASE-SIGNALING-PATHWAY	0.000245218	1.537811834
GOBP-GENERATION-OF-PRECURSOR-METABOLITES-AND-ENERGY	0.000245218	-1.525724525
GOBP-NEGATIVE-REGULATION-OF-CELL-DIFFERENTIATION	0.000245218	1.508918511
GOBP-NEGATIVE-REGULATION-OF-CELL-POPULATION-PROLIFERATION	0.009504337	1.301325522
GOBP-ENDOCYTOSIS	0.043287671	1.24571892

Table 4.1: Individual values from GSEA analysis.

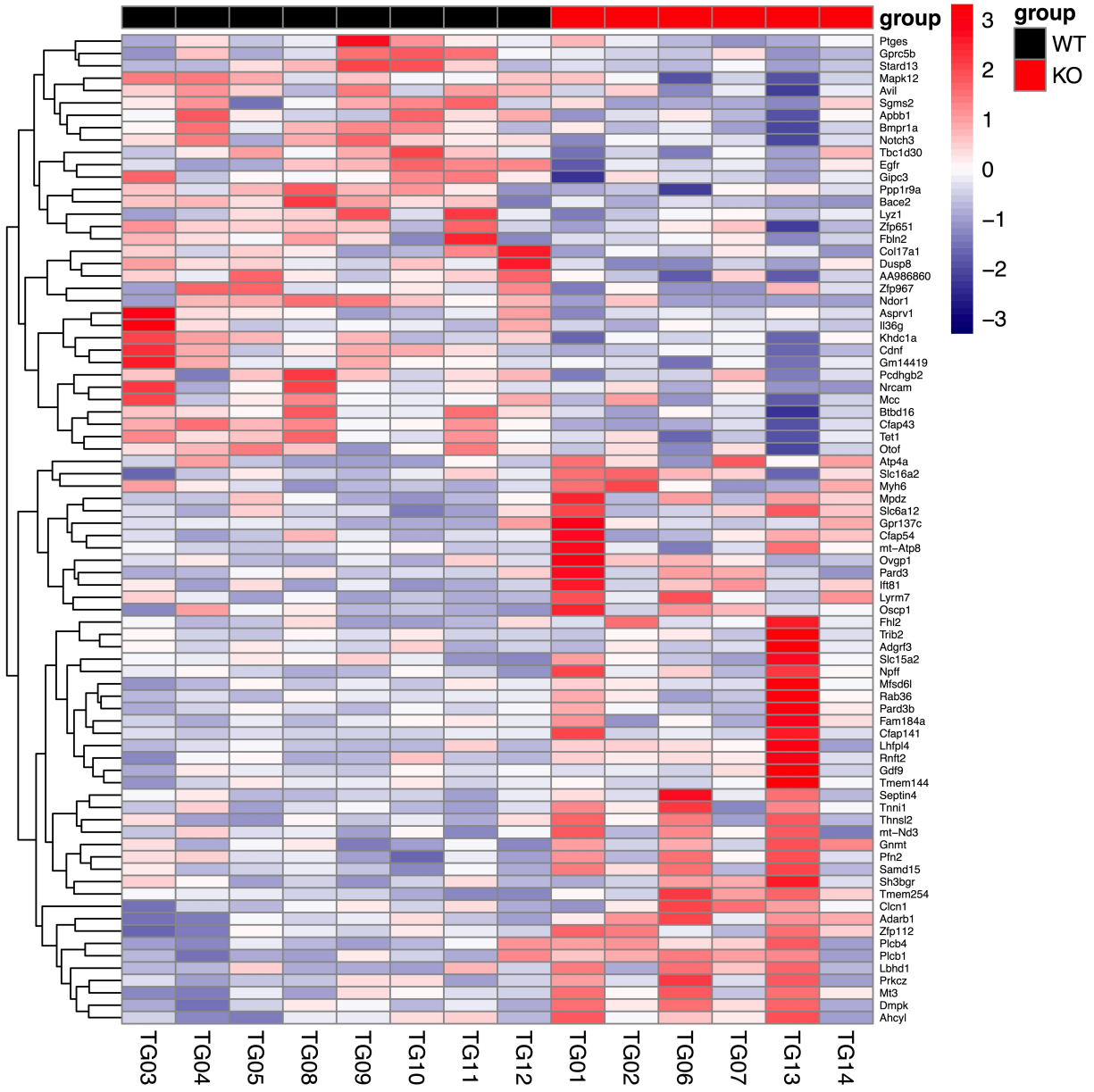

Figure 4.6: Heatmap of differentially expressed genes from RNAseq of intratumoral CD11c$^+$ DCs. Following analysis and normalization of gene expression, the top differentially expressed genes were plotted to compare changes in gene expression between WT and PTPN22 cKO CD11c$^+$ DCs. Relative gene expression is represented by the color gradient where a positive number signifies higher relative expression and a negative number represents decreased relative expression. Data were generated in R.

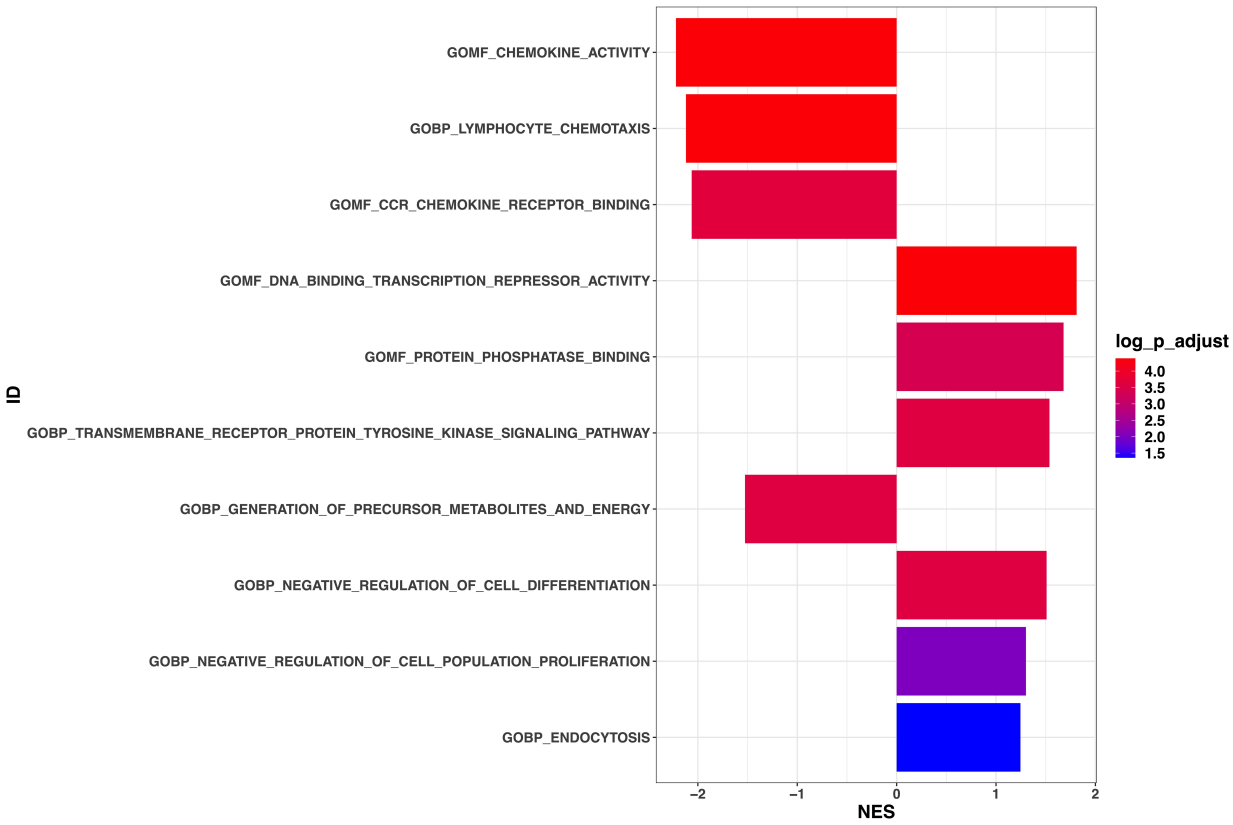

Figure 4.7: Gene signature enrichment analysis from RNAseq. Gene enrichment analysis (GSEA) of biologically relevant pathways was compared between WT and EXP (PTPN22 cKO) samples. The normalized enrichment score (NES) on the x-axis represents the relative enrichment between WT compared to EXP, where positive values represent an enrichment in WT and negative values represent an enrichment in EXP. The color gradient represents the log of the adjusted p-values.

These pathways primarily suggest a more activated phenotype in PTPN22 cKO and an increased regulatory program in wild-type DCs. For example, PTPN22 cKO DCs are enriched for pathways involved in chemokine activity and induction of lymphocyte chemotaxis. This suggests that PTPN22 cKO DCs may be more capable of recruiting other cells (such as $CD8^+$ T cells) for cognate interactions. In contrast, WT DCs were enriched for negative regulatory pathways, such as negative regulators of proliferation and differentiation. WT DCs were also enriched for genes related to endocytosis, a process by which DCs take up and sample antigens in their environment. Endocytic activity is decreased upon DC maturation, and high endocytic potential is associated with DC immaturity [164, 165, 166]. Together, these data suggest that PTPN22 KO DCs are shifted to a more mature state geared towards T cell activation. These results align with the higher levels of MHC II and co-stimulatory markers CD80 and CD86 observed.

4.2.3 Intratumoral dendritic cell accumulation is driven by the preferential expansion of tumor antigen-loaded cells

A greater number of activated DCs in PTPN22 cKO mice suggested the possibility that there was greater functionality of those cells from the perspective of antigen uptake and/or processing and presentation in the context of class I MHC molecules. To begin to address this question, we took advantage of the B16.SIY model, as these cells stably express dsRed linked to the SIY antigen. The linked expression of dsRed to this model antigen allows us to identify which DCs in the tumor are taking up tumor-derived material within the TME by dsRed fluorescence. A schematic highlighting this detection is shown in **Figure 4.8**. We further employed the use of the proliferation marker Ki67 along with the apoptosis marker activated-Caspase3 (aCasp3). The use of these markers along with dsRed thus allows for the identification of antigen-loaded DCs while simultaneously assaying their proliferation and apoptosis in order to gain further insights into the maintenance of this cellular compartment.

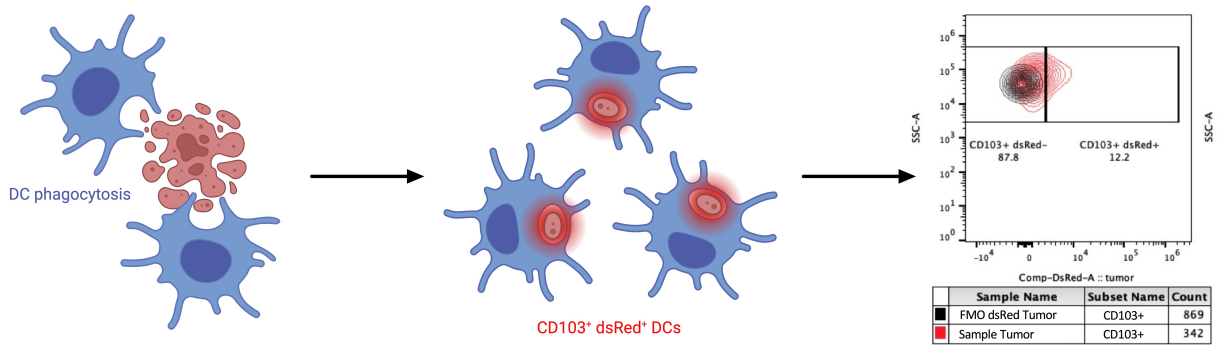

Figure 4.8: Schematic representing DCs loaded with tumor-derived material and their identification via flow cytometry. Female PTPN22$^{fl/fl}$ x Cre^{+} and Cre^{-} aged-matched litter-mates were injected with 1 million B16.SIY cells and harvested on day 20. Three independent experiments were performed (N $\geq$ 20 per group).

For this, mice were injected with B16.SIY cells and tumors were harvested on day 20. This time point was chosen to represent the effector phase prior to endpoint. At this time point, intratumoral DCs were more numerous per gram of tumor and represented a greater

percentage of all tumor-infiltrating immune cells. This was particularly due to an increase in $CD103^+$ DCs that were more numerous per gram of tumor and trended towards increasing in percentage as well. No trends or significant changes were observed in the $CD11b^+$ DC compartment (**Figure 4.9**). The activation profile of DCs was again determined by the expression of the co-stimulatory markers CD80 and CD86. Similar to prior experiments, there was an increase in the number and percentage of $CD103^+$ $CD80^+$ DCs and $CD103^+$ $CD86^+$ DCs in PTPN22 cKO animals. $CD11b^+$ DCs showed similar trends, but only the percentage of $CD11b^+$ $CD86^+$ DCs was significantly increased in PTPN22 cKO mice. Lastly, we checked the MFI of these markers to determine if there was greater expression per cell. However, the MFI of these co-stimulatory markers was the same across both DC types in WT and PTPN22 cKO mice (**Figure 4.10**). Differences in the number and percentage of DCs and active DCs, but not the amount of activation markers per cell, suggested potential differences in the dynamics of these populations.

Because of this, we then examined markers of proliferation and apoptosis to gain further insights into the dynamics of these cellular subsets. $CD103^+$ DCs were increased in the number and percentage of cells expressing Ki67. However, there were no changes in Ki67 expression in $CD11b^+$ DCs. There were also no changes in the number or percentage of cells expressing aCasp3, suggesting similar rates of apoptosis in WT and PTPN22 cKO mice. The ratio of the number of cells positive for Ki67 over the number of cells positive for aCasp3 was used to interrogate the overall dynamics. Thus, deletion of PTPN22 appears to support greater proliferation of $CD103^+$ DCs within the TME (**Figure 4.11**).

To assess the capacity for uptake of tumor-derived material, we used the acquisition of dsRed. In fact, the number and percentage of $CD103^+$ DCs positive for dsRed were increased in PTPN22 cKO mice. The MFI of dsRed was used to quantify how much tumor-derived material was present per cell. Interestingly, WT and PTPN22 cKO DCs had similar amounts of dsRed (**Figure 4.12**). We further checked the levels of CD80 and CD86 to

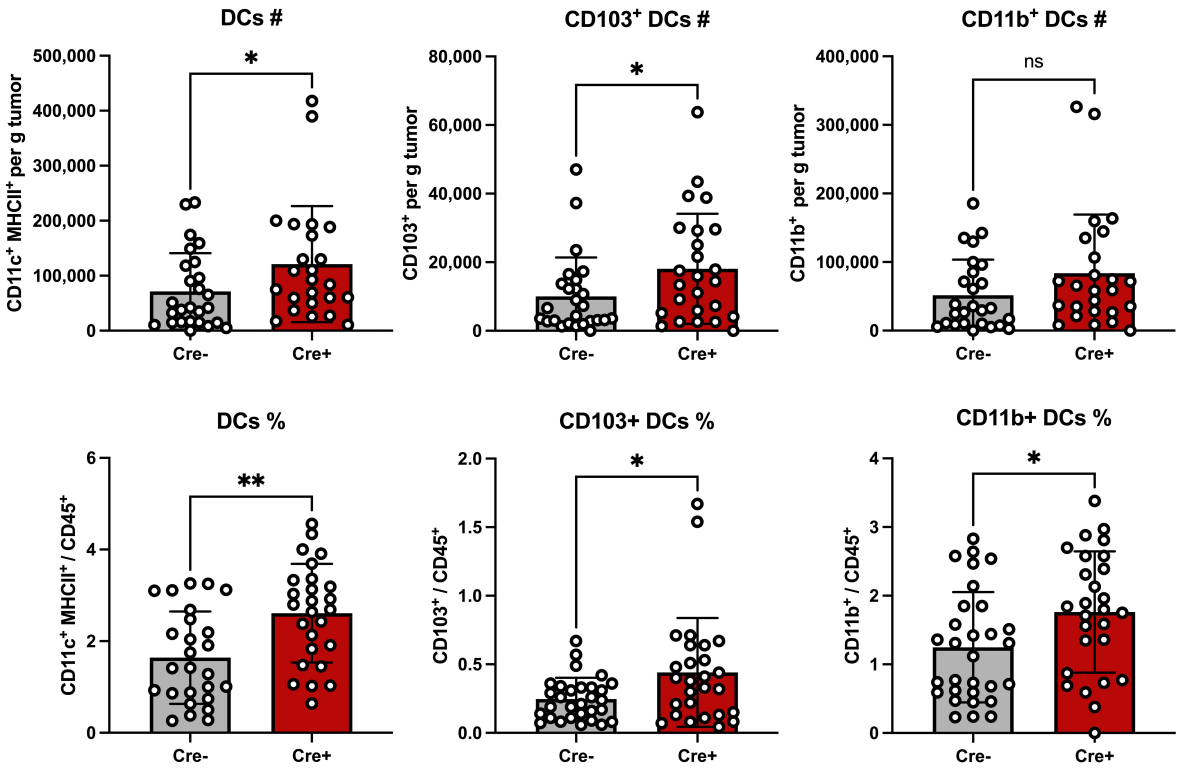

Figure 4.9: Intratumoral DCs were increased in PTPN22 cKO mice in the effector phase. Intratumoral DCs from day 20 tumor-bearing mice were quantified by number per gram of tumor and as the percentage of total $CD45^+$ cells. Pooled data from three independent experiments are plotted ($N \geq 20$ per group).

profile the activation of $dsRed^+$ DCs. In this case, there was a strong increase in the number and percentage of $CD103^+$ $dsRed^+$ $CD80^+$ DCs and $CD103^+$ $dsRed^+$ $CD86^+$ DCs. The number and percentage of $CD11b^+$ $dsRed^+$ $CD86^+$ DCs was also increased in PTPN22 cKO mice, though to a lesser extent than in $CD103^+$ $dsRed^+$ DCs, and the percentage of $CD11b^+$ $dsRed^+$ $CD80^+$ DCs did not reach significance. Lastly, as in all $CD103^+$ and $CD11b^+$ DCs, the MFI of CD80 and CD86 were not any different in the $CD103^+$ $dsRed^+$ and $CD11b^+$ $dsRed^+$ DCs of PTPN22 cKO mice (**Figure 4.13**). These data indicate that there is an increase in the number of activated, antigen-loaded DCs, especially of the $CD103^+$ subset, in PTPN22 cKO mice. However, the amount of uptake of tumor-derived material per DC was comparable.

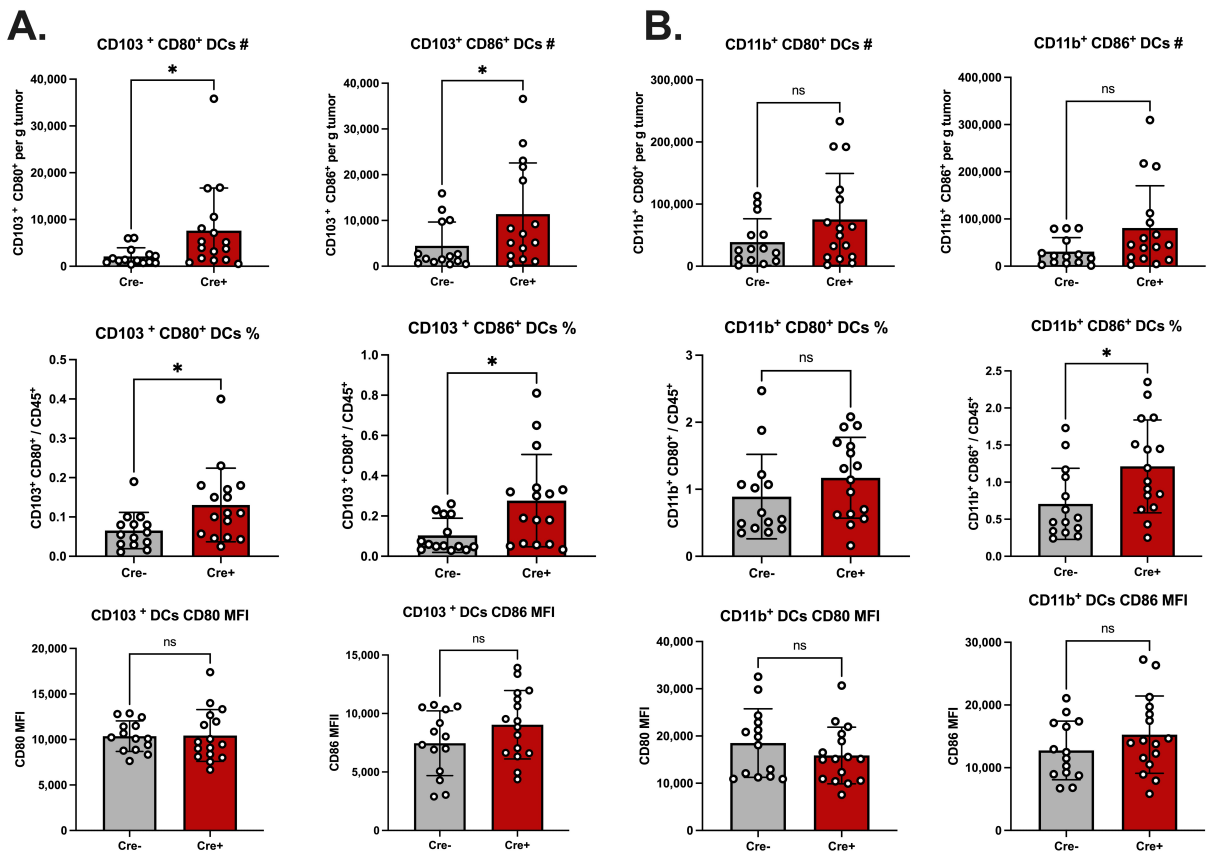

Figure 4.10: More activated CD103$^+$ DCs are present in the tumors of PTPN22 cKO mice in the effector phase. Intratumoral DCs from day 20 tumor-bearing mice were subtyped and profiled for activation markers. The number, percentage, and MFI of CD80 and CD86 in **(A)** CD103$^+$ DCs and **(B)** CD11b$^+$ DCs. Pooled data from two independent experiments are plotted (N $\geq$ 14 per group).

To test whether changes in population dynamics again drove this increase in number and percentage, we checked for the expression of Ki67 and aCasp3 in dsRed$^+$ DCs. Similar to what we observed in the general CD103$^+$ and CD11b$^+$ DC subsets, CD103$^+$ dsRed$^+$, but not CD11b$^+$ dsRed$^+$, DCs had a preferential expansion as measured by the ratio of cells positive for Ki67 to those positive for aCasp3 (**Figure 4.14**). To address whether there was a relationship between the acquisition of tumor-derived material and activation status, we checked the correlation of the co-stimulatory markers CD80 and CD86 with the acquisition of dsRed. Linear regressions of these correlations showed that the relationship between

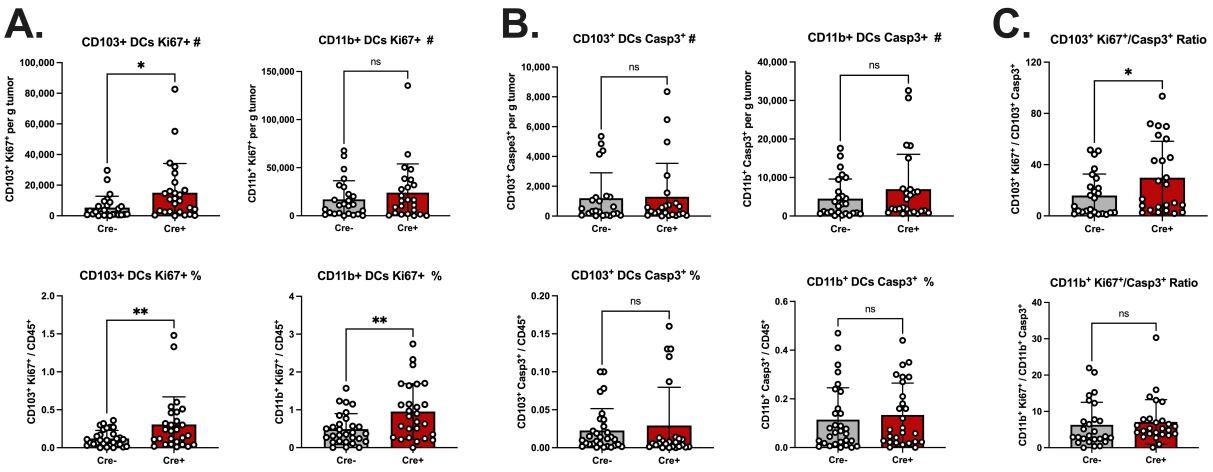

Figure 4.11: CD103$^+$ but not CD11b$^+$ DCs show a preference towards proliferation and expansion. Intratumoral DCs from day 20 tumor-bearing mice were subtyped and profiled for activation markers. The number and percentage of **(A)** Ki67 and **(B)** activated-Caspase 3 (aCasp3) in CD103$^+$ DCs and CD11b$^+$ DCs. **(C)** The ratio of the number of Ki67$^+$ cells per gram of tumor divided by the number of aCasp3$^+$ cells per gram of tumor in CD103$^+$ and CD11b$^+$ DCs. Pooled data from three independent experiments are plotted (N $\geq$ 20 per group).

dsRed acquisition and co-expression of CD80$^+$ CD86$^+$ was stronger in CD103$^+$ DCs than in CD11b$^+$ DCs, though both correlations were significant (**Figure 4.15**). This confirms that the amount of tumor-derived material acquired by DCs correlates with their expression of the co-stimulatory markers.

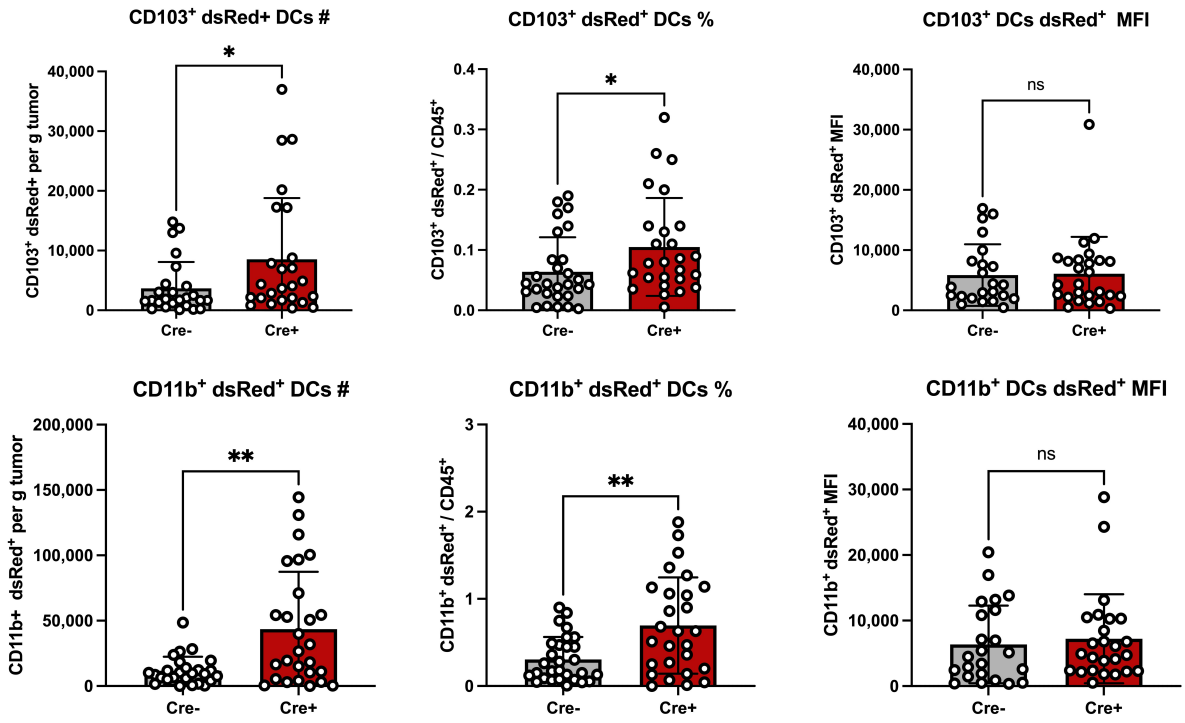

Figure 4.12: PTPN22 cKO mice have more intratumoral, antigen-loaded DCs. Intratumoral DCs were subtyped and assayed for the presence of tumor-derived material (dsRed). Data are shown as the number per gram of tumor, percentage of $CD45^+$ cells, and MFI. Pooled data from three independent experiments are plotted ($N \geq 20$ per group).

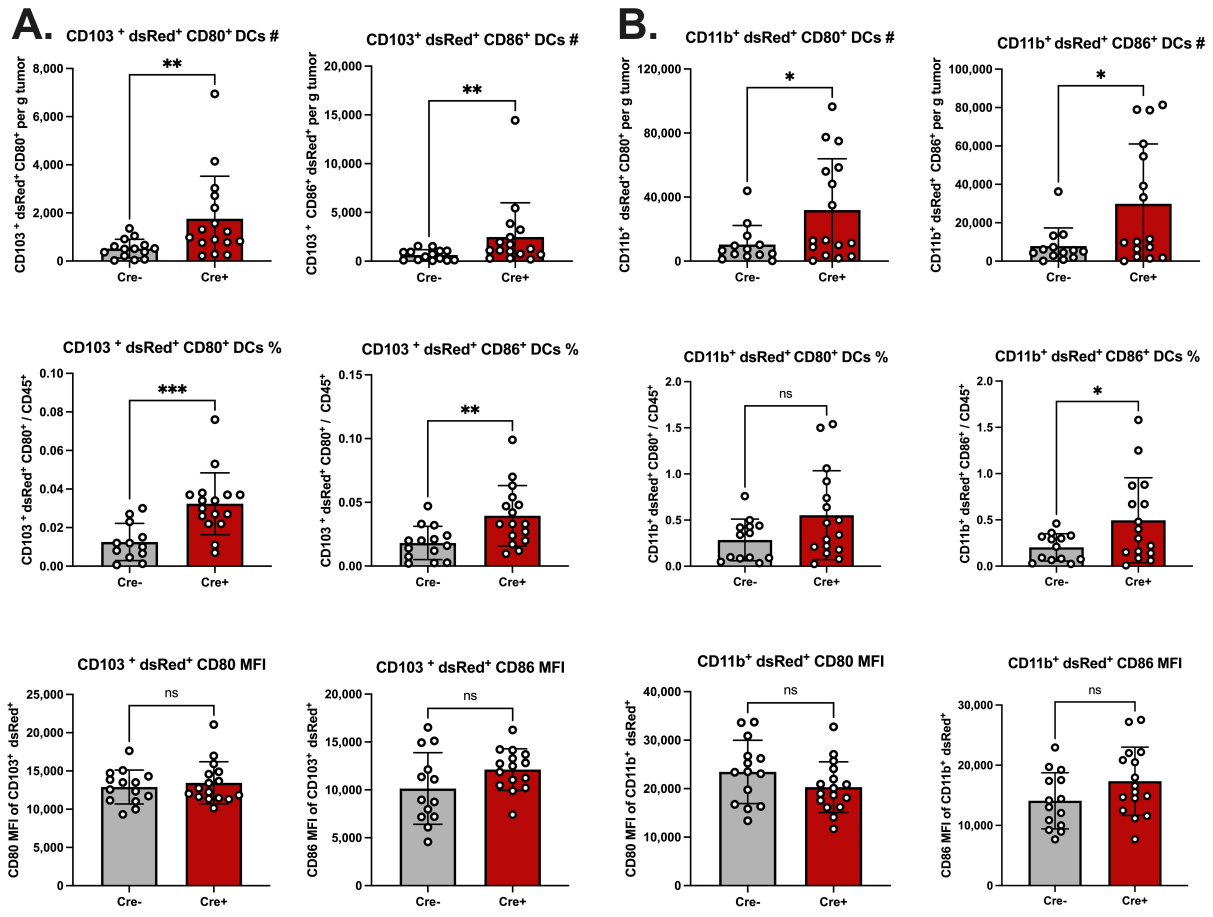

Figure 4.13: PTPN22 cKO mice have an increase of activated, antigen-loaded CD103$^+$ DCs. The number, percentage, and MFI of CD80 and CD86 in **(A)** CD103$^+$ dsRed$^+$ DCs and **(B)** CD11b$^+$ dsRed$^+$ DCs. Pooled data from two independent experiments are plotted (N $\geq$ 14 per group).

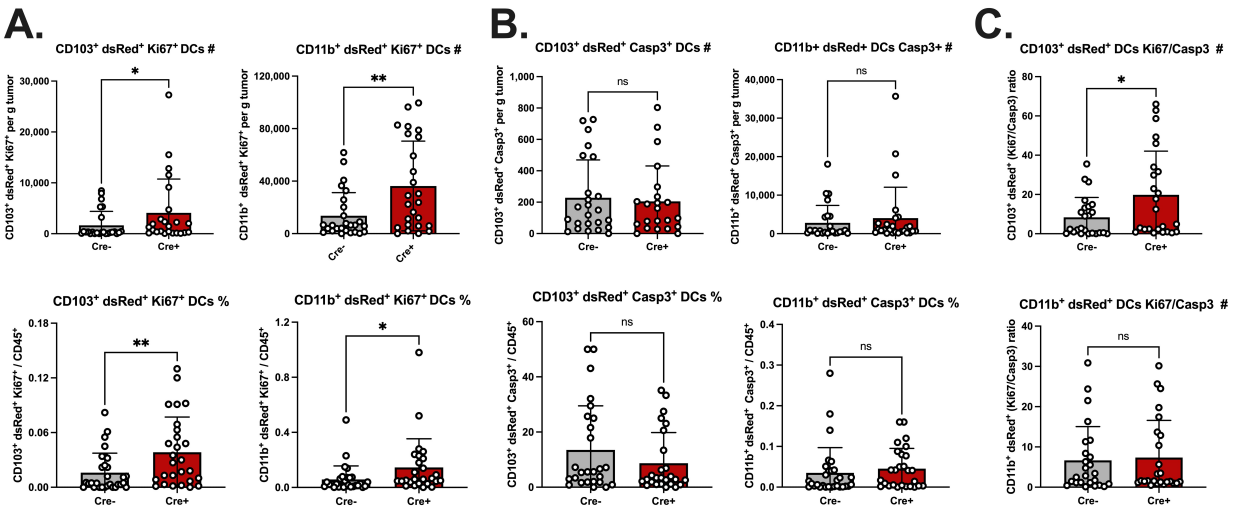

Figure 4.14: Antigen-loaded CD103$^+$ DCs, but not antigen-loaded CD11b$^+$ DCs, show a preference for proliferation and expansion in PTPN22 cKO mice. The number and percentage of **(A)** Ki67 and **(B)** activated-Caspase 3 (aCasp3) in CD103$^+$ dsRed$^+$ DCs and CD11b$^+$ dsRed$^+$ DCs. **(C)** The ratio of the number of Ki67$^+$ cells per gram of tumor divided by the number of aCasp3$^+$ cells per gram of tumor in CD103$^+$ dsRed$^+$ and CD11b$^+$ dsRed$^+$ DCs. Pooled data from three independent experiments are plotted (N $\geq$ 20 per group).

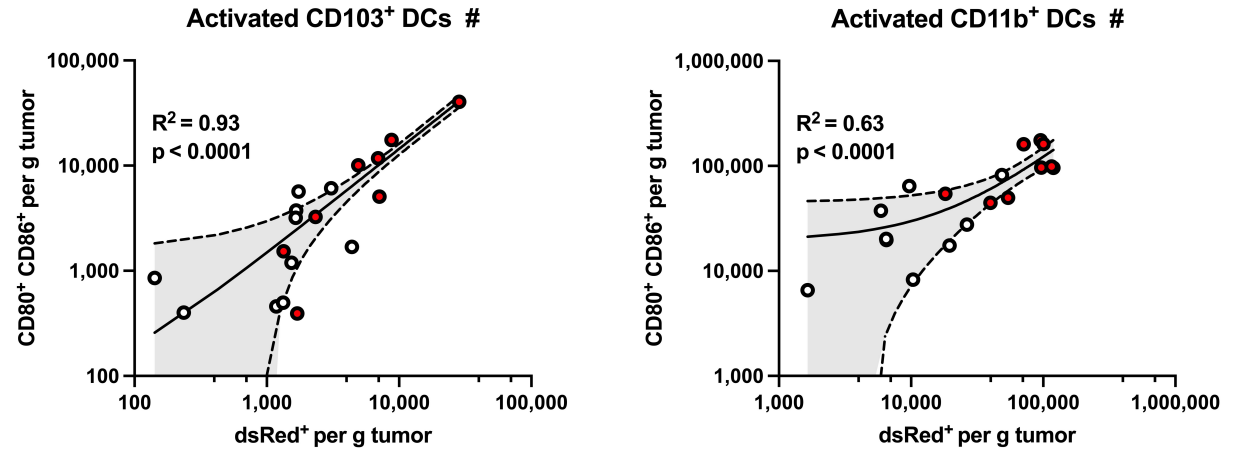

Figure 4.15: Aquisition of tumor-derived material is correlated with co-expression of CD80 and CD86. The number of CD103$^+$ DCs and CD11b$^+$ Dcs are plotted showing the relationship between CD80$^+$ CD86$^+$ and dsRed$^+$. Pooled data from two independent experiments are plotted (N $\geq$ 14 per group).

4.2.4 CD11c$^+$ cells lacking the PTPN22 process and present more antigen in vitro

Although the amount of uptake of tumor-derived material was comparable in wildtype and PTPN22-deleted DCs on a per-cell basis, it was important to additionally address the level of processing and presentation of peptide antigen presented by class I MHC molecules. For these experiments, we took advantage of the model antigen OVA, which has tools available to probe its acquisition, processing, and presentation on MHC I. We first utilized OVA conjugated to the fluorophore AF647 to measure the general uptake of antigen in CD11c$^+$ isolated from the spleens of naive mice. WT and PTPN22 cKO DCs showed similar levels of OVA-AF647 uptake across a range of concentrations (**Figure 4.16**).

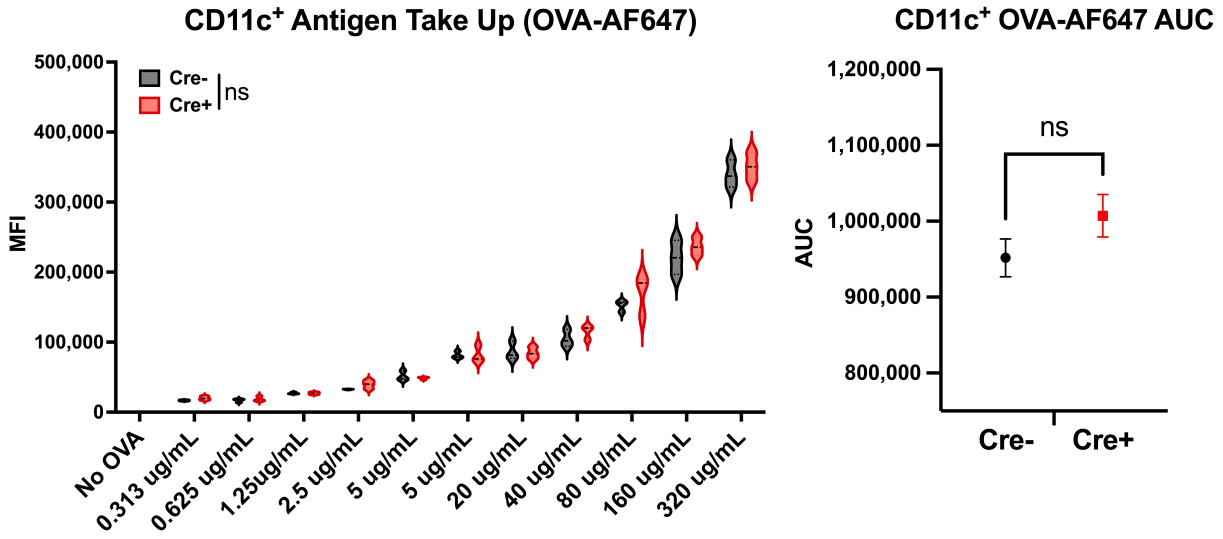

Figure 4.16: CD11c$^+$ cells from WT and PTPN22 cKO mice take up equal amounts of antigen in vitro. Spleens from PTPN22$^{fl/fl}$ x Cre$^+$ and Cre$^-$ aged-matched litter-mates were harvested and purified by MACS. Enriched CD11c$^+$ were incubated with increasing amounts of OVA-AF647 for 2 hours. Uptake of the substrate was measured by the normalized MFI. The area under the curve (AUC) was also calculated and compared for each dose-response. Each dose was run in triplicate, and the experiment was repeated twice in male and female mice.

Next, we examined the DQ-OVA substrate that is hydrolyzed under acidic conditions

only found in the lysosome; upon hydrolysis, this substrate fluoresces, allowing for the quantification of antigen processing of a given cell. Incubation of $CD11c^+$ DCs with DQ-OVA showed an increase in the MFI of signal across a range of concentrations in PTPN22 cKO DCs as well as the overall area under the curve (AUC) (**Figure 4.17**). This prompted us to ask whether there was a difference in antigen processing in both major subtypes of $CD11c^+$ DCs. Both the $CD103^+$ and $CD11b^+$ DCs of PTPN22 cKO mice displayed greater antigen processing per cell assessed by the MFI of hydrolyzed DQ-OVA (**Figure 4.18**). These results suggest that $CD11c^+$ from PTPN22 cKO mice took up equal amounts of antigen in comparison to WT $CD11c^+$ DCs, but processed antigens to a greater extent.

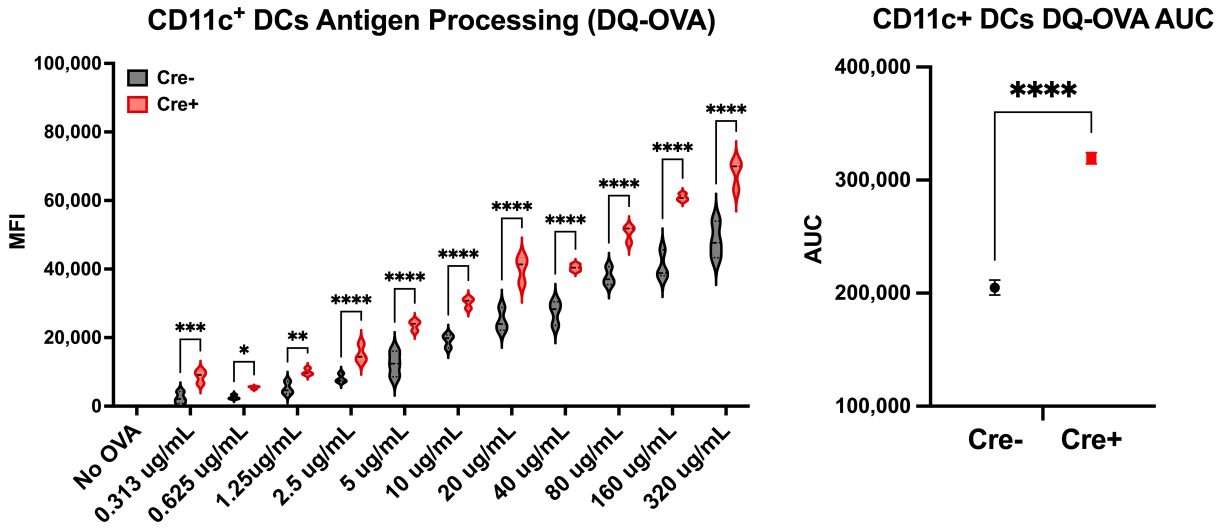

Figure 4.17: $CD11c^+$ DCs from PTPN22 cKO mice process more antigen in vitro. Spleens from $PTPN22^{fl/fl}$ x Cre^+ and Cre^- aged-matched litter-mates were harvested and purified by MACS. Enriched $CD11c^+$ were incubated with increasing amounts of DQ-OVA for 2 hours. Antigen processing was measured by the normalized MFI produced upon hydrolyzation of the DQ-OVA substrate under acidic conditions (lysosome). The area under the curve (AUC) was also calculated and compared for each dose-response. Each dose was run in triplicate, and the experiment was repeated four times in both male and female mice.

To measure the amount of processed antigenic peptide presented by class I MHC, we utilized a monoclonal antibody (mAb) specific for OVA peptide 257-264 bound to H2-K^b. Following the incubation with DQ-OVA, DCs were stained with OVA-H2k^b. In this case,

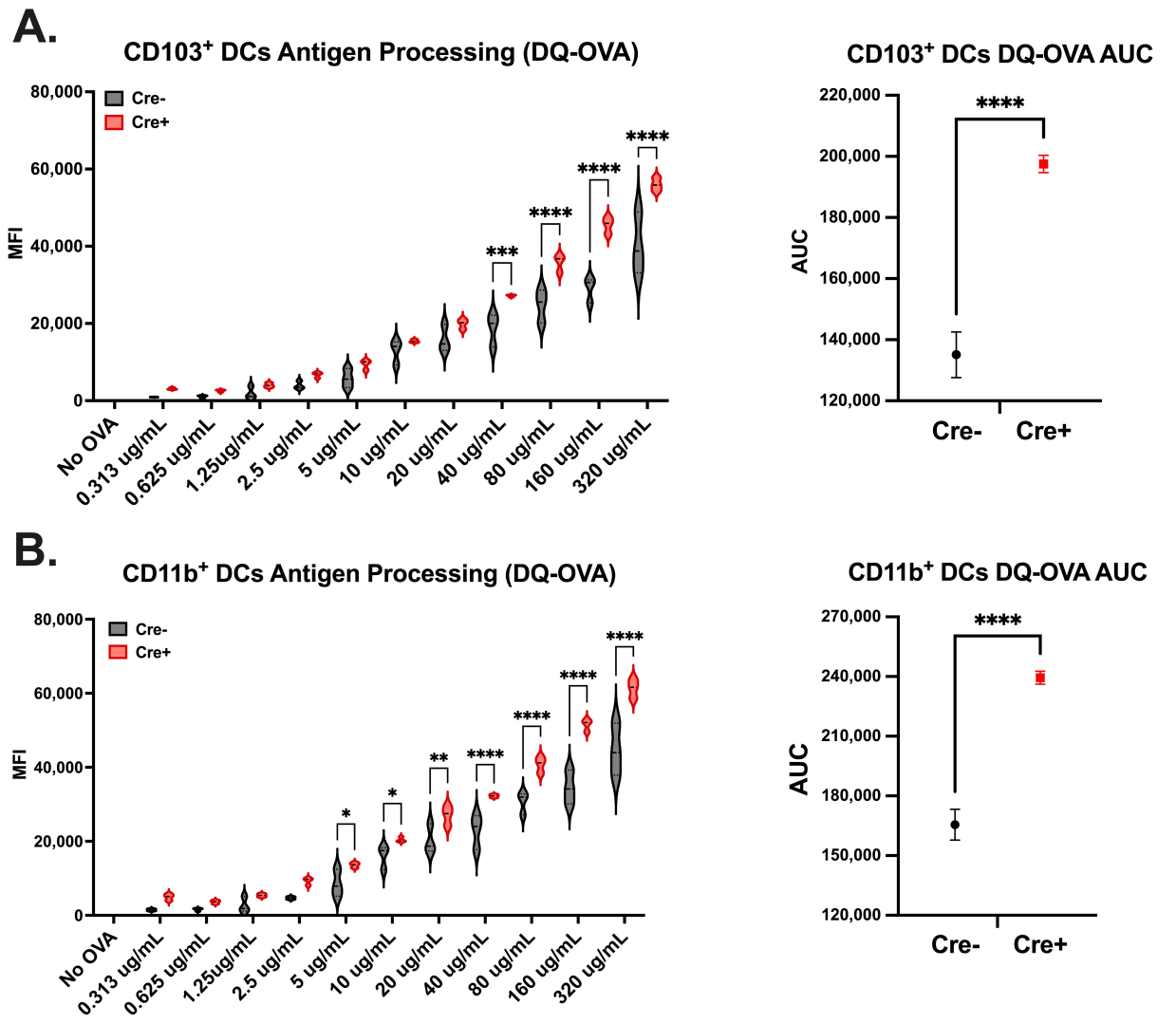

Figure 4.18: Both CD103$^+$ and CD11b$^+$ DCs from PTPN22 cKO mice process more antigen in vitro. Spleens from PTPN22$^{fl/fl}$ x Cre$^+$ and Cre$^-$ aged-matched litter-mates were harvested and purified by MACS. Enriched CD11c$^+$ were incubated with increasing amounts of DQ-OVA for 2 hours. Antigen processing was measured by the normalized MFI produced upon hydrolyzation of the DQ-OVA substrate under acidic conditions (lysosome). The area under the curve (AUC) was also calculated and compared for each dose-response. CD11c$^+$ DCs were subtyped by **(A)** CD103$^+$ and **(B)** CD11b$^+$ for analysis. Each dose was run in triplicate, and the experiment was repeated four times in both male and female mice.

the percentage of cells positive for OVA-H2k^b was only increased in CD103$^+$ DCs but not in CD11b$^+$ DCs (**Figure 4.19**). These results are in accordance with the notion that CD103$^+$

are specialized in presenting antigen on MHC I while CD11b^{+} primarily present antigen on MHC II. We further confirmed this by comparing the amount of OVA-H2k^{b} positive cells in CD103^{+} and CD11b^{+} DCs. This comparison clearly showed the increase in the percentage of OVA-H2k^{b} positive CD103^{+} cells, but not CD11b^{+} cells (**Figure 4.20 A**) Lastly, we tested the correlation between DQ-OVA MFI and OVA-H2k^{b} positive CD103^{+} cells (**Figure 4.20 B**). This positive correlation confirmed the linear relationship of CD103^{+} where the antigen is processed and then presented on MHC I.

Taken together, these results indicate that PTPN22 cKO CD103^{+} DCs take up equal amounts of antigen as WT CD103^{+} DCs but are superior at processing antigen, leading to an increased percentage of cells expressing mature peptide-MHC complexes on the surface.

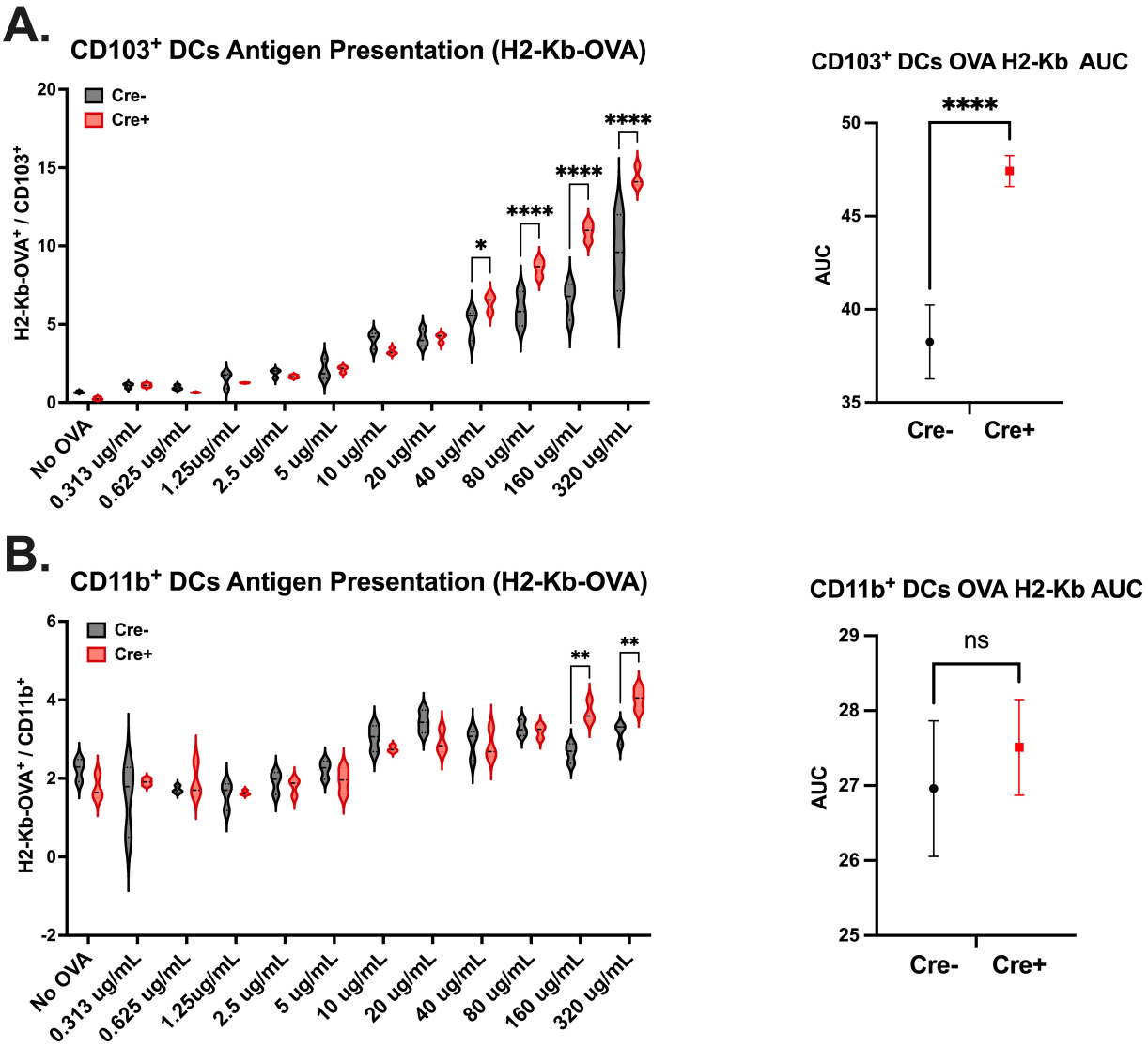

Figure 4.19: CD103$^+$ but not CD11b$^+$ DCs from PTPN22 cKO mice present more antigen on MHC I. Spleens from PTPN22$^{fl/fl}$ x Cre$^+$ and Cre$^-$ aged-matched litter-mates were harvested and purified by MACS. Enriched CD11c$^+$ were incubated with increasing amounts of DQ-OVA for 2 hours. Antigen presentation was measured by the percentage of cells positive for OVA-H2Kb staining. The area under the curve (AUC) was also calculated and compared for each dose-response. CD11c$^+$ DCs were subtyped by **(A)** CD103$^+$ and **(B)** CD11b$^+$ for analysis. Each dose was run in triplicate, and the experiment was repeated four times in both male and female mice.

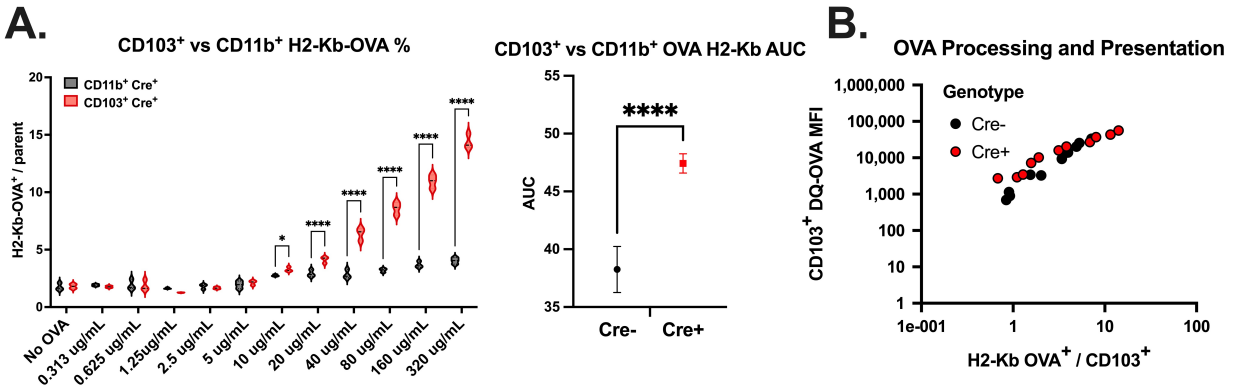

Figure 4.20: Only CD103$^+$ DCs present antigen on MHC I in response to antigen pulsing. Spleens from PTPN22$^{fl/fl}$ x Cre$^+$ and Cre$^-$ aged-matched litter-mates were harvested and purified by MACS. Enriched CD11c$^+$ were incubated with increasing amounts of DQ-OVA for 2 hours. Antigen presentation was measured by the percentage of cells positive for OVA-H2Kb staining. The area under the curve (AUC) was also calculated and compared for each dose response. **(A)** CD103$^+$ and CD11b$^+$ were compared for their ability to present antigen on MHC I in response to increasing amounts of OVA peptide. **(B)** Antigen processing correlates positively with H2Kb-OVA presentation in CD103$^+$ DCs. Each dose was run in triplicate, and the experiment was repeated four times in both male and female mice.

4.2.5 PTPN22 is a negative regulator of Flt3L mediated DC proliferation

Experiments utilizing OVA substrates in vitro shed light on the potential regulation of PTPN22 on antigen processing in DCs. However, altered antigen encounter does not explain why intratumoral PTPN22 cKO DCs were preferentially expanding. We thus investigated potential growth factors that might be mediating DC proliferation. Flt3-ligand (Flt3L) is a critical growth factor for DC development and drives DC proliferation in vivo [167, 168]. This led us to ask if perhaps loss of PTPN22 might increase sensitivity to FLT3L in the TME. We first used single-cell RNAseq (scRNAseq) data from MC38.SIY tumors from our laboratory to probe whether Flt3 and Flt3L are expressed by cells within the TME. Interestingly, the $CD103^+$ DC cluster had the highest expression of Flt3, with pDCs also expressing Flt3 at high levels. Moreover, $CD8^+$ T cells were amongst the cells with the highest expression of FLT3L (**Figure 4.21 A** and **B**). This is in keeping with recent work from our laboratory showing that $CD8^+$ T cells and Batf3-lineage DCs preferentially cluster in the TME. In order to test whether PTPN22 deficiency could impact DC proliferation in response to Flt3L, we isolated splenic and lymph node-derived DCs from Cre^+ and Cre^- mice and stimulated them with soluble Flt3L in vitro. Indeed, PTPN22 cKO DCs showed augmented proliferation as measured by intracellular Ki67 staining when treated with 100ng/mL of soluble Flt3L in vitro m(**Figure 4.21 C**). These experiments suggest that augmented Flt3 signaling is likely contributing to the greater expansion of PTPN22 cKO DCs in the TME. Moreover, these experiments also suggest that PTPN22 negatively regulates multiple biological processes in DCs.

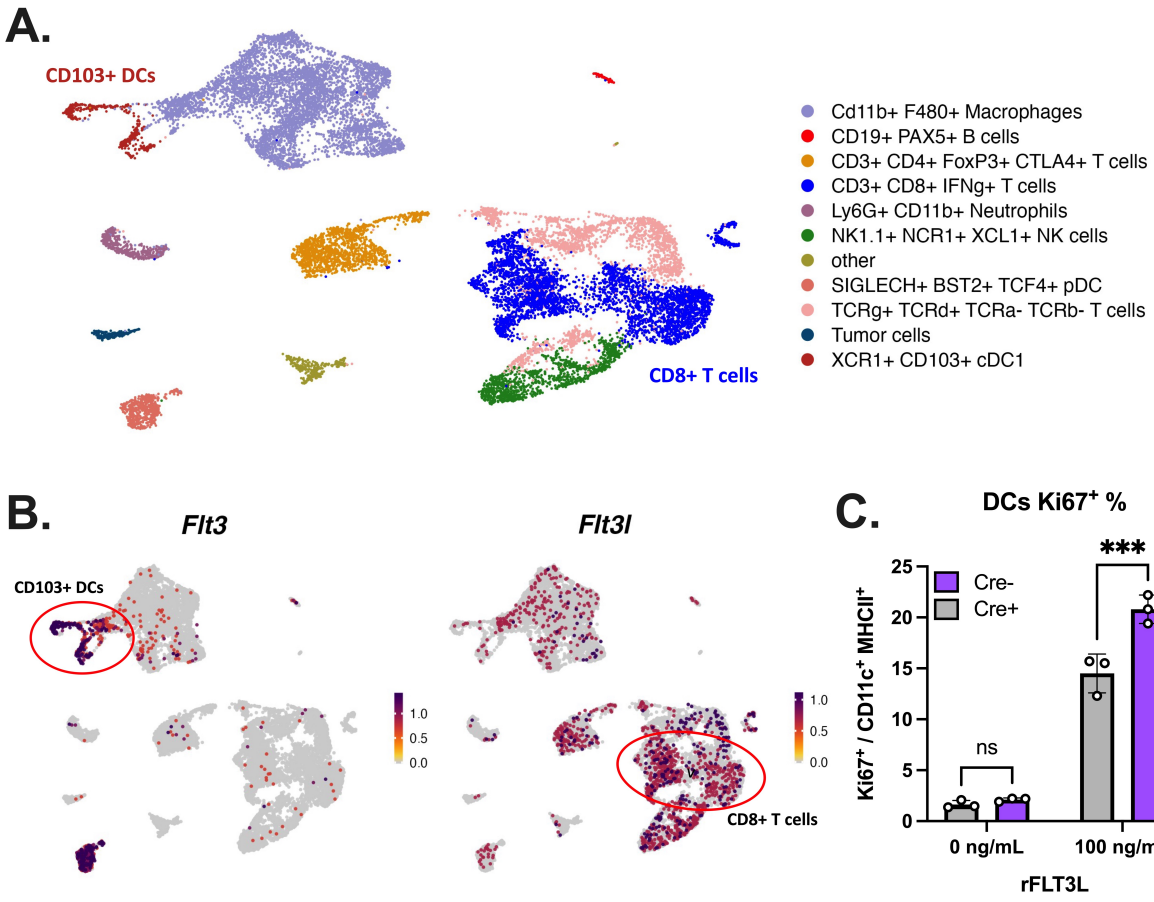

Figure 4.21: CD11c^{+} DCs have increased sensitivity to FLT3L stimulation in vitro. scRNAseq data were used to test for the expression FLT3 and FLT3L in MC38.SIY tumors. **A** UMAP of cell clusters and **B** expression of FLT3 and FLT3L. **C** Spleens and lymph nodes (inguinal and axillary) from PTPN22$^{fl/fl}$ x Cre^{+} and Cre^{-} aged-matched littermates were harvested and purified by MACS. Enriched CD11c^{+} cells were incubated with soluble Flt3L for 48 hours. Response to Flt3L was measured by the percentage of cells positive for Ki67. Each dose was run in triplicate. Data are representative of two independent experiments in male and female mice.

4.2.6 Deletion of PTPN22 in the CD11c$^+$ compartment improves anti-PD-L1-based therapy

Given the increased activation properties of DCs in PTPN22 cKO mice, as well as the increased number of antigen-specific CD8$^+$ T cells, it was of interest to investigate whether anti-PD-L1 checkpoint blockade therapy might be more effective. Blockade of the PD-L1/PD-1 axis has been shown largely to drive re-invigoration of activated T cells already in the TME [169, 170]. Further, DCs have been shown to be important for the efficacy of checkpoint blockade [154, 171]. We first tested aPD-L1 treatment on mice bearing B16.SIY tumors. In this model PBS treated PTPN22 cKO animals displayed improved tumor control in comparison to PBS treated WT animals. Anti-PD-L1 therapy was already quite efficacious in WT mice, and the PTPN22 cKO context only generated modestly improved tumor control. However, the survival of PTPN22 cKO mice was significantly improved with the combination approach (**Figure 4.22 A**). We also tested this intervention in the MC38.SIY model, yet this more immunogenic tumor showed maximal benefit with anti-PD-L1 alone (**Figure 4.22 B**).

Realizing that we needed to test potential synergy in a less immunogenic system, MC38 parental tumors lacking the expression of model antigens were used. In this model, the anti-PD-L1 therapy was more efficacious in PTPN22 cKO animals, which translated into improved overall survival of the mice. (**Fig 4.23**) Thus, in a less immunogenic tumor model, PTPN22 cKO deletion was synergistic with aPD-L1 treatment, resulting in complete control of these tumors.

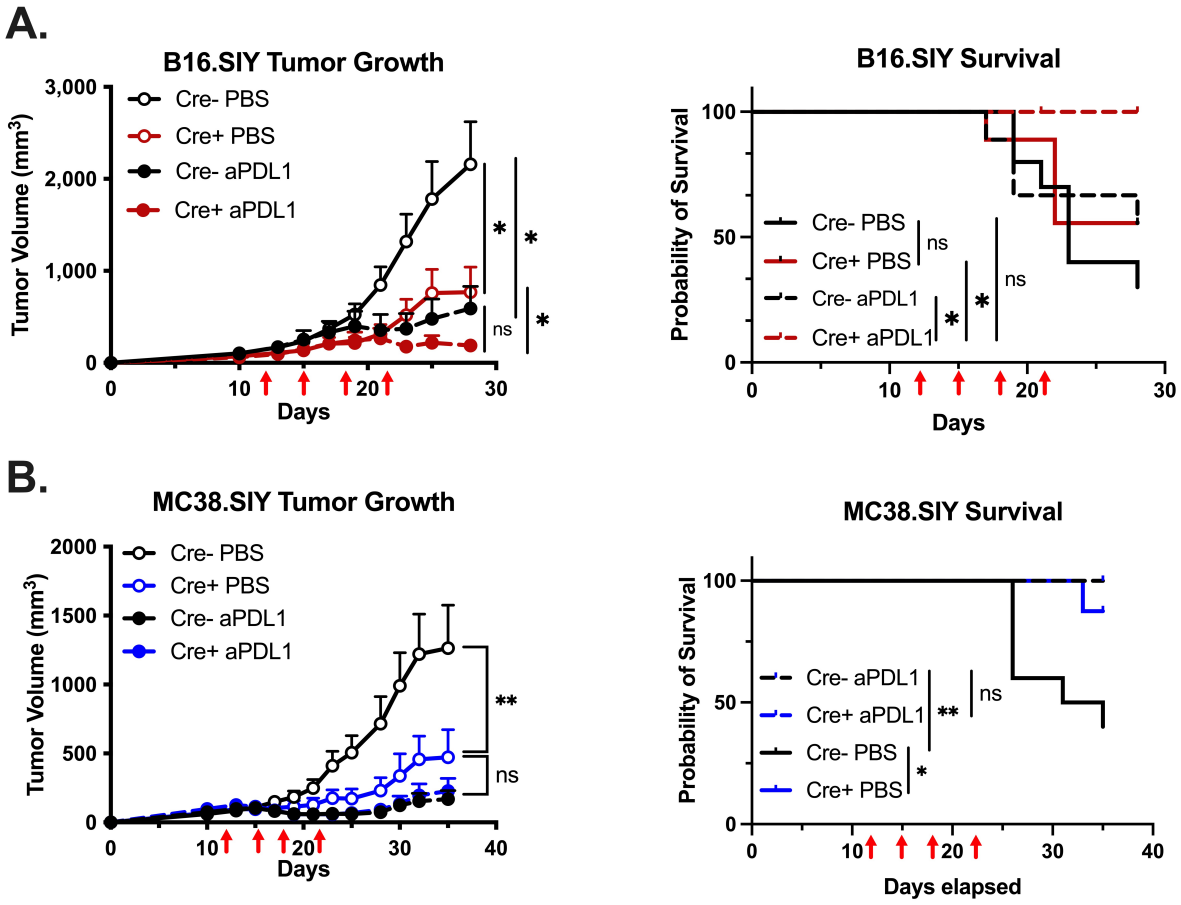

Figure 4.22: PTPN22 cKO mice are responsive to aPD-L1 therapy. PTPN22$^{fl/fl}$ x Cre^{+} and Cre^{-} aged-matched litter-mates were injected with **(A)** B16.SIY (N $\geq$ 8 per group) and **(B)** MC38.SIY (N $\geq$ 9 per group) tumors and treated with 100ng of anti-PD-L1 or PBS intraperitoneally. Tumor growth and survival were evaluated for both; open circles and dashed lines represent PBS treated animals, respectively. Experiments were repeated at least twice, using female mice for B16.SIY and male mice for MC38.SIY.

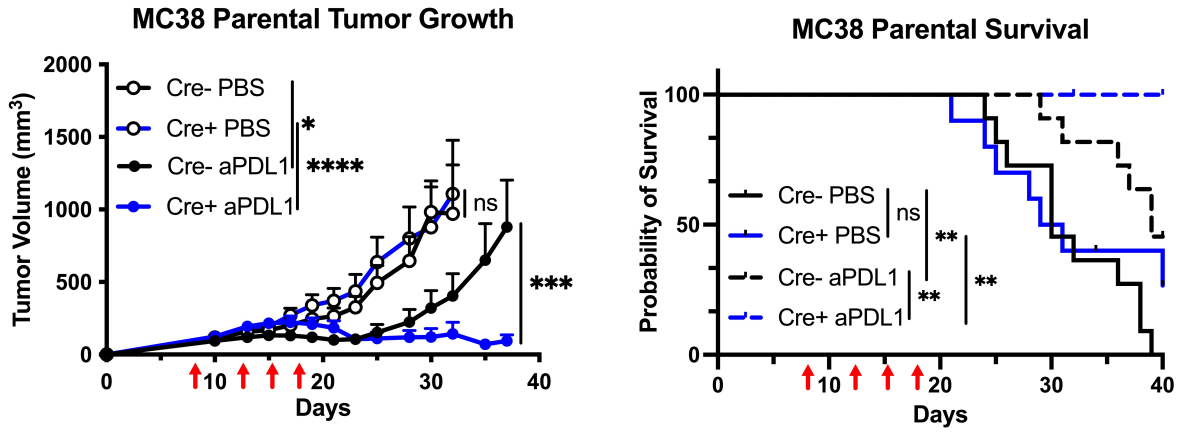

Figure 4.23: aPD-L1 treatment synergizes with PTPN22 cKO in the absence of a model antigen. PTPN22$^{fl/fl}$ x Cre^{+} and Cre^{-} aged-matched litter-mates were injected with MC38 (N $\geq$ 10 per group) tumors and treated with 100ng of anti-PD-L1 or PBS intraperitoneally. Tumor growth and survival were evaluated; open circles and dashed lines represent PBS treated animals, respectively. Experiments were repeated at least twice using male mice.

4.3 Summary of findings

The experiments described in Chapter 4 were aimed at understanding the mechanisms and biological processes altered by the conditional deletion of PTPN22 in the $CD11c^+$ compartment. We found that priming of tumor antigen-specific $CD8^+$ T cells was improved in PTPN22 cKO mice. Further, bulk RNAseq of intratumoral DCs transcriptional changes suggested improved activation, maturation, and proliferation of DCs in this context. In vivo, PTPN22 cKO mice had increased numbers of tumor antigen-loaded DCs, which were also more activated and proliferative, driving the expansion of these populations. In vitro, assays of antigen uptake and presentation indicated that, while PTPN22 cKO DCs showed comparable levels of antigen uptake, they showed superior antigen processing and presentation, yielding a greater number of peptide antigen-MHC I complexes on the cell surface. Lastly, mice bearing MC38 parental tumors revealed a synergistic relationship between PTPN22 cKO and aPD-L1 therapy. Overall, these data underscore the potential of therapeutically targeting PTPN22, especially in the context of dendritic cells, for cancer treatment (**Fig 4.24**).

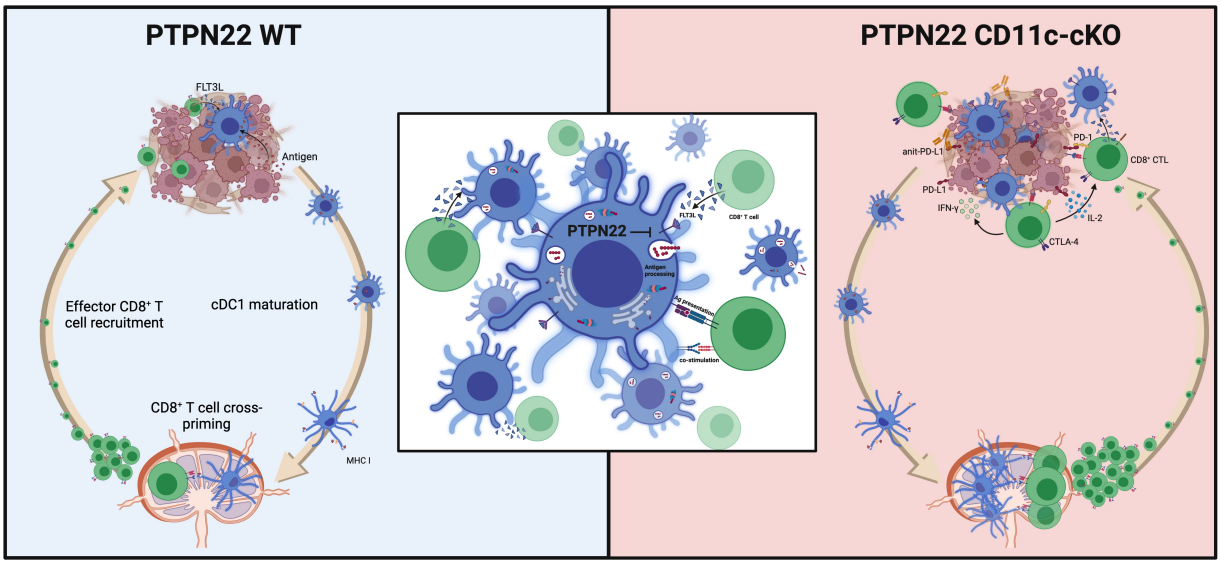

Figure 4.24: Model for PTPN22 regulation of dendritic cells in the context of anti-tumor immunity. The left side represents a wildtype setting where PTPN22 negatively regulates antigen processing and proliferation in response to FLT3L, limiting the endogenous anti-tumor immune response. The right panel represents a context in which DCs lack PTPN22 and are able to elicit a better immune response against the tumor. The center panel focuses on the DC intrinsic roles of PTPN22 uncovered in this thesis, chiefly regulation of antigen processing and FLT3/L signaling.

CHAPTER 5

CHAPTER 5: DISCUSSION

5.1 Conclusions

5.1.1 Repurposing drivers of autoimmunity for cancer immunotherapy

The discovery and development of immune checkpoint blockade have revolutionized cancer care. This same knowledge has also been applied to autoimmunity, where instead of blocking immune checkpoints, their engagement reduces immune activity [172, 173]. This is not surprising as mice lacking PD-1 or CTLA-4 developed severe autoimmune-like symptoms [60, 52]. Similarly, single nucleotide polymorphisms (SNPs) in these genes are linked to a variety of autoimmune diseases [174, 175, 176, 177]. Moreover, genome-wide association studies (GWAS) have played a major role in identifying causative mutations in autoimmunity. In this way, an inverse relationship between causative and therapeutic targets exists in autoimmunity and cancer [107, 178]. Recent work from our laboratory performed by Dr. Kyle Cron similarly found that the loss of PKCδ, a gene for which SNPs are associated with autoimmunity, could also drive improved tumor control in mouse models. These observations emphasize the potential for loss of functions in SNPs associated with autoimmunity as a source for novel immunotherapy targets.

A single SNP resulting in R620W in PTPN22 is the single greatest known genetic risk factor for autoimmune disease outside of polymorphisms in the HLA locus. This mutation results in a loss of function phenotype [141, 115, 179]. Moreover, PTPN22 is exclusively expressed in hematopoietic cells that give rise to immune cells. These observations underscore the immune regulatory nature of PTPN22. Work carried out in a universal PTPN22 KO (only KOd in immune cells, given its exclusive expression) led to the realization that PTPN22 acts primarily as a negative regulator of receptor-mediated signaling, especially in T and B cells. PTPN22 KO mice accordingly accumulate immune cells throughout their life

span, resulting in splenomegaly primarily driven by an accumulation of effector $CD8^+$ T cells [118]. This discovery that PTPN22 de-phosphorylates residues involved in TCR signaling, acting as a sensor for TCR signaling strength. Experiments carried out using antigens of varying immunogenicity showed that loss of PTPN22 only increased the expansion of T cells stimulated against low-affinity antigens, but was disposable for high-affinity antigen stimulation [124, 125]. This role of PTPN22 as an activation rheostat is in alignment with its loss of function phenotype, leading to an increase in the risk of developing autoimmunity, where T cells are thought to become reactive to self-antigens in the absence of proper regulation. In the context of cancer, improved tumor control of PTPN22 KO mice has been attributed to its role in regulating T cells. However, experiments exploring the potential of PTPN22 deletion in T cell-based therapies have yielded less encouraging results [133, 134]. These data, along with the improved tumor control observed in universal PTPN22 KO mice, point to the potentially major role of PTPN22 regulation in other immune compartments. The work summarized here characterized the role of PTPN22 deletion within the dendritic cell compartment.

5.1.2 Conditional deletion of PTPN22 in $CD11c^+$ cells does not impact immune homeostasis

The use of gene KO mice has proved crucial to the characterization of gene functions and the evaluation of the resulting proteins as therapeutic targets. Despite these advantages, results with whole KO mice can be confounding when the gene of interest is expressed in multiple tissues or cell types, hindering mechanistic understanding of where gene products are dominantly important. In the context of PTPN22, the generation of a global KO mouse led to key realizations PTPN22 is a negative regulator of T cell responses and that PTPN22 KO mice are endowed with improved tumor control [118, 135, 136, 137]. Nonetheless, PTPN22 KO T cells alone do not explain the phenotypes observed in global PTPN22 KO mice. To

address this issue, we developed a novel PTPN22 conditional knockout (cKO) model in order to allow for the specific deletion of PTPN22 in a cell lineage-specific manner. Data from PTPN22 KO mice had shown dependence on T cells given the loss of tumor control upon $CD8^+$ depletion. However, experiments with OT-I PTPN22 KO T cells implied that while T cells are ultimately responsible for tumor control, they are not necessarily driving the phenotype observed in these mice [133]. Myeloid cells are the most abundant cell type in solid tumors and are critical mediators of the endogenous anti-tumor immune response. Our lab has previously shown the importance of BATF3 DCs, a type of myeloid cell, in mouse tumor models [180, 145]. DCs are also involved at every step of the anti-tumor immunity cycle, leading us to probe the potential role of PTPN22 in DCs. We crossed our novel $PTPN22^{fl/fl}$ mice to CD11c-Cre mice in order to generate mice with the constitutive deletion of PTPN22 exclusively in the $CD11c^+$ DC compartment.

We first sought to confirm the conditional deletion of PTPN22 in the $CD11c^+$ compartment and characterize these mice at baseline. The availability of reliable and commercially available PTPN22 antibodies is lacking. We utilized qPCR to test for the expression of PTPN22 in order to verify its conditional deletion, showing a complete loss of expression only in $CD11c^+$ splenocytes from CD11c-Cre^+ mice (**Figure 3.1**). Next, we tested whether the deletion of PTPN22 in DCs affected immune homeostasis in naive mice. We utilized spectral flow cytometry to perform thorough immune profiling of these mice at baseline. Unlike the global PTPN22 KO, PTPN22 cKO mice did not display any changes across immune compartments, including T cells and DCs (**Figure 3.2**). Furthermore, we aged PTPN22 cKO mice to 20 months to maximize potential age-associated differences. Aged PTPN22 cKO mice did not differ in spleen or body weight, and similarly to young mice, PTPN22 cKO mice aged to 20 months showed no differences in immune cell populations (**Figure 3.3**).

5.1.3 Deletion of PTPN22 in the CD11c$^+$ compartment results in improved anti-tumor immunity

We were interested to find that PTPN22 cKO mice in the CD11c$^+$ compartment showed augmented tumor control as compared to WT controls. Similar to global PTPN22 KO mice, PTPN22 cKO mice controlled tumors more efficiently in multiple tumor models (**Figure 3.4**). Within the DC compartment, an increase in the maturation status and proliferation of CD103$^+$ DCs was noted in PTPN22 cKO mice. While there were also more CD11b$^+$ DCs, their activation status was not altered. Tumor-infiltrating T cells were also increased in PTPN22 cKO tumors. Further characterization showed only an increase of CD8$^+$ T cells in the B16.SIY model, and an increase in all T cell subsets in MC38.SIY tumors, likely due to their more immunogenic nature.

The use of tumor models expressing the model antigen SIY enabled us to probe endogenous, tumor antigen-specific CD8$^+$ cell responses through pentamer staining. This analysis revealed an overall increase in the number and activation status of CD8$^+$SIY$^+$ T cells in the tumors of PTPN22 cKO mice, accompanied by an increase in the percentage of cells expressing the proliferation marker Ki67. These results suggested that CD8$^+$ T cells might ultimately be responsible for the increased tumor control observed in PTPN22 cKO mice. We confirmed this dependency by depleting CD8$^+$ T cells with an anti-CD8β mAb, which resulted in complete loss of tumor control in both the B16.SIY and MC38.SIY models (**Figure 3.11**). The dependence on CD8$^+$ T cells for tumor controls in this model is in accordance with previous work from our group and others and establishes that the improved tumor control observed in PTPN22 cKO mice is ultimately dependent on CD8$^+$ T cells.

Probing more deeply into the DC-T cell interface, we investigated DCs and T cells in the tdLNs of day 7 tumor-bearing mice, a time point that represents the priming phase. Tumors are not yet palpable during this early priming phase, but DCs will have acquired tumor-derived material and traveled to the tdLNs where they can cross-present tumor-derived

antigens to and activate tumor antigen-specific $CD8^+$ T cells represented by $CD8^+SIY^+$ T cells in this model. PTPN22 cKO mice had a greater number and percentage of DCs in the tdLNs. This expansion was primarily driven by an increase in proliferating $CD103^+$ DCs, without significant changes in $CD11b^+$ or $CD8\alpha^+$ DCs. Only the $CD103^+$ DCs of PTPN22 cKO mice had an increase in the number and percentage of cells positive for the co-stimulatory markers CD80 and CD86 (**Figure 4.2**). These results are consistent with observations in the field that only migratory cDC1s classified by expression of $CD103^+$ possess tumor-derived material for priming of $CD8^+$ T cells in the tdLNs [181]. Thus, improved $CD103^+$ DC numbers and activation state were likely responsible for improved priming of $CD8^+$ T cells. As expected then, PTPN22 cKO mice had an increased number and percentage of proliferating $CD8^+SIY^+$ T cells. IFNγ ELISpot was used to confirm an increased number of functional SIY-reactive T cells. Together, these data, along with the rest of the chapter, show that the conditional deletion of PTPN22 in $CD11c^+$ cells is sufficient to improve the endogenous anti-tumor immune $CD8^+$ T cell response beginning with improved priming in the tdLNs.

5.1.4 Potential molecular mechanisms for PTPN22 regulating $CD11c^+$ cells

To begin understanding the underlying molecular mechanisms driving improved DC responses in PTPN22 cKO mice, we employed bulk RNAseq of intratumoral $CD11c^+$ DCs (**Figure 4.5**). GSEA showed that PTPN22 cKO DCs were enriched for pathways suggestive of activation and maturation, while WT DCs were increased for regulatory pathways (**Figure 4.7**). We chose to investigate two critical aspects of DC biology: population homeostasis, assayed by proliferative and apoptotic markers, and the steps of antigen uptake, processing, and presentation.

In order to assess antigen uptake in vivo, we examined the acquisition of tumor-derived dsRed, an indicator of antigen uptake (**Figure 4.8**). We found that a greater number

of dsRed^{+}CD103^{+} DCs were positive for co-stimulatory markers and were preferentially expanding as a population (**Figures 4.12 - 4.14**). However, the amount of dsRed per cell was the same across PTPN22 cKO and WT DCs. In order to look more deeply into antigen processing and presentation, we employed tools available in the OVA system for in vitro studies. We found that, while DCs from PTPN22 cKO and WT mice had equal levels of antigen uptake, PTPN22 cKO DCs had more antigen processing per cell and also generated more OVA peptide/K^{b} complexes on the surface (**Figures 4.16 - 4.20**).

We also investigated the mechanism by which PTPN22 regulates DC proliferation. Flt3L is a critical growth factor for DCs, and using scRNAseq, we found that Flt3 is highly expressed in CD103^{+} DCs and pDCs within the TME, and that Flt3L was expressed by multiple cell types but predominantly present on CD8^{+} T cells (**Figure 4.21**). In vitro, we found that PTPN22 cKO DCs were more responsive to Flt3L stimulation, as evidenced by an increase in the percentage of cells positive for Ki67 (**Figure 4.21 C**). Previous data has shown that FLT3L is expressed in response to infection and specifically drives the expansion of BATF3-lineage DCs in mice [182]. This possess the potential for a similar mechanism in the context of an immunological challenge by tumor cells.

These data support the notion that CD103^{+} DCs from PTPN22 cKO mice are better able to mount an anti-cancer immune response through their increased ability to process and present antigens, as well as from their increased sensitivity to FLT3L, allowing them to expand therefore amplifying their net ability to activate and maintain tumor antigen-specific CD8^{+} T cells.

5.2 Considerations for Future Directions

Biologically, the loss of PTPN22 seems to regulate DC activation, specifically their ability to process and present antigens and also heighten their ability to proliferate in response to Flt3L. DCs are able to take up antigens by multiple mechanisms, such as phagocytosis,

endocytosis, macropinocytosis, and others [183]. Interestingly, phosphorylation status determines different signaling cascades in these pathways, including cytoskeletal rearrangement, phagosome formation, and receptor-mediated signaling. PTPN22 may regulate one of these processes. Flt3 ligand sensitivity also is increased, and it will be of interest to determine whether PTPN22 regulates the phosphorylation of STAT proteins downstream from FLT3 engagement.

5.2.1 PTPN22-mediated post-translational regulation of DC activation

RNA sequencing suggested a role for PTPN22 in the ability of DCs to process and present antigen and their ability to respond to stimulatory factors in the TME. Whether one process is a consequence of the other warrants further investigation, but together, this points towards the biological processes driving improved tumor control in PTPN22 cKO mice. Moving forward, next-generation phosphoproteomics will be of interest to pursue in order to identify potential direct substrates for the dephosphorylation activity of PTPN22. This will be challenging for a small number of cells.

There is also a need for improved cataloging of intratumoral DCs by single-cell RNA sequencing methods. Identifying and characterizing cellular subsets and cellular states are critical for advancing further our understanding of anti-tumor immunity. DCs exist in a variety of flavors that dictate their capabilities and the immune processes they elicit or impede [75, 76, 77]. While scRNAseq has provided key insights, this sequencing comes at the expense of sequencing depth. Our results serve as a starting point for understanding the role of PTPN22 in DCs but advances in phosphoproteomics on small cell numbers will be necessary to elucidate its molecular mechanisms fully.

5.2.2 Expression of PTPN22 in other myeloid cells

In T cells, PTPN22 forms a complex with CSK where they dephosphorylate activating marks and phosphorylate activating ones upon TCR signaling to ensure only high-affinity TCR signaling results in T cell activation [115]. Similarly, PTPN22 is also implicated in regulating B cell receptor (BCR) signaling. However, there are conflicting results as to whether it functions as negative or positive regulator, which are further confounded by the functional status of the pro-autoimmune variant [184, 185]. On the other hand, as one of the most abundant cell types in tumors, macrophages are an additional cell type that should be investigated regarding a functional role of PTPN22 [81, 82].

The work outlined here shows that DC-intrinsic PTPN22 plays a role in the improved anti-tumor response observed in the global PTPN22 KO model, but it does disqualify other myeloid cells as potentially important by means of different or redundant mechanisms.

To this end, we have also begun to characterize the potential role of PTPN22 in macrophages by employing a LysM-Cre system crossed with our PTPN22 cKO mice. A second Cre transgenic (CD64-Cre) also is being employed, as LysM is not entirely macrophage-specific.

Preliminary data from these experiments have unexpectedly shown that deletion of PTPN22 in the LysM compartment exacerbates tumor growth. However, the LysM-Cre system has been shown to have activity in 60-70% of neutrophils in addition to macrophages. Future experiments depleting macrophages with clodronate and neutrophils with anti-Ly6G will help clarify the dominant LysM-expressing cell in the context of PTPN22 [186]. Lastly, we have also begun breeding PTPN22 cKO mice on a CD64-Cre background for more targeted macrophage depletion. These and other experiments will be needed to clarify the role of PTPN22 in various myeloid cell compartments beyond $CD11c^+$ cells in the context of cancer.

5.2.3 Understanding the therapeutic potential of PTPN22 inhibition

As a negative regulator of anti-tumor immunity, PTPN22 is an attractive therapeutic target for cancer immunotherapy, but understanding its role in a cell-specific manner may aid in the development of efficacious and safe therapies. One strategy considered thus far is the deletion of PTPN22 from T cells used for adoptive therapy. Initial studies utilizing OVA as a model antigen in ovarian and lymphoma models showed promise for PTPN22 KO TCR transgenic T cells, but this was only true in the context of low-affinity antigens [124, 125]. These OVA-specific (OT-I) T cells also seemed to be better able to produce inflammatory cytokines, driving resistance to TGF-β in solid tumor models [132]. Of note, PTPN22 KO OT-I T cells were more resistant to host Tregs but equally sensitive to PTPN22 KO Tregs that were similarly more suppressive in comparison to their WT counterparts. However, PTPN22 KO OT-I cells failed to control other tumors, such as colorectal and mammary models, thus diminishing enthusiasm [133]. Accordingly, a recent report found that loss of PTPN22 in CAR-T cells drove expedited exhaustion, as TCR over-stimulation drove dysfunction [134].

Another approach is to target PTPN22 systemically through small molecule inhibitors. However, the generation of inhibitors with sufficient potency and specificity has proven difficult in regard to the PTP family of proteins. Nevertheless, two recent examples highlight the potential for this approach. A quinolone derivative targeting PTPN22 was developed, showing 7 to 10-fold selectivity over other PTPs. Administration of this PTPN22 inhibitor phenocopied tumor control observed in PTPN22 KO mice and improved efficacy of anti-PD-1 treatment. More recently, Baumgartner and colleagues showed the development of a PTPN1/N2-specific inhibitor. In this case, PTPN1 and PTPN2 have redundant functions, and their inhibition across immune and tumor cells proves beneficial in a variety of tumor models [187]. Together, these show the potential for small molecule inhibitors targeting PTPN22 for cancer immunotherapy.

Our new findings suggest a new set of therapeutic strategies based on a DC-intrinsic role for PTPN22. DC-based therapeutics have been of great interest but have been primarily hindered by the scarcity of DCs in circulation and the lack of universally applicable antigens for DC vaccines. Still, DC vaccines are FDA-approved for the treatment of metastatic castrate-resistant prostate cancer (mCRPC). This vaccine works by isolating DCs from patients and culturing them with growth factors and the antigen prostatic acid phosphatase (PAP) that is expressed on 95% of prostate tumors [188]. Our lab has explored similar approaches whereby DCs are injected intratumorally to restore T cell infiltration into solid tumors [145].

Targeting DCs specifically is also an attractive approach. These approaches include the modification of lipid nanoparticles to target the delivery of siRNA to DCs as well as monoclonal antibodies targeting inhibitory molecules on DCs [189, 190]. However, these approaches are predicated on the discovery and characterization of negative regulators and inhibitory molecules specific to DCs in the TME [191]. Thus, improved cataloging of DCs in the TME by scRNAseq and spatial transcriptomics followed by DC-intrinsic characterization will be critical for the development of novel DC-based therapies for cancer.

In conclusion, the novel findings presented here, along with future discoveries regarding the cell-intrinsic roles of PTPN22, and with innovations in medicinal chemistry and drug delivery systems, suggest the potential development of safe and efficacious PTPN22-targeted therapies for cancer. Thus, it is imperative to continue developing targeted and selective inhibitors while simultaneously characterising the molecular mechanisms of PTPN22 regulation in different immune cell subtypes.

REFERENCES

[1] Rebecca L. Siegel, Kimberly D. Miller, Nikita Sandeep Wagle, and Ahmedin Jemal. Cancer statistics, 2023. *CA: A Cancer Journal for Clinicians*, 73(1):17–48, 2023.

[2] Seper Ekhtiari, Kentaro Chiba, Snezana Popovic, Rhianne Crowther, Gregory Wohl, Andy Kin On Wong, Darren H. Tanke, Danielle M. Dufault, Olivia D. Geen, Naveen Parasu, Mark A. Crowther, and David C. Evans. First case of osteosarcoma in a dinosaur: a multimodal diagnosis. *The Lancet Oncology*, 21(8):1021–1022, 8 2020.

[3] American Cancer Society medical and editorial content team. Understanding What Cancer Is: Ancient Times to Present. *American Cancer Society*, pages 1–34, 2018.

[4] Maroeska M. Rovers Ph.D. Jorine M. Molenaar M.D. Pauline L. Winkler-Seinstra M.Sc. Adam Meijer Ph.D. Jan L.L. Kimpen M.D. Ph.D. Maarten O. Blanken, M.D. and Ph.D. Louis Bont, M.D. Respiratory Syncytial Virus and Recurrent Wheeze in Healthy Preterm Infants. *N Engl J Med*, 368(19):1791–1800, 2013.

[5] Lawrence Koblenz and Kenneth T Jackson. From Sin to Science: The Cancer Revolution of the Nineteenth Century. 3557914:1118, 2013.

[6] A. Karpozilos and N. Pavlidis. The treatment of cancer in Greek antiquity. *European Journal of Cancer*, 40(14):2033–2040, 9 2004.

[7] Anna di Lonardo, Sergio Nasi, and Simonetta Pulciani. Cancer: We Should Not Forget The Past. *Journal of Cancer*, 6(1):29, 2015.

[8] A. Korniluk, O. Koper, H. Kemona, and V. Dymicka-Piekarska. From inflammation to cancer. *Irish Journal of Medical Science*, 186(1):57, 2 2017.

[9] Fran Balkwill and Alberto Mantovani. Inflammation and cancer: back to Virchow? *The Lancet*, 357(9255):539–545, 2 2001.

[10] Lisa M. Coussens and Zena Werb. Inflammation and cancer. *Nature*, 420(6917):860, 12 2002.

[11] Kim R. Kampen. The discovery and early understanding of leukemia. *Leukemia Research*, 36(1):6–13, 1 2012.

[12] Guy B. Faguet. A brief history of cancer: Age-old milestones underlying our current knowledge database. *International Journal of Cancer*, 136(9):2022–2036, 2015.

[13] Paula Dobosz and Tomasz Dzieciątkowski. The Intriguing History of Cancer Immunotherapy. *Frontiers in Immunology*, 10:496087, 12 2019.

[14] Robert D. Carlson, John C. Flickinger, and Adam E. Snook. Talkin' Toxins: From Coley's to Modern Cancer Immunotherapy. *Toxins*, 12(4), 4 2020.

[15] Matthew Tontonoz. What Ever Happened to Coley's Toxins? - Cancer Research Institute, 2015.

[16] Yvonne Bordon. The many sides of Paul Ehrlich. *Nature Immunology 2016 17:1*, 17(1):S6–S6, 12 2016.

[17] Alison Farrell. Hide and seek. *Nature Reviews Cancer*, 6(1):S8–S9, 4 2006.

[18] Paul Ehrlich. Über den jetzigen stand der karzinomforschung. *Nederlandsch Tijdschrift voor Geneeskunde*, 5:273–290, 1909.

[19] F. M. Burnet. The concept of immunological surveillance. *Immunol. Asp. Neoplasia.*, 13:1–27, 1970.

[20] L. Thomas. On immunosurveillance in human cancer. *The Yale Journal of Biology and Medicine*, 55(3-4):329, 1982.

[21] Osias Stutman. Tumor Development after 3-Methylcholanthrene in Immunologically Deficient Athymic-Nude Mice. *Science*, 183(4124):534–536, 2 1974.

[22] W. Budzynski and C. Radzikowski. Cytotoxic cells in immunodeficient athymic mice. *Immunopharmacology and Immunotoxicology*, 16(3):319–346, 1994.

[23] Richard E. Kouri, Leonard H. Billups, Thomas H. Rude, Carrie E. Whitmire, Bernard Sass, and Carol J. Henry. Correlation of inducibility of aryl hydrocarbon hydroxylase with susceptibility to 3-methylcholanthrene-induced lung cancers. *Cancer Letters*, 9(4):277–284, 6 1980.

[24] Yoichi Shinkai, 0Gary Rathbun, Kong Peng Lam, Eugene M. Oltz, Valerie Stewart, Monica Mendelsohn, Jean Charron, Milton Datta, Faith Young, Alan M. Stall, and Frederick W. Alt. RAG-2-deficient mice lack mature lymphocytes owing to inability to initiate V(D)J rearrangement. *Cell*, 68(5):855–867, 3 1992.

[25] Vijay Shankaran, Hiroaki Ikeda, Allen T. Bruce, J. Michael White, Paul E. Swanson, Lloyd J. Old, and Robert D. Schreiber. IFNγ and lymphocytes prevent primary tumour development and shape tumour immunogenicity. *Nature 2001*, 410(6832):1107–1111, 4 2001.

[26] Sylvia Lee and Kim Margolin. Cytokines in Cancer Immunotherapy. *Cancers*, 3(4):3856, 12 2011.

[27] Thomas J. Gryczan. Etymologia: Cytokines. *Emerging Infectious Diseases*, 24(7):1227, 7 2018.

[28] ISAACS A and LINDENMANN J. Virus interference. I. The interferon. *Proceedings of the Royal Society of London. Series B, Biological sciences*, 147(927):258–267, 9 1957.

[29] E. Frederick Wheelock. Interferon-like virus-inhibitor induced in human leukocytes by phytohemagglutinin. *Science*, 149(3681):310–311, 1965.

[30] Stanley Cohen, Pierluigi E. Bigazzi, and Takeshi Yoshida. Similarities of T cell function in cell-mediated immunity and antibody production. *Cellular Immunology*, 12(1):150–159, 4 1974.

[31] Igal Gery, Richard K. Gershon, and Byron H. Waksman. POTENTIATION OF THE T-LYMPHOCYTE RESPONSE TO MITOGENS : I. THE RESPONDING CELL. *The Journal of Experimental Medicine*, 136(1):128, 7 1972.

[32] Karl Welte, Chang Yi Wang, Roland Mertelsmann, Salvatore Venuta, Stuart P. Feldman, and Malcolm A.S. Moore. Purification of human interleukin 2 to apparent homogeneity and its molecular heterogeneity. *The Journal of experimental medicine*, 156(2):454–464, 8 1982.

[33] Steven A. Rosenberg, James J. Mulé, Paul J. Spiess, Cheryl M. Reichert, and Susan L. Schwarz. Regression of established pulmonary metastases and subcutaneous tumor mediated by the systemic administration of high-dose recombinant interleukin 2. *The Journal of experimental medicine*, 161(5):1169–1188, 5 1985.

[34] Timothy J. Eberlein, Maury Rosenstein, and Steven A. Rosenberg. Regression of a disseminated syngeneic solid tumor by systemic transfer of lymphoid cells expanded in interleukin 2. *The Journal of experimental medicine*, 156(2):385–397, 8 1982.

[35] John M. Kirkwood, Joseph G. Ibrahim, Vernon K. Sondak, Jon Richards, Lawrence E. Flaherty, Marc S. Ernstoff, Thomas J. Smith, Uma Rao, Mary Steele, and Ronald H. Blum. High- and low-dose interferon alfa-2b in high-risk melanoma: first analysis of intergroup trial E1690/S9111/C9190. *Journal of clinical oncology : official journal of the American Society of Clinical Oncology*, 18(12):2444–2458, 2000.

[36] Chia Chi Ku, Masaaki Murakami, Akemi Sakamoto, John Kappler, and Philippa Marrack. Control of homeostasis of CD8+ memory T cells by opposing cytokines. *Science (New York, N.Y.)*, 288(5466):675–678, 4 2000.

[37] Timothy R. Hercus, Daniel Thomas, Mark A. Guthridge, Paul G. Ekert, Jack King-Scott, Michael W. Parker, and Angel F. Lopez. The granulocyte-macrophage colony-stimulating factor receptor: linking its structure to cell signaling and its role in disease. *Blood*, 114(7):1289–1298, 2009.

[38] T Yokochi, R D Holly, and E A Clark. B lymphoblast antigen (BB-1) expressed on Epstein-Barr virus-activated B cell blasts, B lymphoblastoid cell lines, and Burkitt's lymphomas. *Journal of immunology (Baltimore, Md. : 1950)*, 128(2):823–827, 2 1982.

[39] Hans GMÜNDER and Werner LESSLAUER. A 45-kDa human T-cell membrane glycoprotein functions in the regulation of cell proliferative responses. *European journal of biochemistry*, 142(1):153–160, 1984.

[40] G J Freeman, A S Freedman, J M Segil, G Lee, J F Whitman, and L M Nadler. B7, a new member of the Ig superfamily with unique expression on activated and neoplastic B cells. *The Journal of Immunology*, 143(8):2714–2722, 10 1989.

[41] C. B. Thompson, T. Lindsten, J. A. Ledbetter, S. L. Kunkel, H. A. Young, S. G. Emerson, J. M. Leiden, and C. H. June. CD28 activation pathway regulates the production of multiple T-cell-derived lymphokines/cytokines. *Proceedings of the National Academy of Sciences*, 86(4):1333–1337, 2 1989.

[42] Peter S. Linsley, Edward A. Clark, and Jeffrey A. Ledbetter. T-cell antigen CD28 mediates adhesion with B cells by interacting with activation antigen B7/BB-1. *Proceedings of the National Academy of Sciences*, 87(13):5031–5035, 7 1990.

[43] Arda Shahinian, Klaus Pfefer, Kelvin P. Lee, Thomas M. Kündig, Kenji Kishihara, Andrew Wakeham, Kazuhiro Kawai, Pamela S. Ohashi, Craig B. Thompson, and Tak W. Mak. Differential T cell costimulatory requirements in CD28-deficient mice. *Science (New York, N.Y.)*, 261(5121):609–612, 1993.

[44] I C Rulifson, A I Sperling, P E Fields, F W Fitch, and J A Bluestone. CD28 costimulation promotes the production of Th2 cytokines. *Journal of immunology (Baltimore, Md. : 1950)*, 158(2):658–665, 1 1997.

[45] Jean Fraṇois Brunet, Fraṇois Denizot, Marie Fraṇoise Luciani, Magali Roux-Dosseto, Marie Suzan, Marie Geneviève Mattei, and Pierre Golstein. A new member of the immunoglobulin superfamily—CTLA-4. *Nature 1987 328:6127*, 328(6127):267–270, 1987.

[46] Peter S. Linsley, William Brady, Laura Grosmaire, Alejandro Aruffo, Nitin K. Damle, and Jeffrey A. Ledbetter. Binding of the B cell activation antigen B7 to CD28 costimulates T cell proliferation and interleukin 2 mRNA accumulation. *The Journal of Experimental Medicine*, 173(3):721, 3 1991.

[47] Gordon J. Freeman, John G. Gribben, Vassiliki A. Boussiotis, Judy W. Ng, Vincent A. Restivo, Lisa A. Lombard, Gary S. Gray, and Lee M. Nadler. Cloning of B7-2: a CTLA-4 Counter-Receptor That Costimulates Human T Cell Proliferation. *Science*, 262(5135):909–911, 1993.

[48] Miyuki Azuma, Daisuke Ito, Hideo Yagita, Ko Okumura, Joseph H. Phillips, Lewis L. Lanier, and Chamorro Somoza. B70 antigen is a second ligand for CTLA-4 and CD28. *Nature 1993 366:6450*, 366(6450):76–79, 1993.

[49] K Harper, C Balzano, E Rouvier, M G Mattéi, M F Luciani, and P Golstein. CTLA-4 and CD28 activated lymphocyte molecules are closely related in both mouse and human as to sequence, message expression, gene structure, and chromosomal location. *Journal of immunology (Baltimore, Md. : 1950)*, 147(3):1037–1044, 8 1991.

[50] Theresa L. Walunas, Deborah J. Lenschow, Christina Y. Bakker, Peter S. Linsley, Gordon J. Freeman, Jonathan M. Green, Craig B. Thompson, and Jeffrey A. Bluestone. CTLA-4 can function as a negative regulator of T cell activation. *Immunity*, 1(5):405–413, 8 1994.

[51] Matthew F. Krummel and James P. Allison. CD28 and CTLA-4 have opposing effects on the response of T cells to stimulation. *The Journal of Experimental Medicine*, 182(2):459, 8 1995.

[52] Elizabeth A. Tivol, Frank Borriello, A. Nicola Schweitzer, William P. Lynch, Jeffrey A. Bluestone, and Arlene H. Sharpe. Loss of CTLA-4 leads to massive lymphoproliferation and fatal multiorgan tissue destruction, revealing a critical negative regulatory role of CTLA-4. *Immunity*, 3(5):541–547, 11 1995.

[53] Paul Waterhouse, Josef M. Penninger, Emma Timms, Andrew Wakeham, Arda Shahinian, Kelvin P. Lee, Craig B. Thompson, Henrik Griesser, and Tak W. Mak. Lymphoproliferative Disorders with Early Lethality in Mice Deficient in Ctla-4. *Science*, 270(5238):985–988, 11 1995.

[54] Dana R. Leach, Matthew F. Krummel, and James P. Allison. Enhancement of Antitumor Immunity by CTLA-4 Blockade. *Science*, 271(5256):1734–1736, 3 1996.

[55] Ajay V. Maker, James C. Yang, Richard M. Sherry, Suzanne L. Topalian, Udai S. Kammula, Richard E. Royal, Marybeth Hughes, Michael J. Yellin, Leah R. Haworth, Catherine Levy, Tamika Allen, Sharon A. Mavroukakis, Peter Attia, and Steven A. Rosenberg. Intrapatient dose escalation of anti-CTLA-4 antibody in patients with metastatic melanoma. *Journal of immunotherapy (Hagerstown, Md. : 1997)*, 29(4):455–463, 7 2006.

[56] F. Stephen Hodi, Steven J. O'Day, David F. McDermott, Robert W. Weber, Jeffrey A. Sosman, John B. Haanen, Rene Gonzalez, Caroline Robert, Dirk Schadendorf, Jessica C. Hassel, Wallace Akerley, Alfons J.M. van den Eertwegh, Jose Lutzky, Paul Lorigan, Julia M. Vaubel, Gerald P. Linette, David Hogg, Christian H. Ottensmeier, Celeste Lebbé, Christian Peschel, Ian Quirt, Joseph I. Clark, Jedd D. Wolchok, Jeffrey S. Weber, Jason Tian, Michael J. Yellin, Geoffrey M. Nichol, Axel Hoos, and Walter J. Urba. Improved Survival with Ipilimumab in Patients with Metastatic Melanoma. *New England Journal of Medicine*, 363(8):711–723, 8 2010.

[57] Caroline Robert, Luc Thomas, Igor Bondarenko, Steven O'Day, Jeffrey Weber, Claus Garbe, Celeste Lebbe, Jean-François Baurain, Alessandro Testori, Jean-Jacques Grob, Neville Davidson, Jon Richards, Michele Maio, Axel Hauschild, Wilson H. Miller, Pere Gascon, Michal Lotem, Kaan Harmankaya, Ramy Ibrahim, Stephen Francis, Tai-Tsang Chen, Rachel Humphrey, Axel Hoos, and Jedd D. Wolchok. Ipilimumab plus Dacarbazine for Previously Untreated Metastatic Melanoma. *New England Journal of Medicine*, 364(26):2517–2526, 6 2011.

[58] Dirk Schadendorf, F. Stephen Hodi, Caroline Robert, Jeffrey S. Weber, Kim Margolin, Omid Hamid, Debra Patt, Tai Tsang Chen, David M. Berman, and Jedd D. Wolchok. Pooled analysis of long-term survival data from phase II and phase III trials of ipilimumab in unresectable or metastatic melanoma. *Journal of Clinical Oncology*, 33(17):1889–1894, 6 2015.

[59] Yasumasa Ishida, Yasutoshi Agata, Keiichi Shibahara, and Tasuku Honjo1. Induced expression of PD-1, a novel member of the immunoglobulin gene superfamily, upon programmed cell death. *The EMBO Journal*, 11(11):3887–3895, 11 1992.

[60] Hiroyuki Nishimura, Masato Nose, Hiroshi Hiai, Nagahiro Minato, and Tasuku Honjo. Development of lupus-like autoimmune diseases by disruption of the PD-1 gene encoding an ITIM motif-carrying immunoreceptor. *Immunity*, 11(2):141–151, 1999.

[61] Haidong Dong, Gefeng Zhu, Koji Tamada, and Lieping Chen. B7-H1, a third member of the B7 family, co-stimulates T-cell proliferation and interleukin-10 secretion. *Nature Medicine 1999 5:12*, 5(12):1365–1369, 12 1999.

[62] Gordon J. Freeman, Andrew J. Long, Yoshiko Iwai, Karen Bourque, Tatyana Chernova, Hiroyuki Nishimura, Lori J. Fitz, Nelly Malenkovich, Taku Okazaki, Michael C. Byrne, Heidi F. Horton, Lynette Fouser, Laura Carter, Vincent Ling, Michael R. Bowman, Beatriz M. Carreno, Mary Collins, Clive R. Wood, and Tasuku Honjo. Engagement of the Pd-1 Immunoinhibitory Receptor by a Novel B7 Family Member Leads to Negative Regulation of Lymphocyte Activation. *The Journal of Experimental Medicine*, 192(7):1027, 10 2000.

[63] Yoshiko Iwai, Masayoshi Ishida, Yoshimasa Tanaka, Taku Okazaki, Tasuku Honjo, and Nagahiro Minato. Involvement of PD-L1 on tumor cells in the escape from host immune system and tumor immunotherapy by PD-L1 blockade. *Proceedings of the National Academy of Sciences of the United States of America*, 99(19):12293–12297, 9 2002.

[64] Tyler J. Curiel, Shuang Wei, Haidong Dong, Xavier Alvarez, Pui Cheng, Peter Mottram, Roman Krzysiek, Keith L. Knutson, Ben Daniel, Maria Carla Zimmermann, Odile David, Matthew Burow, Alan Gordon, Nina Dhurandhar, Leann Myers, Ruth Berggren, Akseli Hemminki, Ronald D. Alvarez, Dominique Emilie, David T. Curiel, Lieping Chen, and Weiping Zou. Blockade of B7-H1 improves myeloid dendritic cell–mediated antitumor immunity. *Nature Medicine 2003 9:5*, 9(5):562–567, 4 2003.

[65] Yoshiko Iwai, Seigo Terawaki, and Tasuku Honjo. PD-1 blockade inhibits hematogenous spread of poorly immunogenic tumor cells by enhanced recruitment of effector T cells. *International immunology*, 17(2):133–144, 2 2005.

[66] Julie R. Brahmer, Scott S. Tykodi, Laura Q.M. Chow, Wen-Jen Hwu, Suzanne L. Topalian, Patrick Hwu, Charles G. Drake, Luis H. Camacho, John Kauh, Kunle Odunsi, Henry C. Pitot, Omid Hamid, Shailender Bhatia, Renato Martins, Keith

Eaton, Shuming Chen, Theresa M. Salay, Suresh Alaparthy, Joseph F. Grosso, Alan J. Korman, Susan M. Parker, Shruti Agrawal, Stacie M. Goldberg, Drew M. Pardoll, Ashok Gupta, and Jon M. Wigginton. Safety and activity of anti-PD-L1 antibody in patients with advanced cancer. *The New England journal of medicine*, 366(26):2455–2465, 6 2012.

[67] Edward B. Garon, Naiyer A. Rizvi, Rina Hui, Natasha Leighl, Ani S. Balmanoukian, Joseph Paul Eder, Amita Patnaik, Charu Aggarwal, Matthew Gubens, Leora Horn, Enric Carcereny, Myung-Ju Ahn, Enriqueta Felip, Jong-Seok Lee, Matthew D. Hellmann, Omid Hamid, Jonathan W. Goldman, Jean-Charles Soria, Marisa Dolled-Filhart, Ruth Z. Rutledge, Jin Zhang, Jared K. Lunceford, Reshma Rangwala, Gregory M. Lubiniecki, Charlotte Roach, Kenneth Emancipator, and Leena Gandhi. Pembrolizumab for the treatment of non-small-cell lung cancer. *The New England journal of medicine*, 372(21):2018–2028, 5 2015.

[68] Caroline Robert, Jacob Schachter, Georgina V. Long, Ana Arance, Jean Jacques Grob, Laurent Mortier, Adil Daud, Matteo S. Carlino, Catriona McNeil, Michal Lotem, James Larkin, Paul Lorigan, Bart Neyns, Christian U. Blank, Omid Hamid, Christine Mateus, Ronnie Shapira-Frommer, Michele Kosh, Honghong Zhou, Nageatte Ibrahim, Scot Ebbinghaus, and Antoni Ribas. Pembrolizumab versus Ipilimumab in Advanced Melanoma. *New England Journal of Medicine*, 372(26):2521–2532, 6 2015.

[69] Robert J. Motzer, Nizar M. Tannir, David F. McDermott, Osvaldo Arén Frontera, Bohuslav Melichar, Toni K. Choueiri, Elizabeth R. Plimack, Philippe Barthélémy, Camillo Porta, Saby George, Thomas Powles, Frede Donskov, Victoria Neiman, Christian K. Kollmannsberger, Pamela Salman, Howard Gurney, Robert Hawkins, Alain Ravaud, Marc-Oliver Grimm, Sergio Bracarda, Carlos H. Barrios, Yoshihiko Tomita, Daniel Castellano, Brian I. Rini, Allen C. Chen, Sabeen Mekan, M. Brent McHenry, Megan Wind-Rotolo, Justin Doan, Padmanee Sharma, Hans J. Hammers, and Bernard Escudier. Nivolumab plus Ipilimumab versus Sunitinib in Advanced Renal-Cell Carcinoma. *New England Journal of Medicine*, 378(14):1277–1290, 4 2018.

[70] Douglas Hanahan. Hallmarks of Cancer: New Dimensions. *Cancer Discovery*, 12(1):31–46, 1 2022.

[71] Tamara J. Laskowski, Alexander Biederstädt, and Katayoun Rezvani. Natural killer cells in antitumour adoptive cell immunotherapy. *Nature Reviews Cancer 2022 22:10*, 22(10):557–575, 7 2022.

[72] C. H. Takimoto, M. P. Chao, C. Gibbs, M. A. McCamish, J. Liu, J. Y. Chen, R. Majeti, and I. L. Weissman. The Macrophage 'Do not eat me' signal, CD47, is a clinically validated cancer immunotherapy target. *Annals of Oncology*, 30(3):486–489, 3 2019.

[73] Bettina Weigelin and Peter Friedl. T cell-mediated additive cytotoxicity – death by multiple bullets. *Trends in Cancer*, 8(12):980–987, 12 2022.

[74] Ira Mellman, Daniel S. Chen, Thomas Powles, and Shannon J. Turley. The cancer-immunity cycle: Indication, genotype, and immunotype. *Immunity*, 56(10):2188–2205, 2023.

[75] Rahul Kushwah and Jim Hu. Complexity of dendritic cell subsets and their function in the host immune system. *Immunology*, 133(4):409, 8 2011.

[76] Thiago A. Patente, Mariana P. Pinho, Aline A. Oliveira, Gabriela C.M. Evangelista, Patrícia C. Bergami-Santos, and José A.M. Barbuto. Human dendritic cells: Their heterogeneity and clinical application potential in cancer immunotherapy. *Frontiers in Immunology*, 10(JAN):422571, 1 2019.

[77] Annalisa Del Prete, Valentina Salvi, Alessandra Soriani, Mattia Laffranchi, Francesca Sozio, Daniela Bosisio, and Silvano Sozzani. Dendritic cell subsets in cancer immunity and tumor antigen sensing, 5 2023.

[78] Jérôme Galon, Anne Costes, Fatima Sanchez-Cabo, Amos Kirilovsky, Bernhard Mlecnik, Christine Lagorce-Pagès, Marie Tosolini, Matthieu Camus, Anne Berger, Philippe Wind, Franck Zinzindohoué, Patrick Bruneval, Paul Henri Cugnenc, Zlatko Trajanoski, Wolf Herman Fridman, and Franck Pagès. Type, density, and location of immune cells within human colorectal tumors predict clinical outcome. *Science (New York, N.Y.)*, 313(5795):1960–1964, 9 2006.

[79] Helena Harlin, Yuru Meng, Amy C. Peterson, Yuanyuan Zha, Maria Tretiakova, Craig Slingluff, Mark McKee, and Thomas F. Gajewski. Chemokine expression in melanoma metastases associated with CD8+ T-cell recruitment. *Cancer research*, 69(7):3077–3085, 4 2009.

[80] Mark Ayers, Jared Lunceford, Michael Nebozhyn, Erin Murphy, Andrey Loboda, David R. Kaufman, Andrew Albright, Jonathan D. Cheng, S. Peter Kang, Veena Shankaran, Sarina A. Piha-Paul, Jennifer Yearley, Tanguy Y. Seiwert, Antoni Ribas, and Terrill K. McClanahan. IFN-γ–related mRNA profile predicts clinical response to PD-1 blockade. *The Journal of Clinical Investigation*, 127(8):2930, 8 2017.

[81] Zicong He and Shuixing Zhang. Tumor-Associated Macrophages and Their Functional Transformation in the Hypoxic Tumor Microenvironment. *Frontiers in Immunology*, 12, 9 2021.

[82] Xinyu Cheng, Huilan Wang, Zhongyu Wang, Bo Zhu, and Haixia Long. Tumor-associated myeloid cells in cancer immunotherapy. *Journal of Hematology & Oncology 2023 16:1*, 16(1):1–21, 7 2023.

[83] Stefani Spranger, Riyue Bao, and Thomas F. Gajewski. Melanoma-intrinsic β-catenin signalling prevents anti-tumour immunity. *Nature*, 523(7559):231–235, 7 2015.

[84] Ayelet Sivan, Leticia Corrales, Nathaniel Hubert, Jason B. Williams, Keston Aquino-Michaels, Zachary M. Earley, Franco W. Benyamin, Yuk Man Lei, Bana Jabri,

Maria Luisa Alegre, Eugene B. Chang, and Thomas F. Gajewski. Commensal Bifidobacterium promotes antitumor immunity and facilitates anti-PD-L1 efficacy. *Science*, 350(6264):1084–1089, 11 2015.

[85] Vyara Matson, Jessica Fessler, Riyue Bao, Tara Chongsuwat, Yuanyuan Zha, Maria Luisa Alegre, Jason J. Luke, and Thomas F. Gajewski. The commensal microbiome is associated with anti-PD-1 efficacy in metastatic melanoma patients. *Science*, 359(6371):104–108, 1 2018.

[86] Christine N. Spencer, Jennifer L. McQuade, Vancheswaran Gopalakrishnan, John A. McCulloch, Marie Vetizou, Alexandria P. Cogdill, Md A. Wadud Khan, Xiaotao Zhang, Michael G. White, Christine B. Peterson, Matthew C. Wong, Golnaz Morad, Theresa Rodgers, Jonathan H. Badger, Beth A. Helmink, Miles C. Andrews, Richard R. Rodrigues, Andrey Morgun, Young S. Kim, Jason Roszik, Kristi L. Hoffman, Jiali Zheng, Yifan Zhou, Yusra B. Medik, Laura M. Kahn, Sarah Johnson, Courtney W. Hudgens, Khalida Wani, Pierre Olivier Gaudreau, Angela L. Harris, Mohamed A. Jamal, Erez N. Baruch, Eva Perez-Guijarro, Chi Ping Day, Glenn Merlino, Barbara Pazdrak, Brooke S. Lochmann, Robert A. Szczepaniak-Sloane, Reetakshi Arora, Jaime Anderson, Chrystia M. Zobniw, Eliza Posada, Elizabeth Sirmans, Julie Simon, Lauren E. Haydu, Elizabeth M. Burton, Linghua Wang, Minghao Dang, Karen Clise-Dwyer, Sarah Schneider, Thomas Chapman, Nana Ama A.S. Anang, Sheila Duncan, Joseph Toker, Jared C. Malke, Isabella C. Glitza, Rodabe N. Amaria, Hussein A. Tawbi, Adi Diab, Michael K. Wong, Sapna P. Patel, Scott E. Woodman, Michael A. Davies, Merrick I. Ross, Jeffrey E. Gershenwald, Jeffrey E. Lee, Patrick Hwu, Vanessa Jensen, Yardena Samuels, Ravid Straussman, Nadim J. Ajami, Kelly C. Nelson, Luigi Nezi, Joseph F. Petrosino, P. Andrew Futreal, Alexander J. Lazar, Jianhua Hu, Robert R. Jenq, Michael T. Tetzlaff, Yan Yan, Wendy S. Garrett, Curtis Huttenhower, Padmanee Sharma, Stephanie S. Watowich, James P. Allison, Lorenzo Cohen, Giorgio Trinchieri, Carrie R. Daniel, and Jennifer A. Wargo. Dietary fiber and probiotics influence the gut microbiome and melanoma immunotherapy response. *Science*, 374(6575):1632–1640, 12 2021.

[87] Bertrand Routy, John G. Lenehan, Wilson H. Miller, Rahima Jamal, Meriem Messaoudene, Brendan A. Daisley, Cecilia Hes, Kait F. Al, Laura Martinez-Gili, Michal Punčochář, Scott Ernst, Diane Logan, Karl Belanger, Khashayar Esfahani, Corentin Richard, Marina Ninkov, Gianmarco Piccinno, Federica Armanini, Federica Pinto, Mithunah Krishnamoorthy, Rene Figueredo, Pamela Thebault, Panteleimon Takis, Jamie Magrill, Lee Ann Ramsay, Lisa Derosa, Julian R. Marchesi, Seema Nair Parvathy, Arielle Elkrief, Ian R. Watson, Rejean Lapointe, Nicola Segata, S. M. Mansour Haeryfar, Benjamin H. Mullish, Michael S. Silverman, Jeremy P. Burton, and Saman Maleki Vareki. Fecal microbiota transplantation plus anti-PD-1 immunotherapy in advanced melanoma: a phase I trial. *Nature Medicine 2023 29:8*, 29(8):2121–2132, 7 2023.

[88] Joon Seok Park, Francesca S. Gazzaniga, Meng Wu, Amalia K. Luthens, Jacob Gillis,

Wen Zheng, Martin W. LaFleur, Sarah B. Johnson, Golnaz Morad, Elizabeth M. Park, Yifan Zhou, Stephanie S. Watowich, Jennifer A. Wargo, Gordon J. Freeman, Dennis L. Kasper, and Arlene H. Sharpe. Targeting PD-L2–RGMb overcomes microbiome-related immunotherapy resistance. *Nature 2023 617:7960*, 617(7960):377–385, 5 2023.

[89] Yoong Wearn Lim, Haiyin Chen-Harris, Oleg Mayba, Steve Lianoglou, Arthur Wuster, Tushar Bhangale, Zia Khan, Sanjeev Mariathasan, Anneleen Daemen, Jens Reeder, Peter M. Haverty, William F. Forrest, Matthew Brauer, Ira Mellman, and Matthew L. Albert. Germline genetic polymorphisms influence tumor gene expression and immune cell infiltration. *Proceedings of the National Academy of Sciences of the United States of America*, 115(50):E11701–E11710, 12 2018.

[90] Vylyny Chat, Robert Ferguson, and Tomas Kirchhoff. Germline genetic host factors as predictive biomarkers in immuno-oncology. *Immuno-Oncology Technology*, 2:14–21, 9 2019.

[91] Rosalyn W. Sayaman, Mohamad Saad, Vésteinn Thorsson, Donglei Hu, Wouter Hendrickx, Jessica Roelands, Eduard Porta-Pardo, Younes Mokrab, Farshad Farshidfar, Tomas Kirchhoff, Randy F. Sweis, Oliver F. Bathe, Carolina Heimann, Michael J. Campbell, Cynthia Stretch, Scott Huntsman, Rebecca E. Graff, Najeeb Syed, Laszlo Radvanyi, Simon Shelley, Denise Wolf, Francesco M. Marincola, Michele Ceccarelli, Jérôme Galon, Elad Ziv, and Davide Bedognetti. Germline genetic contribution to the immune landscape of cancer. *Immunity*, 54(2):367, 2 2021.

[92] Meghana Pagadala, Timothy J. Sears, Victoria H. Wu, Eva Pérez-Guijarro, Hyo Kim, Andrea Castro, James V. Talwar, Cristian Gonzalez-Colin, Steven Cao, Benjamin J. Schmiedel, Shervin Goudarzi, Divya Kirani, Jessica Au, Tongwu Zhang, Teresa Landi, Rany M. Salem, Gerald P. Morris, Olivier Harismendy, Sandip Pravin Patel, Ludmil B. Alexandrov, Jill P. Mesirov, Maurizio Zanetti, Chi Ping Day, Chun Chieh Fan, Wesley K. Thompson, Glenn Merlino, J. Silvio Gutkind, Pandurangan Vijayanand, and Hannah Carter. Germline modifiers of the tumor immune microenvironment implicate drivers of cancer risk and immunotherapy response. *Nature Communications 2023 14:1*, 14(1):1–22, 5 2023.

[93] Davide Mangani, Dandan Yang, and Ana C. Anderson. Learning from the nexus of autoimmunity and cancer. *Immunity*, 56(2):256–271, 2 2023.

[94] Eli P. Darnell, Meghan J. Mooradian, Erez N. Baruch, Melis Yilmaz, and Kerry L. Reynolds. Immune-Related Adverse Events (irAEs): Diagnosis, Management, and Clinical Pearls. *Current oncology reports*, 22(4), 4 2020.

[95] Michael Conroy and Jarushka Naidoo. Immune-related adverse events and the balancing act of immunotherapy. *Nature Communications 2022 13:1*, 13(1):1–4, 1 2022.

[96] Camille Hua, Lise Boussemart, Christine Mateus, Emilie Routier, Céline Boutros, Hugo Cazenave, Roxane Viollet, Marina Thomas, Séverine Roy, Naima Benannoune,

Gorana Tomasic, Jean Charles Soria, Stéphane Champiat, Matthieu Texier, Emilie Lanoy, and Caroline Robert. Association of Vitiligo With Tumor Response in Patients With Metastatic Melanoma Treated With Pembrolizumab. *JAMA Dermatology*, 152(1):45–51, 1 2016.

[97] M. Guida, S. Strippoli, M. Maule, P. Quaglino, A. Ramondetta, V. Chiaron Sileni, G. Antonini Cappellini, P. Queirolo, L. Ridolfi, M. Del Vecchio, E. Cocorocchio, A. M. Di Giacomo, L. Festino, B. Merelli, M. Occelli, S. Brugnara, A. Minisini, S. Sava, S. Tommasi, and S. De Summa. Immune checkpoint inhibitor associated vitiligo and its impact on survival in patients with metastatic melanoma: an Italian Melanoma Intergroup study. *ESMO Open*, 6(2):100064, 4 2021.

[98] Nicole Mastacouris, Andrew Strunk, and Amit Garg. Incidence and Prevalence of Diagnosed Vitiligo According to Race and Ethnicity, Age, and Sex in the US. *JAMA Dermatology*, 159(9):986–990, 9 2023.

[99] Mark A. Socinski, Robert M. Jotte, Federico Cappuzzo, Makoto Nishio, Tony S.K. Mok, Martin Reck, Gene G. Finley, Monika D. Kaul, Wei Yu, Nindhana Paranthaman, Ilze Bāra, and Howard J. West. Association of Immune-Related Adverse Events With Efficacy of Atezolizumab in Patients With Non–Small Cell Lung Cancer: Pooled Analyses of the Phase 3 IMpower130, IMpower132, and IMpower150 Randomized Clinical Trials. *JAMA Oncology*, 9(4):527–535, 4 2023.

[100] Martina Damo, Noah I. Hornick, Aarthi Venkat, Ivana William, Kathryn Clulo, Srividhya Venkatesan, Jiaming He, Eric Fagerberg, Jennifer L. Loza, Darwin Kwok, Aya Tal, Jessica Buck, Can Cui, Jaiveer Singh, William E. Damsky, Jonathan S. Leventhal, Smita Krishnaswamy, and Nikhil S. Joshi. PD-1 maintains CD8 T cell tolerance towards cutaneous neoantigens. *Nature*, 619(7968):151–159, 7 2023.

[101] Jacy Gameiro, Patrícia Nagib, and Liana Verinaud. The thymus microenvironment in regulating thymocyte differentiation. *Cell Adhesion & Migration*, 4(3):382, 2010.

[102] Mohamed Elsherif Badr, Zhongmei Zhang, Xuguang Tai, and Alfred Singer. CD8 T cell tolerance results from eviction of immature autoreactive cells from the thymus. *Science*, 382(6670):534–541, 11 2023.

[103] Mohammad Reza Zamani, Saeed Aslani, Arash Salmaninejad, Mohammad Reza Javan, and Nima Rezaei. PD-1/PD-L and autoimmunity: A growing relationship. *Cellular immunology*, 310:27–41, 12 2016.

[104] Md Munnaf Hossen, Yanmei Ma, Zhihua Yin, Yuhao Xia, Jing Du, Jim Yi Huang, Jennifer Jin Huang, Linghua Zou, Zhizhong Ye, and Zhong Huang. Current understanding of CTLA-4: from mechanism to autoimmune diseases. *Frontiers in Immunology*, 14, 2023.

[105] Zia Khan, Christian Hammer, Ellie Guardino, G. Scott Chandler, and Matthew L. Albert. Mechanisms of immune-related adverse events associated with immune checkpoint blockade: Using germline genetics to develop a personalized approach. *Genome Medicine*, 11(1):1–3, 6 2019.

[106] Ik Shin Chin, Aman Khan, Anna Olsson-Brown, Sophie Papa, Gary Middleton, and Claire Palles. Germline genetic variation and predicting immune checkpoint inhibitor induced toxicity. *NPJ Genomic Medicine*, 7(1), 12 2022.

[107] Vylyny Chat, Robert Ferguson, Danny Simpson, Esther Kazlow, Rebecca Lax, Una Moran, Anna Pavlick, Dennie Frederick, Genevieve Boland, Ryan Sullivan, Antoni Ribas, Keith Flaherty, Iman Osman, Jeffrey Weber, and Tomas Kirchhoff. Autoimmune genetic risk variants as germline biomarkers of response to melanoma immune checkpoint inhibition. *Cancer immunology, immunotherapy : CII*, 68(6):897, 2019.

[108] Xiao Yu, Jin Peng Sun, Yantao He, Xiaoling Guo, Sijiu Liu, Bo Zhou, Andy Hudmon, and Zhong Yin Zhang. Structure, inhibitor, and regulatory mechanism of Lyp, a lymphoid-specific tyrosine phosphatase implicated in autoimmune diseases. *Proceedings of the National Academy of Sciences of the United States of America*, 104(50):19767–19772, 12 2007.

[109] Sophia J. Tsai, Udayaditya Sen, Lei Zhao, William B. Greenleaf, Jhimli Dasgupta, Edoardo Fiorillo, Valeria Orrú, Nunzio Bottini, and Xiaojiang S. Chen. Crystal structure of the human lymphoid tyrosine phosphatase catalytic domain: insights into redox regulation. *Biochemistry*, 48(22):4838–4845, 6 2009.

[110] R. James Matthews, David B. Bowne, Edwin Flores, and Matthew L. Thomas. Characterization of hematopoietic intracellular protein tyrosine phosphatases: description of a phosphatase containing an SH2 domain and another enriched in proline-, glutamic acid-, serine-, and threonine-rich sequences. *Molecular and cellular biology*, 12(5):2396–2405, 5 1992.

[111] Jean François Cloutier and André Veillette. Association of inhibitory tyrosine protein kinase p50csk with protein tyrosine phosphatase PEP in T cells and other hemopoietic cells. *EMBO J.*, 15(18):4909–4918, 9 1996.

[112] Ann B. Begovich, Victoria E.H. Carlton, Lee A. Honigberg, Steven J. Schrodi, Anand P. Chokkalingam, Heather C. Alexander, Kristin G. Ardlie, Qiqing Huang, Ashley M. Smith, Jill M. Spoerke, Marion T. Conn, Monica Chang, Sheng Yung P. Chang, Randall K. Saiki, Joseph J. Catanese, Diane U. Leong, Veronica E. Garcia, Linda B. McAllister, Douglas A. Jeffery, Annette T. Lee, Franak Batliwalla, Elaine Remmers, Lindsey A. Criswell, Michael F. Seldin, Daniel L. Kastner, Christopher I. Amos, John J. Sninsky, and Peter K. Gregersen. A missense single-nucleotide polymorphism in a gene encoding a protein tyrosine phosphatase (PTPN22) is associated with rheumatoid arthritis. *Am. J. Hum. Genet.*, 75(2):330–337, 2004.

[113] Nunzio Bottini, Lucia Musumeci, Andres Alonso, Souad Rahmouni, Konstantina Nika, Masoud Rostamkhani, James MacMurray, Gian Franco Meloni, Paola Lucarelli, Maurizio Pellecchia, George S. Eisenbarth, David Comings, and Tomas Mustelin. A functional variant of lymphoid tyrosine phosphatase is associated with type I diabetes. *Nat. Genet.*, 36(4):337–338, 4 2004.

[114] Chieko Kyogoku, Carl D. Langefeld, Ward A. Ortmann, Annette Lee, Scott Selby, Victoria E.H. Carlton, Monica Chang, Paula Ramos, Emily C. Baechler, Franak M. Batliwalla, Jill Novitzke, Adrienne H. Williams, Clarence Gillett, Peter Rodine, Robert R. Graham, Kristin G. Ardlie, Patrick M. Gaffney, Kathy L. Moser, Michelle Petri, Ann B. Begovich, Peter K. Gregersen, and Timothy W. Behrens. Genetic Association of the R620W Polymorphism of Protein Tyrosine Phosphatase PTPN22 with Human SLE. *American Journal of Human Genetics*, 75(3):504, 2004.

[115] Stephanie M. Stanford and Nunzio Bottini. PTPN22: The archetypal non-HLA autoimmunity gene, 2014.

[116] Torkel Vang, Mauro Congia, Maria Doloretta Macis, Lucia Musumeci, Valeria Orrú, Patrizia Zavattari, Konstantina Nika, Lutz Tautz, Kjetil Taskén, Francesco Cucca, Tomas Mustelin, and Nunzio Bottini. Autoimmune-associated lymphoid tyrosine phosphatase is a gain-of-function variant. *Nat. Genet.*, 37(12):1317–1319, 12 2005.

[117] Jinyi Zhang, Naima Zahir, Qiuhong Jiang, Helen Miliotis, Stephanie Heyraud, Xianwang Meng, Baoxia Dong, Gang Xie, Frank Qiu, Zhenyue Hao, Christopher A. McCulloch, Edward C. Keystone, Alan C. Peterson, and Katherine A. Siminovitch. The autoimmune diseaseg-associated PTPN22 variant promotes calpain-mediated Lyp/Pep degradation associated with lymphocyte and dendritic cell hyperresponsiveness. *Nature Genetics*, 43(9):902–907, 9 2011.

[118] Kiminori Hasegawa, Flavius Martin, Guangming Huang, Dan Tumas, Lauri Diehl, and Andrew C. Chan. PEST Domain-Enriched Tyrosine Phosphatase (PEP) Regulation of Effector/Memory T Cells. *Science*, 303(5658):685–689, 1 2004.

[119] Shatakshi Sood, Rebecca J. Brownlie, Celine Garcia, Graeme Cowan, Robert J. Salmond, Shimon Sakaguchi, and Rose Zamoyska. Loss of the Protein Tyrosine Phosphatase PTPN22 Reduces Mannan-Induced Autoimmune Arthritis in SKG Mice. *Journal of immunology (Baltimore, Md. : 1950)*, 197(2):429–440, 7 2016.

[120] Xiaotian Lin, Stephane Pelletier, Sebastien Gingras, Stephanie Rigaud, Christian J. Maine, Kristi Marquardt, Yang D. Dai, Karsten Sauer, Alberto R. Rodriguez, Greg Martin, Sergey Kupriyanov, Ling Jiang, Liping Yu, Douglas R. Green, and Linda A. Sherman. CRISPR-Cas9-Mediated Modification of the NOD Mouse Genome With Ptpn22R619W Mutation Increases Autoimmune Diabetes. *Diabetes*, 65(8):2134–2138, 8 2016.

[121] Yaya Wang, Iftach Shaked, Stephanie M. Stanford, Wenbo Zhou, Julie M. Curtsinger, Zbigniew Mikulski, Zachary R. Shaheen, Genhong Cheng, Kristy Sawatzke, Amanda M. Campbell, Jennifer L. Auger, Hatice Bilgic, Fernanda M. Shoyama, David O. Schmeling, Henry H. Balfour, Kiminori Hasegawa, Andrew C. Chan, John A. Corbett, Bryce A. Binstadt, Matthew F. Mescher, Klaus Ley, Nunzio Bottini, and Erik J. Peterson. The Autoimmunity-Associated Gene PTPN22 Potentiates Toll-like Receptor-Driven, Type 1 Interferon-Dependent Immunity. *Immunity*, 39(1):111–122, 7 2013.

[122] Songtao Tang, Wenjia Peng, Changjiang Wang, Haiqin Tang, and Qiu Zhang. Association of the PTPN22 gene (+1858C/T, -1123G/C) polymorphisms with type 1 diabetes mellitus: a systematic review and meta-analysis. *Diabetes research and clinical practice*, 97(3):446–452, 9 2012.

[123] M. Galeazzi, G. Gasbarrini, A. Ghirardello, S. Grandemange, H. M. Hoffman, R. Manna, M. Podswiadek, L. Punzi, G. D. Sebastiani, I. Touitou, and Andrea Doria. Autoinflammatory syndromes. *Clinical and experimental rheumatology*, 24(1 Suppl 40), 1 2006.

[124] Robert J Salmond, Rebecca J Brownlie, Vicky L Morrison, and Rose Zamoyska. The tyrosine phosphatase PTPN22 discriminates weak self peptides from strong agonist TCR signals. *Nature Immunology*, 15, 2014.

[125] Rebecca J. Brownlie, David Wright, Rose Zamoyska, and Robert J. Salmond. Deletion of PTPN22 improves effector and memory CD8+ T cell responses to tumors. *JCI Insight*, 4(16), 8 2019.

[126] Georgia Fousteri, Stamatis Nick C. Liossis, and Manuela Battaglia. Roles of the protein tyrosine phosphatase PTPN22 in immunity and autoimmunity, 12 2013.

[127] Rebecca J Brownlie, Lisa A Miosge, Demetrios Vassilakos, Lena M Svensson, Andrew Cope, and Rose Zamoyska. Lack of the Phosphatase PTPN22 Increases Adhesion of Murine Regulatory T Cells to Improve Their Immunosuppressive Function. *Science Signaling*, 5(252), 2012.

[128] Fiona Clarke, Christine K. Jordan, Enrique Gutiérrez-Martinez, Jack A. Bibby, Cristina Sanchez-Blanco, Georgina H. Cornish, Xuezhi Dai, David J. Rawlings, Rose Zamoyska, Pierre Guermonprez, Andrew P. Cope, and Harriet A. Purvis. Protein tyrosine phosphatase PTPN22 is dispensable for dendritic cell antigen processing and promotion of T-cell activation by dendritic cells. *PLoS ONE*, 12(10), 10 2017.

[129] Fiona Clarke, Harriet A. Purvis, Cristina Sanchez-Blanco, Enrique Gutiérrez-Martinez, Georgina H. Cornish, Rose Zamoyska, Pierre Guermonprez, and Andrew P. Cope. The protein tyrosine phosphatase PTPN22 negatively regulates presentation of immune complex derived antigens. *Scientific Reports*, 8(1):12692, 12 2018.

[130] Harriet A. Purvis, Fiona Clarke, Anna B. Montgomery, Chloe Colas, Jack A. Bibby, Georgina H. Cornish, Xuezhi Dai, Diana Dudziak, David J. Rawlings, Rose Zamoyska, Pierre Guermonprez, and Andrew P. Cope. Phosphatase PTPN22 Regulates Dendritic Cell Homeostasis and cDC2 Dependent T Cell Responses. *Frontiers in Immunology*, 11, 3 2020.

[131] Hui-Hsin Chang, Shi-Chuen Miaw, William Tseng, Yi-Wei Sun, Chih-Chun Liu, Hsiao-Wei Tsao, and I-Cheng Ho. PTPN22 Modulates Macrophage Polarization and Susceptibility to Dextran Sulfate Sodium–Induced Colitis. *The Journal of Immunology*, 191(5):2134–2143, 9 2013.

[132] Rebecca J. Brownlie, Celine Garcia, Mate Ravasz, Dietmar Zehn, Robert J. Salmond, and Rose Zamoyska. Resistance to TGFβ suppression and improved anti-tumor responses in CD8+ T cells lacking PTPN22. *Nature Communications*, 8(1):1–10, 12 2017.

[133] Xin Du, Phillip K. Darcy, Florian Wiede, and Tony Tiganis. Targeting Protein Tyrosine Phosphatase 22 Does Not Enhance the Efficacy of Chimeric Antigen Receptor T Cells in Solid Tumors. *Molecular and Cellular Biology*, 42(3), 3 2022.

[134] Alexandra Rose Teagle, Patricia Castro-Sanchez, Rebecca J Brownlie, Nicola Logan, Simran S Kapoor, David Wright, Robert J Salmond, and Rose Zamoyska. Deletion of the protein tyrosine phosphatase PTPN22 for adoptive T cell therapy facilitates CTL effector function but promotes T cell exhaustion. *Journal for ImmunoTherapy of Cancer*, 11(12):e007614, 12 2023.

[135] Rafael Cubas, Zia Khan, Qian Gong, Marina Moskalenko, Huizhong Xiong, Qinglin Ou, Christine Pai, Ryan Rodriguez, Jeanne Cheung, and Andrew C. Chan. Autoimmunity linked protein phosphatase PTPN22 as a target for cancer immunotherapy. *Journal for ImmunoTherapy of Cancer*, 8(2):1439, 10 2020.

[136] Won Jin Ho, Sarah Croessmann, Jianping Lin, Zaw H. Phyo, Soren Charmsaz, Ludmila Danilova, Aditya A. Mohan, Nicole E. Gross, Fangluo Chen, Jiajun Dong, Devesh Aggarwal, Yunpeng Bai, Janey Wang, Jing He, James M. Leatherman, Mark Yarchoan, Todd D. Armstrong, Neeha Zaidi, Elana J. Fertig, Joshua C. Denny, Ben H. Park, Zhong-Yin Zhang, and Elizabeth M. Jaffee. Systemic inhibition of PTPN22 augments anticancer immunity. *The Journal of Clinical Investigation*, 7 2021.

[137] Robin C. Orozco, Kristi Marquardt, Kerri Mowen, and Linda A. Sherman. Proautoimmune Allele of Tyrosine Phosphatase, PTPN22, Enhances Tumor Immunity. *The Journal of Immunology*, 207(6):1662–1671, 9 2021.

[138] Christian Blank, Ian Brown, Amy C. Peterson, Mike Spiotto, Yoshiko Iwai, Tasuku Honjo, and Thomas F. Gajewski. PD-L1/B7H-1 Inhibits the Effector Phase of Tumor Rejection by T Cell Receptor (TCR) Transgenic CD8+ T Cells. *Cancer Research*, 64(3):1140–1145, 2 2004.

[139] Alberto Mantovani, Federica Marchesi, Alberto Malesci, Luigi Laghi, and Paola Allavena. Tumour-associated macrophages as treatment targets in oncology, 7 2017.

[140] Torkel Vang, Wallace H. Liu, Laurence Delacroix, Shuangding Wu, Stefan Vasile, Russell Dahl, Li Yang, Lucia Musumeci, Dana Francis, Johannes Landskron, Kjetil Tasken, Michel L. Tremblay, Benedicte A. Lie, Rebecca Page, Tomas Mustelin, Souad Rahmouni, Robert C. Rickert, and Lutz Tautz. LYP inhibits T-cell activation when dissociated from CSK. *Nature Chemical Biology*, 8(5):437–446, 2012.

[141] Sharon A. Chung and Lindsey A. Criswell. PTPN22: Its role in SLE and autoimmunity, 12 2007.

[142] Mercedes B. Fuertes, Aalok K. Kacha, Justin Kline, Seng Ryong Woo, David M. Kranz, Kenneth M. Murphy, and Thomas F. Gajewski. Host type I IFN signals are required for antitumor CD8+ T cell responses through CD8α+ dendritic cells. *Journal of Experimental Medicine*, 208(10):2005–2016, 9 2011.

[143] Edward W. Roberts, Miranda L. Broz, Mikhail Binnewies, Mark B. Headley, Amanda E. Nelson, Denise M. Wolf, Tsuneyasu Kaisho, Dusan Bogunovic, Nina Bhardwaj, and Matthew F. Krummel. Critical Role for CD103(+)/CD141(+) Dendritic Cells Bearing CCR7 for Tumor Antigen Trafficking and Priming of T Cell Immunity in Melanoma. *Cancer cell*, 30(2):324–336, 8 2016.

[144] Alycia Gardner and Brian Ruffell. Dendritic Cells and Cancer Immunity. *Trends in immunology*, 37(12):855, 12 2016.

[145] Stefani Spranger, Daisy Dai, Brendan Horton, and Thomas F. Gajewski. Tumor-Residing Batf3 Dendritic Cells Are Required for Effector T Cell Trafficking and Adoptive T Cell Therapy. *Cancer Cell*, 31(5):711–723, 5 2017.

[146] Miriam Merad, Priyanka Sathe, Julie Helft, Jennifer Miller, and Arthur Mortha. The Dendritic Cell Lineage: Ontogeny and Function of Dendritic Cells and Their Subsets in the Steady State and the Inflamed Setting. *Annual review of immunology*, 31:563–604, 3 2013.

[147] Qi Peng, Xiangyan Qiu, Zihan Zhang, Silin Zhang, Yuanyuan Zhang, Yong Liang, Jingya Guo, Hua Peng, Mingyi Chen, Yang Xin Fu, and Haidong Tang. PD-L1 on dendritic cells attenuates T cell activation and regulates response to immune checkpoint blockade. *Nature Communications*, 11(1):1–8, 12 2020.

[148] Philippe Pierre, Shannon J. Turley, Evelina Gatti, Michael Hull, Joseph Meltzer, Asra Mirza, Kayo Inaba, Ralph M. Steinman, and Ira Mellman. Developmental regulation of MHC class II transport in mouse dendritic cells. *Nature 1997 388:6644*, 388(6644):787–792, 1997.

[149] Marina Cella, Anneke Engering, Valerie Pinet, Jean Pieters, and Antonio Lanzavecchia. Inflammatory stimuli induce accumulation of MHC class II complexes on dendritic cells. *Nature 1997 388:6644*, 388(6644):782–787, 1997.

[150] Stefani Spranger, Robbert M. Spaapen, Yuanyuan Zha, Jason Williams, Yuru Meng, Thanh T. Ha, and Thomas F. Gajewski. Up-regulation of PD-L1, IDO, and Tregs in the melanoma tumor microenvironment is driven by CD8+ T cells, 8 2013.

[151] Alexander S. Baras, Charles Drake, Jen Jane Liu, Nilay Gandhi, Max Kates, Mohamed O. Hoque, Alan Meeker, Noah Hahn, Janis M. Taube, Mark P. Schoenberg, George Netto, and Trinity J. Bivalacqua. The ratio of CD8 to Treg tumor-infiltrating lymphocytes is associated with response to cisplatin-based neoadjuvant chemotherapy in patients with muscle invasive urothelial carcinoma of the bladder. *Oncoimmunology*, 5(5), 5 2016.

[152] Luis Alberto Solis-Castillo, Gina Stella Garcia-Romo, Alvaro Diaz-Rodriguez, Diana Reyes-Hernandez, Elizabeth Tellez-Rivera, Victor Hugo Rosales-Garcia, Adolfo Rene Mendez-Cruz, Jose Rafael Jimenez-Flores, Victor Hugo Villafana-Vazquez, and Alexander Pedroza-Gonzalez. Tumor-infiltrating regulatory T cells, CD8/Treg ratio, and cancer stem cells are correlated with lymph node metastasis in patients with early breast cancer. *Breast Cancer*, 27(5):837–849, 9 2020.

[153] Lili Huang, Yeye Guo, Shujing Liu, Huaishan Wang, Jinjin Zhu, Lingling Ou, and Xiaowei Xu. Targeting regulatory T cells for immunotherapy in melanoma. *Molecular Biomedicine*, 2(1), 12 2021.

[154] Jan P. Böttcher and Caetano Reis e Sousa. The Role of Type 1 Conventional Dendritic Cells in Cancer Immunity. *Trends in Cancer*, 4(11):784, 11 2018.

[155] Christopher S. Garris, Sean P. Arlauckas, Rainer H. Kohler, Marcel P. Trefny, Seth Garren, Cécile Piot, Camilla Engblom, Christina Pfirschke, Marie Siwicki, Jeremy Gungabeesoon, Gordon J. Freeman, Sarah E. Warren, Su Fey Ong, Erica Browning, Christopher G. Twitty, Robert H. Pierce, Mai H. Le, Alain P. Algazi, Adil I. Daud, Sara I. Pai, Alfred Zippelius, Ralph Weissleder, and Mikael J. Pittet. Successful Anti-PD-1 Cancer Immunotherapy Requires T Cell-Dendritic Cell Crosstalk Involving the Cytokines IFN-γ and IL-12. *Immunity*, 49(6):1148–1161, 12 2018.

[156] Thomas F. Gajewski, Yuru Meng, and Helena Harlin. Immune suppression in the tumor microenvironment. *Journal of immunotherapy (Hagerstown, Md. : 1997)*, 29(3):233–240, 5 2006.

[157] Thomas F. Gajewski. Failure at the Effector Phase: Immune Barriers at the Level of the Melanoma Tumor Microenvironment. *Clinical Cancer Research*, 13(18):5256–5261, 9 2007.

[158] Nataliya Prokhnevska, Maria A. Cardenas, Rajesh M. Valanparambil, Ewelina Sobierajska, Benjamin G. Barwick, Caroline Jansen, Adriana Reyes Moon, Petra Gregorova, Luke delBalzo, Rachel Greenwald, Mehmet Asim Bilen, Mehrdad Alemozaffar, Shreyas Joshi, Cara Cimmino, Christian Larsen, Viraj Master, Martin Sanda, and Haydn Kissick. CD8+ T cell activation in cancer comprises an initial activation

phase in lymph nodes followed by effector differentiation within the tumor. *Immunity*, 56(1):107–124, 1 2023.

[159] Rhys S. Allan, Chris M. Smith, Gabrielle T. Belz, Allison L. Van Lint, Linda M. Wakim, William R. Heath, and Francis R. Carbone. Epidermal viral immunity induced by CD8α+ dendritic cells but not by langerhans cells. *Science*, 301(5641):1925–1928, 9 2003.

[160] Lionel Franz Poulin, Sandrine Henri, Béatrice De Bovis, Elisabeth Devilard, Adrien Kissenpfennig, and Bernard Malissen. The dermis contains langerin+ dendritic cells that develop and function independently of epidermal Langerhans cells. *The Journal of experimental medicine*, 204(13):3119–3131, 12 2007.

[161] Sandrine Henri, Lionel Franz Poulin, Samira Tamoutounour, Laurence Ardouin, Martin Guilliams, Béatrice De Bovis, Elisabeth Devilard, Christophe Viret, Hiroaki Azukizawa, Adrien Kissenpfennig, and Bernard Malissen. CD207+ CD103+ dermal dendritic cells cross-present keratinocyte-derived antigens irrespective of the presence of Langerhans cells. *The Journal of experimental medicine*, 207(1):189–206, 1 2010.

[162] Samira Tamoutounour, Martin Guilliams, Frédéric MontananaSanchis, Hong Liu, Dorothea Terhorst, Camille Malosse, Emeline Pollet, Laurence Ardouin, Hervé Luche, Cindy Sanchez, Marc Dalod, Bernard Malissen, and Sandrine Henri. Origins and functional specialization of macrophages and of conventional and monocyte-derived dendritic cells in mouse skin. *Immunity*, 39(5):925–938, 11 2013.

[163] Nathalie T. Joncker, Sarah Bettini, Delphine Boulet, Martine Guiraud, and Sylvie Guerder. The site of tumor development determines immunogenicity via temporal mobilization of antigen-laden dendritic cells in draining lymph nodes. *European Journal of Immunology*, 46(3):609–618, 3 2016.

[164] Ralph M. Steinman and Joel Swanson. The endocytic activity of dendritic cells. *Journal of Experimental Medicine*, 182(2):283–288, 8 1995.

[165] Laura Bonifaz, David Bonnyay, Karsten Mahnke, Miguel Rivera, Michel C. Nussenzweig, and Ralph M. Steinman. Efficient Targeting of Protein Antigen to the Dendritic Cell Receptor DEC-205 in the Steady State Leads to Antigen Presentation on Major Histocompatibility Complex Class I Products and Peripheral CD8+ T Cell Tolerance. *Journal of Experimental Medicine*, 196(12):1627–1638, 12 2002.

[166] Ralph M. Steinman. Decisions About Dendritic Cells: Past, Present, and Future. *https://doi.org/10.1146/annurev-immunol-100311-102839*, 30:1–22, 3 2012.

[167] Holger Karsunky, Miriam Merad, Antonio Cozzio, Irving L. Weissman, and Markus G. Manz. Flt3 Ligand Regulates Dendritic Cell Development from Flt3+ Lymphoid and Myeloid-committed Progenitors to Flt3+ Dendritic Cells In Vivo. *The Journal of Experimental Medicine*, 198(2):305, 7 2003.

[168] Claudia Waskow, Kang Liu, Guillaume Darrasse-Jèze, Pierre Guermonprez, Florent Ginhoux, Miriam Merad, Tamara Shengelia, Kaihui Yao, and Michel Nussenzweig. The receptor tyrosine kinase Flt3 is required for dendritic cell development in peripheral lymphoid tissues. *Nature Immunology 2008 9:6*, 9(6):676–683, 5 2008.

[169] Junghwa Lee, Eunseon Ahn, Haydn T Kissick, and Rafi Ahmed. Reinvigorating Exhausted T Cells by Blockade of the PD-1 Pathway.

[170] E. John Wherry and Makoto Kurachi. Molecular and cellular insights into T cell exhaustion. *Nature reviews. Immunology*, 15(8):486–499, 8 2015.

[171] Peng Liu, Liwei Zhao, Guido Kroemer, and Oliver Kepp. Conventional type 1 dendritic cells (cDC1) in cancer immunity. *Biology Direct*, 18(1):71, 12 2023.

[172] Christopher Paluch, Ana Mafalda Santos, Consuelo Anzilotti, Richard J. Cornall, and Simon J. Davis. Immune checkpoints as therapeutic targets in autoimmunity. *Frontiers in Immunology*, 9(OCT):406796, 10 2018.

[173] Asher Mullard. PD1 agonist antibody passes first phase II trial for autoimmune disease. *Nature Reviews Drug Discovery*, 22(7):526, 7 2023.

[174] Ludmila Prokunina, Casimiro Castillejo-López, Fredrik Öberg, Iva Gunnarsson, Louise Berg, Veronica Magnusson, Anthony J. Brookes, Dmitry Tentler, Helga Kristjansdóttir, Gerdur Gróndal, Anne Isine Bolstad, Elisabet Svenungsson, Ingrid Lundberg, Gunnar Sturfelt, Andreas Jönssen, Lennart Truedsson, Guadalupe Lima, Jorge Alcocer-Varela, Roland Jonsson, Ulf B. Gyllensten, John B. Harley, Donato Alarcón-Segovia, Kristján Steinsson, and Marta E. Alarcón-Riquelme. A regulatory polymorphism in PDCD1 is associated with susceptibility to systemic lupus erythematosus in humans. *Nature genetics*, 32(4):666–669, 12 2002.

[175] Marta Barreto, Eugénia Santos, Ricardo Ferreira, Constantin Fesel, Maria Francisca Fontes, Clara Pereira, Berta Martins, Rita Andreia, João Faro Viana, Francisco Crespo, Carlos Vasconcelos, Carlos Ferreira, and Astrid Moura Vicente. Evidence for CTLA4 as a susceptibility gene for systemic lupus erythematosus. *European Journal of Human Genetics 2004 12:8*, 12(8):620–626, 5 2004.

[176] Eric Kai Pang Kong, Ludmila Prokunina-Olsson, Wilfred Hing Sang Wong, Chak Sing Lau, Tak Mao Chan, Marta Alarcón-Riquelme, and Yu Lung Lau. A new haplotype of PDCD1 is associated with rheumatoid arthritis in Hong Kong Chinese. *Arthritis and rheumatism*, 52(4):1058–1062, 4 2005.

[177] Shuo Zhang, Li Wang, Mengtao Li, Fengchun Zhang, and Xiaofeng Zeng. The PD-1/PD-L pathway in rheumatic diseases. *Journal of the Formosan Medical Association*, 120(1):48–59, 1 2021.

[178] Stephanie M. Stanford and Nunzio Bottini. Targeting protein phosphatases in cancer immunotherapy and autoimmune disorders. *Nature Reviews Drug Discovery 2023 22:4*, 22(4):273–294, 1 2023.

[179] Tomas Mustelin, Nunzio Bottini, and Stephanie M. Stanford. The Contribution of PTPN22 to Rheumatic Disease. *Arthritis & Rheumatology*, 71(4):486–495, 4 2019.

[180] Stefani Spranger, Jason J. Luke, Riyue Bao, Yuanyuan Zha, Kyle M. Hernandez, Yan Li, Alexander P. Gajewski, Jorge Andrade, and Thomas F. Gajewski. Density of immunogenic antigens does not explain the presence or absence of the T-cell-inflamed tumor microenvironment in melanoma. *Proceedings of the National Academy of Sciences of the United States of America*, 113(48):E7759–E7768, 11 2016.

[181] Hélène Salmon, Juliana Idoyaga, Adeeb Rahman, Marylène Leboeuf, Romain Remark, Stefan Jordan, Maria Casanova-Acebes, Makhzuna Khudoynazarova, Judith Agudo, Navpreet Tung, Svetoslav Chakarov, Christina Rivera, Brandon Hogstad, Marcus Bosenberg, Daigo Hashimoto, Sacha Gnjatic, Nina Bhardwaj, Anna Karolina Palucka, Brian D. Brown, Joshua Brody, Florent Ginhoux, and Miriam Merad. Expansion and Activation of CD103(+) Dendritic Cell Progenitors at the Tumor Site Enhances Tumor Responses to Therapeutic PD-L1 and BRAF Inhibition. *Immunity*, 44(4):924–938, 4 2016.

[182] Pierre Guermonprez, Julie Helft, Carla Claser, Stephanie Deroubaix, Henry Karanje, Anna Gazumyan, Guillaume Darasse-Jèze, Stephanie B. Telerman, Gaëlle Breton, Heidi A. Schreiber, Natalia Frias-Staheli, Eva Billerbeck, Marcus Dorner, Charles M. Rice, Alexander Ploss, Florian Klein, Melissa Swiecki, Marco Colonna, Alice O. Kamphorst, Matthew Meredith, Rachel Niec, Constantin Takacs, Fadi Mikhail, Aswin Hari, David Bosque, Tom Eisenreich, Miriam Merad, Yan Shi, Florent Ginhoux, Laurent Rénia, Britta C. Urban, and Michel C. Nussenzweig. Inflammatory Flt3L is essential to mobilize dendritic cells and for T
}cell responses during Plasmodium infection. *Nature medicine*, 19(6):730, 6 2013.

[183] Yingying Wang, Ying Xiang, Victoria W. Xin, Xian Wang Wang, Xiao Chun Peng, Xiao Qin Liu, Dong Wang, Na Li, Jun Ting Cheng, Yan Ning Lyv, Shu Zhong Cui, Zhaowu Ma, Qing Zhang, and Hong Wu Xin. Dendritic cell biology and its role in tumor immunotherapy. *Journal of Hematology and Oncology*, 13(1):1–18, 8 2020.

[184] Jean Nicolas Schickel, Marcel Kuhny, Alessia Baldo, Jason M. Bannock, Christopher Massad, Haowei Wang, Nathan Katz, Tyler Oe, Laurence Menard, Pauline Soulas-Sprauel, Till Strowig, Richard Flavell, and Eric Meffre. PTPN22 inhibition resets defective human central B cell tolerance. *Science Immunology*, 1(1):7153, 2016.

[185] Lucas H. Armitage, Mark A. Wallet, and Clayton E. Mathews. Influence of PTPN22 Allotypes on Innate and Adaptive Immune Function in Health and Disease. *Frontiers in Immunology*, 12:636618, 2 2021.

[186] Tivoli Nguyen, Jie Du, and Yan Chun Li. A protocol for macrophage depletion and reconstitution in a mouse model of sepsis. *STAR Protocols*, 2(4), 12 2021.

[187] Christina K. Baumgartner, Hakimeh Ebrahimi-Nik, Arvin Iracheta-Vellve, Keith M. Hamel, Kira E. Olander, Thomas G.R. Davis, Kathleen A. McGuire, Geoff T. Halvorsen, Omar I. Avila, Chirag H. Patel, Sarah Y. Kim, Ashwin V. Kammula, Audrey J. Muscato, Kyle Halliwill, Prasanthi Geda, Kelly L. Klinge, Zhaoming Xiong, Ryan Duggan, Liang Mu, Mitchell D. Yeary, James C. Patti, Tyler M. Balon, Rebecca Mathew, Carey Backus, Domenick E. Kennedy, Angeline Chen, Kenton Longenecker, Joseph T. Klahn, Cara L. Hrusch, Navasona Krishnan, Charles W. Hutchins, Jax P. Dunning, Marinka Bulic, Payal Tiwari, Kayla J. Colvin, Cun Lan Chuong, Ian C. Kohnle, Matthew G. Rees, Andrew Boghossian, Melissa Ronan, Jennifer A. Roth, Meng Ju Wu, Juliette S.M.T. Suermondt, Nelson H. Knudsen, Collins K. Cheruiyot, Debattama R. Sen, Gabriel K. Griffin, Todd R. Golub, Nabeel El-Bardeesy, Joshua H. Decker, Yi Yang, Magali Guffroy, Stacey Fossey, Patricia Trusk, Im Meng Sun, Yue Liu, Wei Qiu, Qi Sun, Marcia N. Paddock, Elliot P. Farney, Mark A. Matulenko, Clay Beauregard, Jennifer M. Frost, Kathleen B. Yates, Philip R. Kym, and Robert T. Manguso. The PTPN2/PTPN1 inhibitor ABBV-CLS-484 unleashes potent anti-tumour immunity. *Nature 2023 622:7984*, 622(7984):850–862, 10 2023.

[188] Rohit Bhargava and David J. Dabbs. Immunohistology of Metastatic Carcinomas of Unknown Primary. *Diagnostic Immunohistochemistry: Theranostic and Genomic Applications, Expert Consult*, pages 206–255, 1 2011.

[189] Joseph A. Katakowski, Gayatri Mukherjee, Samantha E. Wilner, Keith E. Maier, Michael Travis Harrison, Teresa P. Di Lorenzo, Matthew Levy, and Deborah Palliser. Delivery of siRNAs to dendritic cells using DEC205-targeted lipid nanoparticles to inhibit immune responses. *Molecular Therapy*, 24(1):146–155, 2 2016.

[190] Lucía López, Luciano Gastón Morosi, Federica La Terza, Pierre Bourdely, Giuseppe Rospo, Roberto Amadio, Giulia Maria Piperno, Valentina Russo, Camilla Volponi, Simone Vodret, Sonal Joshi, Francesca Giannese, Dejan Lazarevic, Giovanni Germano, Patrizia Stoitzner, Alberto Bardelli, Marc Dalod, Luigia Pace, Nicoletta Caronni, Pierre Guermonprez, and Federica Benvenuti. Dendritic cell-targeted therapy expands CD8 T cell responses to bona-fide neoantigens in lung tumors. *Nature Communications 2024 15:1*, 15(1):1–17, 3 2024.

[191] Barbara Maier, Andrew M. Leader, Steven T. Chen, Navpreet Tung, Christie Chang, Jessica LeBerichel, Aleksey Chudnovskiy, Shrisha Maskey, Laura Walker, John P. Finnigan, Margaret E. Kirkling, Boris Reizis, Sourav Ghosh, Natalie Roy D'Amore, Nina Bhardwaj, Carla V. Rothlin, Andrea Wolf, Raja Flores, Thomas Marron, Adeeb H. Rahman, Ephraim Kenigsberg, Brian D. Brown, and Miriam Merad. A conserved dendritic-cell regulatory program limits antitumour immunity. *Nature 2020 580:7802*, 580(7802):257–262, 3 2020.